nagra.

Technical Report 17-04

An evaluation of sulphide fluxes in the near field of a HLW repository

April 2017

V. Cloet, M. Pekala, P. Smith,
P. Wersin, N. Diomidis

National Cooperative
for the Disposal of
Radioactive Waste

Hardstrasse 73
CH-5430 Wettingen
Switzerland
Tel. +41 56 437 11 11

www.nagra.ch

nagra.

Technical Report 17-04

An evaluation of sulphide fluxes in the near field of a HLW repository

April 2017

V. Cloet [1], M. Pekala [2], P. Smith [3], P. Wersin [2], N. Diomidis [1]

[1] Nagra
[2] University of Bern
[3] SAM (Switzerland)

National Cooperative for the Disposal of Radioactive Waste

Hardstrasse 73
CH-5430 Wettingen
Switzerland
Tel. +41 56 437 11 11

www.nagra.ch

ISSN 1015-2636

Abstract

According to the current reference concept for the deep geological disposal of high-level radioactive waste (HLW) in Switzerland, steel canisters will be used to dispose of the spent fuel and vitrified waste. Surrounding a steel canister, a buffer material will be emplaced to maintain a diffusive transport regime and to retain the released radionuclides after breaching of the canister. Within the buffer, favourable hydrogeochemical conditions guarantee a low canister corrosion rate and thus a long canister life-time. Instead of a steel canister, an alternative concept based on a copper coated canister is currently being developed. Thanks to its negligible corrosion rate in oxygen-free water a copper coating significantly prolongs the canister life-time. In such a case, the presence of sulphide in the near field of the canister requires additional attention, as it is a very effective oxidant for copper. The aim of this report is to investigate the sulphide fluxes in the near field as a function of the buffer material and properties.

The sulphide fluxes in the near field are defined by the hydrogeochemical conditions in the near field, which are to a large part defined by the emplaced buffer material. Three different types of near field are considered in this report: a well-emplaced bentonite buffer, a bentonite buffer with reduced density and a crushed Opalinus Clay buffer. To calculate the sulphide fluxes towards the canister, two different models are used. A simplified transport model in which the diffusive transport of sulphide, produced by the microbial reduction of sulphate, towards the canister is modelled, and a reactive transport model in which the sulphide concentration is defined by the entire chemical environment in the near field (pH, Eh, Fe, microbial activity, …), before being diffusively transported towards the canister. Once the sulphide is at the canister interface, a one-step corrosion mechanism based on the stoichiometry of the simplified corrosion reaction was assumed. This means that the calculated corrosion depths in this report represents an average corrosion depth.

As both models show, the potential corrosion depths after 1'000'000 years in the well-emplaced bentonite buffer scenario are the lowest (0.08 – 0.2 mm), followed by the reduced density bentonite (1.3 – 2 mm) and the crushed Opalinus Clay scenario (3.1 – 3.4 mm). The lower values are provided by the reactive transport model, the upper bound values by the simplified model. With the help of the simplified model, the sensitivity of the sulphide flux to several parameters (e.g. sulphide solubility, anion diffusion coefficient, oxidised pyrite in the EDZ, gypsum concentration in bentonite) could be shown. The most important parameters are shown to be the sulphide solubility, followed by the diffusion coefficient of sulphide and sulphate.

Besides calculating the sulphide fluxes and their impact on corrosion, these models have also illustrated the importance of the sulphide solubility limit. The presence of iron in the near field (arising from goethite in bentonite or siderite in Opalinus Clay) induce the precipitation of FeS minerals, which limits free sulphide in solution. Linked to the solubility limit, are the pH and Eh of the near field, which also influence the free sulphide in solution. Several special cases that influence pH or Eh (such as H_2 production from anoxic corrosion of construction steel, presence of cement liner or the effect of pH decrease due to microbial activity) are evaluated by the reactive transport model. In none of these cases does the corrosion depth increase beyond the reference cases.

Zusammenfassung

Das gegenwärtige Referenzkonzept für die Entsorgung hochaktiver Abfälle in der Schweiz sieht Stahlbehälter vor, um abgebrannte Brennelemente sowie verglaste Abfälle aus der Wiederaufarbeitung in einem geologischen Tiefenlager zu entsorgen. Die Lagerstollen mit den eingelagerten Stahlbehältern werden mit einem geeigneten Material verfüllt, um ein diffusives Transportregime aufrechtzuerhalten und freigesetzte Radionuklide nach dem Behälterversagen zurückzuhalten. Zudem gewährleisten günstige hydrogeochemische Bedingungen eine niedrige Behälterkorrosionsrate und somit eine lange Behälterlebensdauer. Anstelle von Stahl als Behältermaterial könnte der Stahlbehälter auch mit einer Kupferbeschichtung versehen werden. Dank ihrer vernachlässigbaren Korrosionsrate in sauerstofffreiem Wasser verlängert eine solche Kupferbeschichtung die Behälterlebensdauer beträchtlich. In diesem Fall erfordert allerdings die Anwesenheit von Sulfid im Nahfeld der Behälter eine erhöhte Aufmerksamkeit, da dies ein effektives Oxidationsmittel für Kupfer darstellt. Das Ziel des vorliegenden Berichts ist daher die Untersuchung von Sulfid-Flüssen im Nahfeld in Abhängigkeit des Verfüllungsmaterials und dessen Eigenschaften. Die hydrogeochemischen Bedingungen im Nahfeld, welche grösstenteils durch das eingebrachte Verfüllungsmaterial bestimmt werden, beeinflussen die Sulfid-Flüsse. Im vorliegenden Bericht werden drei verschiedene Nahfeldtypen betrachtet: eine gut eingebaute Bentonitverfüllung (ausreichender Dichte und Homogenität), eine schlecht eingebaute Bentonitverfüllung und eine Verfüllung aus gebrochenem Opalinuston. Zur Berechnung der Sulfid-Flüsse zum Behälter werden zwei verschiedene Modelle verwendet: ein vereinfachtes Transportmodell, bei dem der diffusive Transport von mikrobiellp produziertem Sulfid zum Behälter hin modelliert wird und ein reaktives Transportmodell, bei dem die Sulfidkonzentration durch die vorherrschenden chemischen Bedingungen im Nahfeld (pH, Eh, Fe, mikrobielle Aktivität etc.) definiert wird, bevor Sulfid diffusiv zum Behälter transportiert wird. Sobald Sulfid die Behälteroberfläche erreicht, wird ein einstufiger Korrosionsmechanismus basierend auf der Stöchiometrie der vereinfachten Korrosionsreaktion angenommen. Dies bedeutet, dass die berechneten Korrosionstiefen im vorliegenden Bericht einem Mittelwert entsprechen.

Wie beide Modelle zeigen, sind die potenziellen Korrosionstiefen nach 1'000'000 Jahren beim Szenarium der gut eingebauten Bentonitverfüllung am niedrigsten (0.08 – 0.2 mm), gefolgt von den Szenarien schlecht eingebauter Bentonit (1.3 – 2 mm) und gebrochener Opalinuston (3.1 – 3.4 mm). Die niedrigeren Werte werden jeweils durch das reaktive Transportmodell, die höheren durch das vereinfachte Modell berechnet. Mithilfe des vereinfachten Modells konnte die Sensitivität des Sulfid-Flusses gegenüber verschiedenen Parametern (z.B. Sulfid-Löslichkeit, Anionen-Diffusionskoeffizient, Gehalt an oxidiertem Pyrit in der Auflockerungszone, Gipskonzentration im Bentonit) aufgezeigt werden. Es stellte sich heraus, dass die wichtigsten Parameter dabei die Sulfid-Löslichkeit und der Diffusionskoeffizient von Sulfid und Sulfat sind.

Abgesehen von der Berechnung der Sulfid-Flüsse und deren Einfluss auf die Korrosion haben die beiden Modelle auch die Bedeutung der Sulfid-Löslichkeitslimite aufgezeigt. Vorhandenes Eisen im Nahfeld (aus Goethit im Bentonit oder Siderit im Opalinuston stammend) macht die Ausfällung von FeS sehr wahrscheinlich, welches freies Sulfid in Lösung begrenzt. Direkt verbunden mit der Löslichkeitslimite sind pH und Eh im Nahfeld, die ebenfalls freies Sulfid in Lösung beeinflussen. Verschiedene Sonderfälle (wie H_2-Produktion aus der anoxischen Korrosion von für den Ausbau verwendetem Stahl, vorhandener Zementliner oder Effekt der Abnahme des pH-Werts aufgrund mikrobieller Aktivität) werden durch das reaktive Transportmodell evaluiert. In keinem dieser Fälle liegt die Korrosionstiefe höher als diejenige bei den Referenzfällen.

Résumé

Selon le concept de référence actuel pour un dépôt géologique profond destiné aux déchets et haute activité (DHA) en Suisse, les éléments combustibles usés et les déchets vitrifiés seront stockés dans des conteneurs en acier. Ceux-ci seront entourés par un matériau de remplissage visant à maintenir un mode de transport diffusif et à retenir les radionucléides relâchés suite à la perte d'intégrité des conteneurs. Par ailleurs, des conditions hydrogéochimiques favorables dans le matériau de remplissage ont pour corollaire un faible taux de corrosion de l'acier et, de ce fait, une longue durée de vie des conteneurs. Il est en outre possible d'appliquer un revêtement de cuivre sur le haut des conteneurs en acier. Du fait de son taux de corrosion négligeable dans l'eau sans oxygène, un revêtement de cuivre prolonge la durée de vie des conteneurs de manière significative. Si l'on utilise un tel revêtement, il sera nécessaire de surveiller la présence de sulfures dans le champ proche du conteneur, car ceux-ci exacerbent les phénomènes de corrosion du cuivre. Le présent rapport étudie les flux de sulfures dans le champ proche en fonction du matériau de remplissage et de ses propriétés.

Les flux de sulfures dépendent des conditions hydrogéochimiques dans le champ proche, elles-mêmes étant pour une grande part déterminées par le matériau de remplissage. Dans le présent rapport, trois types de champ proche sont postulés: un remplissage de bentonite correctement mis en place, un remplissage de bentonite mis en place de façon imparfaite et un remplissage composé d'Argile à Opalinus concassée. Afin de calculer les flux de sulfures en direction du conteneur, on a utilisé deux modèles différents: d'une part un modèle de transport simplifié où l'on modélise le transport par diffusion vers le conteneur des sulfures produites par la réduction microbienne des sulfates et, d'autre part, un modèle de transport réactif où la concentration des sulfures est déterminée par l'ensemble de l'environnement chimique du champ proche (pH, Eh, Fe, activité microbienne, …), avant que les sulfures ne soient transportés par diffusion vers le conteneur. On a posé comme hypothèse un processus de corrosion en une seule étape, basé sur la stoechiométrie de la réaction de corrosion simplifiée. Ceci signifie que les profondeurs de corrosion calculées présentées ici correspondent à une valeur moyenne.

Les deux modèles montrent que les profondeurs de corrosion potentielles après 1'000'000 ans sont les plus basses (0.08 – 0.2 mm) dans le cas d'un remplissage de bentonite correctement mis en place, suivi du remplissage de bentonite mis en place de façon imparfaite (1.3 - 2 mm) et du remplissage composé d'Argile à Opalinus concassée (3.1 – 3.4 mm). Les valeurs les plus faibles proviennent du modèle de transport réactif, les valeurs les plus hautes du modèle simplifié. A l'aide du modèle simplifié, on a pu observer la sensibilité des flux de sulfures à différents paramètres (p.ex. solubilité des sulphures, coefficient de diffusion des anions, présence de pyrite oxydée dans la zone perturbée par les excavations, concentration de gypse dans la bentonite). Les principal paramètres s'est avéré être la solubilité des sulfures, le coefficient de diffusion des sulfures et sulfates.

Outre leur rôle dans le calcul des flux de sulfures et de leur impact sur la corrosion, les modèles ont également démontré l'importance de la limite de solubilité des sulfures. Du fait de la présence de fer dans le champ proche (provenant de la goethite dans la bentonite ou de la sidérite dans l'Argile à Opalinus), la précipitation des minéraux du sulfure de fer est très probable, ce qui limitera les sulfures en solution. Le pH et l'Eh du champ proche, qui sont liés à la limite de solubilité, ont aussi un impact sur les sulfures en solution. A l'aide du modèle de transport réactif, on a étudié plusieurs cas particuliers entrainant une variation du pH ou de l'Eh (comme la production de H_2 par corrosion anoxique de l'acier utilisé pour la construction, la présence d'un revêtement de ciment ou encore l'activité microbienne entrainant une baisse de pH) (voir annexes). Dans aucun de ces cas on n'a observé de profondeurs de corrosion supérieures à celles des cas de référence.

List of frequently used parameters, symbols and units

Parameter	Symbol	Unit
Tunnel radius	r_0	m
Canister radius	r_{can}	m
EDZ thickness	$a - r_0$	m
Density of copper	ρ_c	kg/m^3
Molar weight of copper	N_c	g/mol
Formula weight of mineral	f	g/mol
Stoichiometry factors	n	-
Dry density	ρ_{hr}	kg/m^3
Hydraulic gradient	i	-
Hydraulic conductivity	K	m/s
Diffusion distance	L	m
Stoichiometry factor	n_c	-
Effective diffusion coefficient	D_e	m^2/s
Total porosity	ϵ	NA
Dry density of EDZ	ρ_{EDZ}	kg/m^3
Stoichiometry factor	n_a	-
Concentration of mineral	C	wt.-%
Flux	F	mol/m/a
Rate of copper corrosion	j_a	m/a
Amount of mineral	w	wt.-%
Mass of mineral per tunnel length	M	mol/m
Solubility limit of mineral	S	mol/m^3
Maximum rate constant	k_{max}	L/s

Table of Contents

List of Tables

List of Figures

1 Introduction

1.1 Background and aims

The Nuclear Energy Law in Switzerland requires that all types of radioactive waste are disposed of in deep geological repositories (KEG 2003). In the current concept a deep geological repository for spent fuel (SF) and high-level waste (HLW) is foreseen. One of the safety principles of a geological repository is the containment of the radioactive waste (Nagra 2002), thus the integrity of steel canisters containing SF and HLW is crucial. The choice of canister material affects its long-term integrity, but equally important are the conditions that prevail in a deep geological repository, which eventually define the lifetime of a canister. For disposal canisters made of metal, corrosion plays an important role in the definition of their lifetime. A steel canister has been Nagra's reference concept for a long time (Nagra 2002).

Of particular interest is the use of copper as a canister material as it reduces H_2 gas production and it can lead to very long canister lifetimes which will delay radionuclide release. The main chemical process that can hamper copper's longevity under disposal conditions is sulphide-enhanced corrosion. The rate and extent of corrosion depends on the availability of sulphide at the surface of the canister. As a result, the flux of sulphide towards the canister is a critical process, which depends on a number of near-field properties and biogeochemical processes occurring in the near field.

Studies on sulphide availability and transport have been reported by other waste management organisations which consider the use of copper-bearing canisters. The Swedish Nuclear Fuel and Waste Management organisation (SKB) has calculated by mass balance that a maximum corrosion depth of 0.1 mm is possible, assuming MX-80 bentonite as buffer material (SKB 2010a). A more advanced sulphide transport model including the geochemistry of the near field was used by Posiva (Wersin et al. 2014). More recently, NWMO has also developed and published a sulphide diffusion model (Briggs et al. 2016, Briggs et al. 2017a, Briggs et al. 2017b). Although a lot can be learned from other studies conducted elsewhere regarding process understanding and the impact of certain parameters on copper canister lifetime, the geological setting and country-specific design options play an important role in the assessment.

The aim of this report is to assess the sulphide fluxes in the HLW repository[1] and their impact on the corrosion of a disposal canister under different near-field scenarios reflecting design options and uncertainties, and the different transport and biogeochemical processes involved. To achieve this aim, two models are used: the first model is a diffusive transport model (including a negligibly small advective transport component) with highly simplified chemical assumptions to estimate maximum sulphide fluxes reaching the canister. The second model, which builds on more complex reactive transport conditions and was derived by Wersin et al. (2014), describes the sulphide pathways in the SF/HLW near field in a more realistic manner. In this report, a copper-coated canister is used as an example of a disposal canister. Different buffer scenarios relevant to the Swiss geological disposal concept are investigated. Although this report focuses on the transport of sulphide in the SF emplacement drifts, this assessment is also valid for the HLW emplacement drifts.

[1] The repository for high-level waste (containing separate emplacement drifts for spent fuel, vitrified and long-lived intermediate level waste) is called a *HLW repository* and should not be confused with the abbreviation for vitrified high-level waste (HLW).

1.2 Elements of the HLW repository

Repository layout and components

The current proposal is to construct horizontal emplacement drifts for SF and HLW canisters at the mid-plane of an Opalinus Clay formation at a depth of 600-900 m. The Opalinus Clay (OPA) in the geological siting regions considered has a thickness of about 100 m so that the radionuclide transport paths to the rock formations above and below is generally of the order of 50 m. Depending on the selected site, aquifers might be lying above and/or below the Opalinus Clay. The reference repository concept (Nagra 2002) foresees approximately 800 m long emplacement drifts which have an inner diameter of 2.5 m (excavated diameter 2.8 m, shotcrete tunnel liner thickness of 0.15 m) and are separated from one another by 40 m.

In view of the upcoming General Licence Application[2], Nagra is developing and evaluating a number of potential disposal canister concepts. A recent feasibility evaluation of candidate canister materials and designs indicated that a promising concept is based on a steel or cast iron supporting structure coated with copper with a thickness of 3 – 5 mm (Holdsworth et al. 2014). This concept can satisfy the canister requirement of a lifetime of 10'000 years without breach of containment. Furthermore, depending on the design, such a concept has the potential to provide significantly longer canister lifetimes. The development of the design of the copper coated canister is progressing based on the experience gained from the development of a carbon steel canister (Patel et al. 2012) and is reported in Bastid et al. (2015) and Allen et al. (2016). The SF canisters will be approximately 5 m long, have a diameter of about 1 m and a wall thickness of 0.12 m. On the other hand, disposal canisters for HLW will have a length of approximately 3 m and a diameter of about 0.7 m and a wall thickness of 0.12 m.

The use of a copper as a canister material was first explored by SKB in 1978 and has since been investigated intensively (KBS 1978, SKB 2010a, SKB 2010b, King 2013, Pedersen 2010). Other waste management organisations that are considering the use of copper in canister design include NWMO and Posiva (Keech et al. 2014, Raiko 2005, King et al. 2013, Scully & Edwards 2013, Posiva 2012). Despite its low corrosion rate, copper may react with sulphide and form a Cu sulphide corrosion product. The interaction between sulphide and Cu also produces H_2, which will lead to reducing conditions in the near field. At reducing potentials below the H_2 / H_2O stability line, Cu_2S remains stable. Hence the amount of sulphide available for corrosion at the canister surface needs to be assessed.

In the reference repository concept, canisters will be emplaced coaxially on a pedestal constructed from blocks of highly compacted bentonite, with a spacing of 3m between the individual canisters (see Fig. 1-1). The remainder of the space around the canisters will then be backfilled. Within this report, two different buffer materials are considered: MX-80 bentonite and crushed Opalinus Clay. The use of a bentonite as buffer has been investigated and tested extensively by Nagra and other waste management organisations. An alternative buffer material could be crushed Opalinus Clay; it will be available in large quantities as a result of the excavation of the emplacement drifts, which has led Nagra to also assess its use as buffer material. From an engineering point of view, using crushed Opalinus Clay is a feasible option, provided that technology is available to crush Opalinus Clay homogeneously and that the oxidation of Opalinus Clay does not cause any harm to the long-term performance of the repository.

[2] German *Rahmenbewilligungsgesuch* (RBG).

The current repository concept uses a cementitious liner, rock bolts and a steel mesh to support the walls of the emplacement drifts and access tunnels, designed to withstand the mechanical loads expected to arise during the construction and operational phases. The concept is illustrated in Fig. 1-1. The impact of clogging on transport at the cement liner – Opalinus Clay interface is not modelled in this work. The coupling between transport properties and the changing porosity at the interface is a topic of continuous research. Extensive research is being done to improve the characterisation of the cement – clay interfaces and to enable the coupling between reactive transport and porosity changes at the interface.

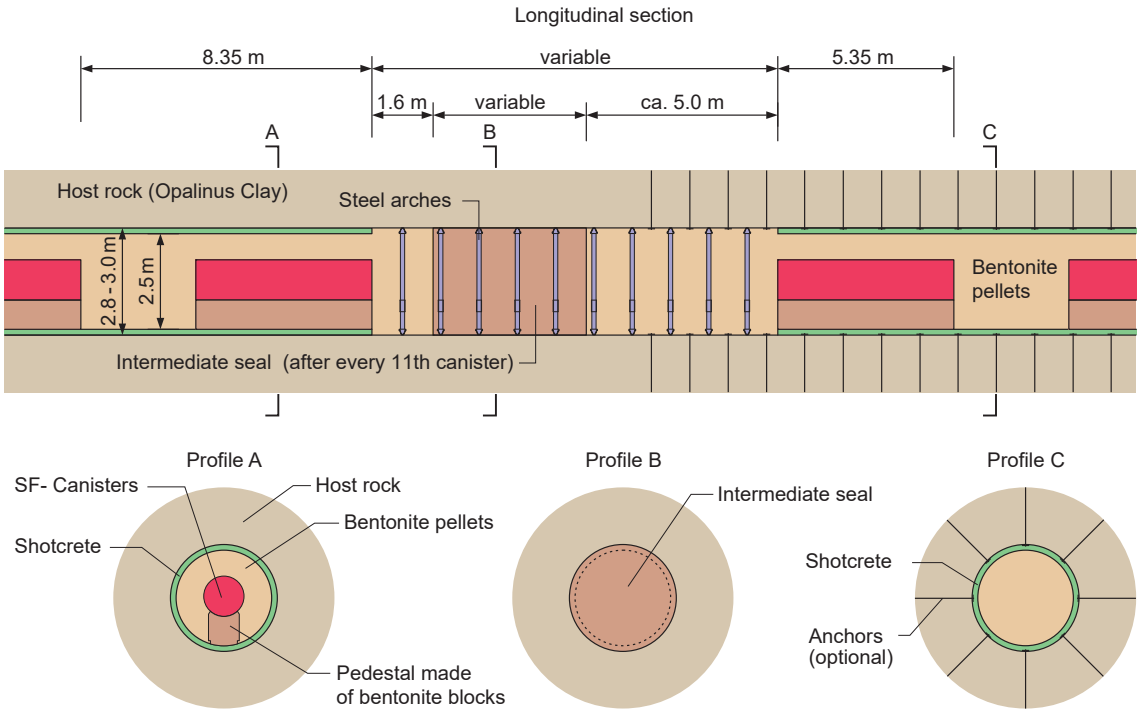

Fig. 1-1: Schematic emplacement concept for SF/HLW canisters including two different types of tunnel stabilisation (shotcrete or steel arches) (Leupin et al. 2016).

Mineralogy of host rock and buffer

Sulphide is naturally present in Opalinus Clay in the form of pyrite (FeS_2) and its concentration is 0.3 – 3.7 wt.-% (Mazurek 2011). Under anoxic and reducing conditions pyrite is very insoluble, which results in very low sulphide concentration in the porewater (< 10^{-8} M, Wersin et al. 2014). Although pyrite is stable under anoxic conditions, the construction and operational phase of the repository will bring oxygen into the emplacement drifts. During these phases, pyrite in the excavation-damaged zone (EDZ) will be partly oxidised. Vinsot et al. (2014) have clearly shown that fractures along boreholes and excavated tunnels in the Bure URL contained oxidised pyrite. The observed oxidised features show that pyrite is transformed into sulphate, which locally reduces pH, dissolves calcite and leads to the precipitation of gypsum. As the age of the boreholes or excavated tunnels increased, oxidised features at greater depths were observed. Within the EDZ, pore space is temporarily larger than in the undisturbed Opalinus Clay due to the excavation of the emplacement drift. This available pore space could enable micro-organisms to reduce the available sulphate to sulphide, which in turn can be transported to the canister surface. As saturation of the near-field progresses, many of the cracks that have been formed in the EDZ will self-

seal and prevent further propagation of an oxidation front. The remaining undisturbed host rock will largely remain in its pristine conditions where no sulphide-sulphate transformations will take place. Based on isotopic records from drillcores of Opalinus Clay (Switzerland) and Callovo-Oxfordian Clay (France), it can be shown that pyrite was formed during the early Jurassic by microbial sulphate reduction in a closed system (Lerouge et al. 2014, Lerouge et al. 2011). As sedimentation increased, the sulphate inventory was depleted and porosity was reduced, bacterial reduction of sulphate came to a halt. Other minor sulphide minerals such as galena and sphalerite were formed after the formation of Fe-rich calcite and siderite. It is suggested that the current day sulphate concentrations in Opalinus Clay in Mont Terri rock laboratory (celestite infillings) originate from an external influx of marine water, which was additionally enriched through evaporation, after the diagenesis of sulphides (Mazurek & Haller 2017).

The sulphate inventory in the host rock minerals may indirectly contribute to sulphide-enhanced Cu-corrosion when sulphate-reducing bacteria are present in the EDZ. The main sulphate-containing mineral in Opalinus Clay is celestite ($SrSO_4$), which can be found in very low concentrations of 0.02 – 0.06 wt.-% (Wersin et al. 2013). In the EDZ, which is estimated to be 0.7 m thick, sulphate-reducing bacteria can encounter suitable conditions to reduce sulphate to sulphide. To achieve this, they need sufficient space, nutrients, water activity, and an electron donor (see Section 2.3). This means that, in the EDZ, sulphate constrained by celestite solubility can potentially be reduced to sulphide when conditions are suitable for microbial activity.

The buffer has a dual impact on sulphide concentrations in the near field. On the one hand, the buffer mineralogy defines the inventory of sulphate in the near field and on the other hand the density and swelling pressure of the buffer determine whether or not sulphate can be reduced to sulphide through microbial activity. As with Opalinus Clay, low concentrations of pyrite are present in bentonite (0.4 – 0.6 wt.-%; Karnland 2010), but also these are very stable under anoxic conditions and result in low concentrations of dissolved sulphide ($< 10^{-8}$ M). Bentonite contains sulphate minerals; in the case of Wyoming bentonite there is 0.5 – 0.9 wt.-% gypsum ($CaSO_4$) present (Karnland 2010).

In addition to the sources/production of sulphide, this report also considers the possible consumption and transport mechanisms for sulphide. Sulphide which is formed in the EDZ and/or within the buffer, depending on the chosen buffer material, can react with Fe-rich corrosion products (in case there are steel bolts or meshes present in the near field) such as magnetite, goethite and siderite, as well as with minerals naturally present in the Opalinus Clay and bentonite (Fe(III) oxides, siderite, ankerite) and form insoluble mackinawite or pyrite or even precipitate as elemental sulphur (S(0)). These mechanisms reduce the dissolved sulphide concentration in the buffer/EDZ.

Initial state and uncertainties

After emplacement of the HLW and SF canisters in the emplacement drifts, the drifts are backfilled with clay material. Anoxic conditions in the near field are expected to prevail after closure of the repository, once all entrapped oxygen that had entered the repository during construction and operations is consumed (Diomidis 2014). Because the corrosion rate of copper in oxygen-free water is extremely low (Ottosson et al. 2016), the longevity of a canister can be prolonged by adding a copper coating. In the assessment of the sulphide fluxes towards the canister, the initial state considered is the fully saturated near field, in which transport is dominated by diffusion and reducing conditions prevail. Nevertheless, some uncertainties related to the design and evolution of the repository remain. The most relevant ones are explicitly addressed in this report and listed hereafter.

The first uncertainty dealt with in this report is the emplacement density. As the emplacement density of the backfill materials plays an important role in limiting microbial activity, it is important to define the required density. Tests of emplacing granular bentonite around a canister have taken place at full scale using presently available technologies (Müller et al. 2017). In the future, other technologies might possibly achieve other (higher) values; the exact emplacement density of bentonite is therefore somewhat uncertain. The uncertainty in this value is taken into account in the sensitivity analysis carried out in this report.

An alternative option for the backfill material is looked at in this report. Although the commonly used reference material for backfilling is MX-80 bentonite, an alternative scenario with crushed Opalinus Clay is calculated as well in this report to assess the impact of a different material on the sulphide flux towards the canister.

Both Opalinus Clay and bentonite contain few sulphide- and sulphate-containing minerals. The sulphate released from the latter can be converted by micro-organisms to sulphide. Depending on the buffer material and microbial activity, sulphide may be locally present in the SF/HLW near field and be transported to the copper-coated canister. If the emplacement density of the buffer material is low, microbial activity in the buffer material may become possible. This report assesses the transport and fate of sulphide in the SF/HLW near field, given different buffer scenarios (varying emplacement density and buffer material). The corresponding copper corrosion depths will be calculated to evaluate the required thickness of the copper coating.

1.3 Methodology

Based on the current Nagra concept, three different scenarios are assessed in this report: a scenario with a well-emplaced MX-80 bentonite backfill, a scenario with a reduced bentonite density and a scenario with a backfill consisting of crushed Opalinus Clay. In order to evaluate the impact of sulphide fluxes on copper corrosion in these three scenarios two different models are used: a simplified model and a reactive transport model.

The simplified model assumes diffusive transport of sulphide from its place of origin towards the canister, where it reacts immediately with the copper. For any given time, the simplified model solves the diffusion equation for quasi-steady-state conditions; the model is time-dependent because the boundary conditions vary. The processes responsible for sulphide production (e.g. microbiology and mineral dissolution) are controlled by the inventory of minerals in the near field.

However, this model does not take into account any reactivity between the transported sulphide and its chemical environment (buffer material). As a result, the simplified model provides an upper bound of the sulphide flux and the corresponding corrosion depth. The advantage of the simplified model is that, because the calculations are much faster, sensitivity analyses can readily be performed. Processes or parameters with larger uncertainties are varied between the expected upper and lower values.

A more complete process understanding and an increased realism is offered by the reactive transport model, where sulphide concentrations in solution are constrained by solid phases present in the near field. In contrast to the simplified model which solves the diffusion equation for steady state conditions, the reactive transport model solves the transient diffusion equation. Which solid phase limits the sulphide solubility depends on the pH and Eh of the geochemical system. Because iron sulphide precipitation plays an important role in limiting the sulphide in solution, Fe-containing minerals play an important role in the reactive transport model.

Whereas the simplified model over-estimates sulphide fluxes to the canister and thus copper corrosion due to the assumption of steady-state concentration profiles, the reactive transport model explicitly calculates the transient concentration profiles, as a result of which sulphide fluxes to the canister increase more gradually.

1.4 Structure of report

In this report the sulphide fluxes and the resulting corrosion depths for three different backfill scenarios, calculated by using two different transport models are compared.

In Chapter 2, the relevant (bio)geochemical processes that are taken into account in the reactive transport models are explained in more detail.

Different buffer materials and/or emplacement densities are considered and calculated to assess the sulphide fluxes under different scenarios. The setup of these scenarios and the assumptions made are described in Chapter 3. Also included in Chapter 3 is a list of the common parameters that were shared between both models.

The two models (simplified and reactive transport) used in this report to estimate the sulphide fluxes in the SF/HLW near field are described in Chapter 4.

In the following three chapters (Chapters 5 – 7) the three scenarios that were defined in Chapter 3 are addressed by both models. The results of the simplified and reactive transport models are presented and compared with each other.

The final discussion and conclusions on the sulphide fluxes in the SF/HLW near field can be found in Chapter 8.

In Appendix A a more in-depth description is given of how the diffusive and advective fluxes were calculated in the simplified model. An additional calculation case exploring the effect of a high pH shotcrete liner is presented in Appendix B. In Appendices C and D, respectively, an assessment of the effect of hydrogen production on corrosion and an assessment of a reduced pH due to microbial activity on sulphide stability can be found.

2 Considered processes in the HLW repository

In the HLW repository many different processes will take place; dependening on hydraulic conditions, temperature, chemistry or rock mechanics. A comprehensive overview of these relevant processes taking place within the HLW repository has been described by Leupin et al. (2016). Among the (bio)geochemical processes in the HLW repository, several processes are in one way or another linked to the sulphide fluxes in the near field. These processes are described in more detail in this chapter. A thorough understanding of these processes is necessary if meaningful modelling of the sulphide fluxes is to be carried out. The reason for this is that most of the processes require a level of abstraction before they can be used in the transport models. Besides sulphide-assisted corrosion and microbial activity, the solubility and geochemical controls of the sulphide concentration are discussed in the paragraphs below. The transport processes (diffusion and advection) that are modelled are briefly described as well. For the modelling in this report, isothermal conditions are assumed. This simplification has its justification, as the transport of species will mainly take place once the saturation of the near field has started (which can only happens when the temperature pulse has passed).

2.1 Microbial processes

Microbial activity in the buffer or in the EDZ depends on the availability of sufficient *pore space, nutrients* (micro- and macronutrients, electron acceptors and electron donors) and *water activity*. If one of these conditions fails; microbial activity will come to a halt. During the transient phase, when the buffer is not yet fully saturated, water activity will be too low close to the canister to sustain microbial activity. Conditions in the EDZ, however, might be suitable for microbial activity, since in the EDZ water activity, pore space and nutrients will be available. As soon as the buffer is saturated and given that the buffer is emplaced with a sufficiently high emplacement density (and the volume remains constant), the swelling pressure will reduce the pore size and thus eliminate microbial activity. The emplacement density and the resulting swelling pressure in the buffer thus play a crucial role in preventing microbial activity close to the canister (Masurat et al. 2010, Pedersen 2010). Masurat demonstrated that as the wet density of compacted bentonite increases from 1500 kg/m^3 to 2000 kg/m^3 (corresponding to swelling pressures of 0.1 MPa and 7.8 MPa), the production of sulphide decreases (Masurat et al. 2010). The mineralogy of the buffer material and especially the clay content also has an impact on the obtained swelling pressure. A buffer made of crushed Opalinus Clay, having a lower percentage of swelling clay minerals than bentonite, will naturally obtain a much lower swelling pressure. In addition, the bentonite buffer is likely to be more homogeneous than a crushed Opalinus Clay buffer, which means that the conditions (e.g. swelling pressure) around the canister will be less prone to fluctuations.

An important group of micro-organisms that is of relevance to the sulphide flux in the SF/HLW near field are the sulphate-reducing bacteria (SRB). These micro-organisms use sulphate as an electron acceptor, and use dissolved organic matter (e.g. lactate, pyruvate, acetate) or hydrogen gas as an electron donor. The latter will be available in large quantities in the repository, coming from the anoxic corrosion of steel components such as rock bolts and steel mesh. As a result of the sulphate reduction that is carried out by SRB, sulphide is produced (see Eq. 2-1 for an example with H_2 as electron donor). The fact that SRB are present in Opalinus Clay porewater has been demonstrated at the Mont Terri rock laboratory (e.g. Stroes-Gascoyne et al. 2011, Bagnoud et al. 2016). Through metagenomics the activity of the sulphate-reducing metabolism could be demonstrated.

$$SO_4^{2-}(aq) + 4H_2(aq) + H^+(aq) \rightarrow HS^-(aq) + 4H_2O \qquad (2\text{-}1)$$

Besides the SRB, the formation of biofilms is also of importance to the corrosion of the canister. Biofilms are assemblages of microbial cells that are attached to a surface and enclosed in an extracellular matrix that is secreted by the micro-organisms themselves. Owing to the extracellular matrix, the micro-organisms are protected against detachment and the biofilm becomes very resilient. Biofilms tend to occlude the surface and promote the development of an environment which is different from the bulk and which can result in localised corrosion. Copper alloys are generally considered to be resistant to biofilms since copper has a broad spectrum of antimicrobial activity (Grass et al. 2011, Sato et al. 2012). Nevertheless, it has been reported that SRB can form a biofilm on copper surfaces in anoxic conditions and this can result in the acceleration of corrosion (Chen et al. 2014). Because the impact and outcome of biofilm formation is uncertain and difficult to predict (King 2009), biofilm formation should be prevented from forming in the first place. This is achieved by the high temperature, desiccation, and radiation field during the early stages of repository evolution, and by the insufficient pore space, low water activity and swelling pressure of the buffer during the later stages.

Availability of electron acceptors

Dissolved sulphate is the electron acceptor required by SRB for microbial sulphate reduction. In the near field of the repository two main sources of sulphate can be distinguished: gypsum (in the MX-80 buffer) and celestite (in the Opalinus Clay). Thanks to fairly reliable thermodynamic data on gypsum and celestite, the initial concentration of sulphate in the porewater near the repository can be constrained with reasonable confidence. The initial sulphate concentration in the MX-80 buffer due to gypsum equilibrium is expected to be roughly ten times higher (ca. 10^{-1} mol/L) compared to the initial sulphate concentration in the Opalinus Clay due to celestite equilibrium (ca. 10^{-2} mol/L) (see Tab. 5-4). However, the total volume of the MX-80 buffer is small compared with the volume of the Opalinus Clay. Therefore, it is expected that, if the microbial reaction is allowed to proceed for a sufficiently long time at a sufficiently high rate, all gypsum in the buffer will be completely consumed. Following this, celestite contained in the Opalinus Clay will remain the sole source of sulphate for microbial activity.

Availability of electron donors

Various chemical species could serve as electron donor for microbial sulphate reduction, including reactive organic carbon (from dissolution of solid organic matter), methane and higher alkanes or hydrogen gas.

Opalinus Clay contains 0.6 wt.-% of solid organic matter (SOM), which translates into 14.7 kg/m^3 rock (or 1'225 mol/m^3 assuming molar mass of pure carbon, 12 g/mol; see Tab. 5-4). MX-80 contains about 0.1 wt.-% of SOM, which equals 1.45 kg/m^3 or 120.8 mol/m^3 (making the same assumption about molar mass; Tab. 5-4). This is much more (especially in the Opalinus Clay) than the total inventories of sulphate (see below).

The solid organic matter in bentonite is, generally speaking, recalcitrant, because it has persisted in this natural material for a long time period. A recent study by Marshall et al. (2015) investigated solid organic matter in several bentonites and concluded that the SOM shows signs of advanced diagenesis and appears to be geochemically recalcitrant and, therefore, unlikely to serve as a microbial substrate. However, when exposed to repository conditions, this SOM might become more reactive. For example, it was observed that heating and irradiation of bentonite-based buffer materials followed by leaching in distilled water stimulated microbial growth in granitic groundwaters by up to two orders of magnitude (Stroes-Gascoyne et al. 1997). In the long run, dissolution

processes of SOM in the compacted buffer are expected to be small as long as microbial activity is restricted. Thus the amount of reactive carbon and dissolved organic carbon concentration in the porewater are expected to be low, but these concentrations are so far not well constrained.

The organic matter in Opalinus Clay consists predominantly of kerogen, a fossilised macromolecular insoluble form of organic matter derived from biomass. Regarding its maturation degree it can be considered as fairly immature but close to the onset of the oil window (Elie & Mazurek 2008). The dissolved organic fraction is fairly low, a few mg C/L. Courdouan et al. (2007) studied the dissolved organic matter (DOM) in Opalinus Clay and confirmed that only a small fraction (< 0.4 %) of the total organic C was extractable in synthetic Opalinus Clay porewater. The concentrations in the anoxic extracts were found to be in the range 4 – 8 mg/L. About 2/3 of this DOM exhibited hydrophilic properties and molecular sizes < 500 Dalton.

Natural methane concentrations in Opalinus Clay determined at the Mont Terri Rock Laboratory are about 0.3 mmol/L and that of higher alkanes at least a factor of 10 lower (Vinsot et al. 2017). From the available experimental observations at Mont Terri (e.g. PC and BN experiments), there are no indications that alkanes play a role as electron donors in the microbial sulphate reduction process (Wersin et al. 2011, Stroes-Gascoyne et al. 2011). Thus anaerobic methane oxidation has so far never been observed in Opalinus Clay. Hydrogen, on the other hand, strongly impacts sulphate reduction when injected into the rock (Vinsot et al. 2014). The natural levels of this species, however, are very low, usually below detection limits (Vinsot et al. 2017). Corrosion of steel materials in the EDZ may produce higher H_2 levels, which could then be utilised by SRB provided that sufficient pore space is available.

2.2 Geochemical control of sulphide concentration in the EDZ

It has been long recognised that in aqueous solutions at ambient temperature and in the presence of Fe(II), sulphide reacts rapidly to produce a brownish black iron(II) monosulphide (Rickard & Luther 2007). This precipitate was identified by Rickard and collaborators (Rickard 2006) to be the tetragonal nano-particulate mackinawite characterised by the stoichiometric formula $Fe_{1.00 \pm 0.01}S$. A recent study by Csákberényi-Malasics et al. (2012) indicates that while under "tightly controlled anoxic conditions" the precipitate was nano-crystalline mackinawite, under sufficient oxygen access the precipitated iron sulphide could be defined as "X-ray amorphous", FeS(am), with no known structure. Nevertheless, conversion of FeS(am) to a mixture of mackinawite and greigite in aqueous solutions at ambient temperature is reported (Csákberényi-Malasics et al. 2012) to be rapid (complete within ca. 10 months).

Greigite (Fe_3S_4) is a tetrahedral and octahedral mixed Fe(II)Fe(III) sulphide that forms from mackinawite and can convert to pyrite, and is a fairly widespread mineral associated particularly with fresh water systems (Rickard & Luther 2007). Owing to their similar structures, mackinawite can transform into greigite via a solid-state mechanism (Hunger & Benning 2007), the reaction strongly depending on geochemical conditions (especially on pH and polysulphide concentration).

Pyrite (FeS_2) is the most common sulphide mineral in natural environments. It has a cubic NaCl-type structure with alternating S_2^{2-} groups and Fe atoms. The composition of pyrite is close to stoichiometric (Fe/S = 0.5). Rickard & Luther 1997) postulated two pathways for pyrite formation with either mackinawite or greigite as reactant. Due to its differing structure from mackinawite and greigite, transformation of mackinawite and greigite to pyrite occurs via a dissolution/ precipitation process rather than a solid-state process.

The relations between the different iron sulphide minerals are schematically shown in Fig. 2-1.

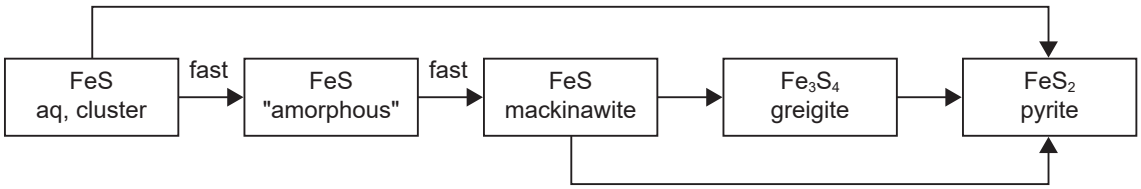

Fig. 2-1: Schematic representation of the formation of iron sulphide minerals.

Other iron sulphide minerals, including for example troilite (FeS), pyrrhotite ($Fe_{1-x}S$) and marcasite (FeS_2) are usually formed at higher temperature and are much less common in low temperature environments.

From the point of view of the sulphide modelling, the important differences between FeS(am), mackinawite, greigite and pyrite are the mineral solubilities and kinetics of dissolution/ precipitation reactions. The reported solubility data for solid FeS are quite variable, which appears to be related to experimental difficulties on the one hand, and to variations in crystallinity and/or grain size of the tested FeS samples on the other (e.g. Davison 1991, Rickard & Luther 2007). Selected data on apparent FeS(am) and mackinawite solubility are shown in Tab. 2-1. The solubility of greigite is rather poorly known. This is related to the experimental difficulty of synthesising a pure phase and maintaining this condition during the tests. The solubility of pyrite is very low and thus virtually impossible to measure experimentally (Tab. 2-1). The formation of pyrite has been shown experimentally to require a high degree of supersaturation. Thus, Harmandas et al. 1998) determined a saturation index of almost 14 at pH 7 in the presence of pyrite seeds before pyrite nucleation started. The supersaturation limit in the presence of organic substrates found by Rickard et al. (2001) was somewhat lower (SI ca. 11), but still remarkably high. The saturation index of pyrite is a strong function of redox, as noted e.g. by Rickard & Morse 2005). Thus, over a very small redox range the saturation degree varies by several orders of magnitude. This is of particular relevance at the low Eh side, where pyrite stability decreases in favour of FeS. The stability of pyrite and FeS (as mackinawite) is illustrated in the pe – pH diagram in Fig. 2-2. The stability of FeS increases both at lower Eh and higher pH.

Overall, the solubility of the different iron sulphide minerals varies by many orders of magnitude (shown in Tab. 2-1), following the solubility trend: pyrite << greigite << mackinawite < FeS(am). This is illustrated in Fig. 2-3 by the greater field of pyrite stability under conditions expected to be approximately representative of the EDZ porewater affected by microbial activity (pH ca. 6.5 to 7.5, and pe ca. -4 to -2) and assuming total Fe and S(-II) concentrations of 5×10^{-5} M and total carbonate concentration of 10^{-2} M. Specifically, pyrite has greater stability than mackinawite under more acidic and less reducing conditions.

Tab. 2-1: Apparent solubility constants ($logK^0$) for selected iron sulphides (based on Wersin et al. 2014).

Mineral	**$logK^0$**	**Reference**	**Database**	**Comments**
FeS(am)	-2.95	Davison (1991)	Thermochimie	
	-3.00	Davison et al. (1999)		at 20° C
	-3.92	Berner (1967)	MINTEQ, PHREEQC	
Mackinawite	-3.60	Davison (1991)	Thermochimie	
	-3.83	Benning et al. (2000)		at 25° C
	-3.48	Rickard (2006)		at 23° C
	-4.65	Berner (1967)	MINTEQ, PHREEQC	
Greigite	-12.84	Rickard & Luther (2007)		Recalculated from Berner (1967)
Pyrite	-15.79	Davison (1991)	Thermochimie	Based on compilation Bard et al. (1985)
	-18.50	Hummel et al. (2002)	Nagra/PSI	
	-18.48	Robie & Waldbaum (1968)	MINTEQ, PHREEQC	

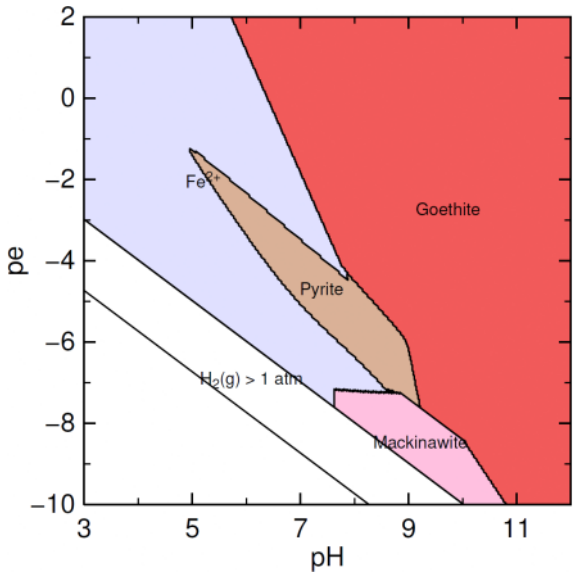

Fig. 2-2: pe – pH diagram of the Fe-S-H_2O system (Fe(II)tot = S(-II)tot = 10^{-5} M) at 25° C and I = 0.1 M showing the stability of pyrite and FeS (as mackinawite).

Calculated with PhreePlot (http://www.phreeplot.org/) using the Thermochimie v.9b thermodynamic database (https://www.thermochimie-tdb.com/).

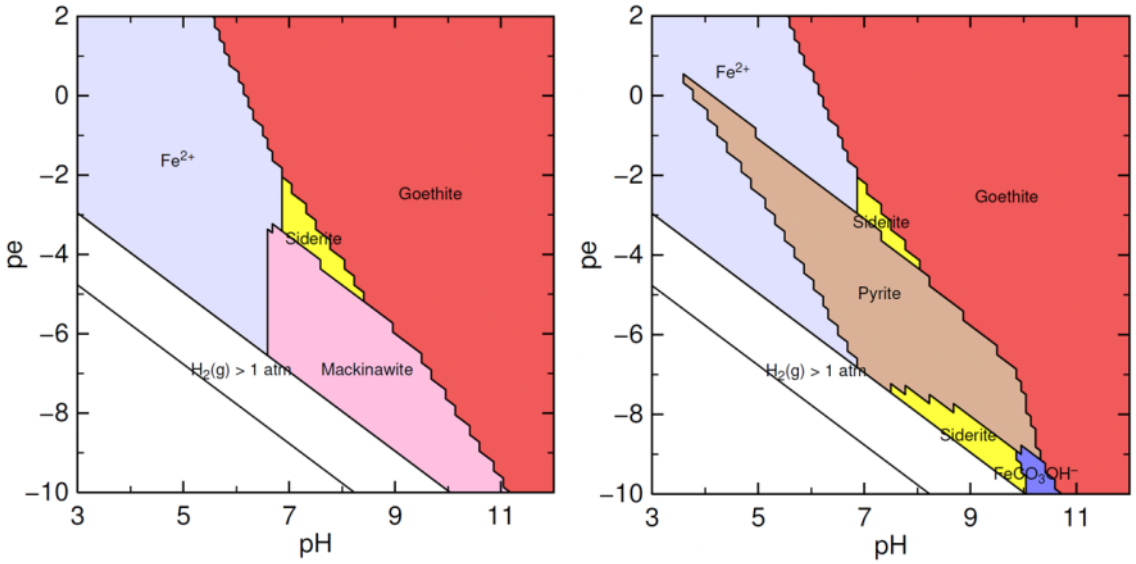

Fig. 2-3: pe – pH diagram of the Fe-S-C-H_2O system (Fe(II)tot = S(-II)tot = 5×10^{-5} M and C(IV)tot = 10^{-2} M) and I = 0.1 M at 25° C comparing the stability of mackinawite (left) and pyrite (right).

Calculated with PhreePlot (http://www.phreeplot.org/) using the Thermochimie v.9b thermodynamic database (https://www.thermochimie-tdb.com/).

In general, the precipitation of mackinawite is fast (Benning et al. 2000). Rickard showed that the mechanism of mackinawite precipitation involves two competing reactions involving aqueous H_2S and HS^-. Kinetics of both reactions are limited by the exchange between water molecules in hexaqua iron(II) sulfide outer sphere complexes. For the precipitation reaction:

$$Fe^{2+} + H_2S \rightarrow FeS + 2H^+ \qquad (2\text{-}2)$$

Rickard & Luther (1997) derived the rate law:

$$R_{FeS}(m) = \delta cFeS/\delta t = k_1(a_{Fe2+} \cdot a_{H2S}) \qquad (2\text{-}3)$$

where a_{Fe2+} and a_{H2S} are the activities of these species in mol/L and k_1 is the rate constant with $k_1 = 7 \pm 1$ mol/(L s). To illustrate, assuming Fe and S(-II) activities at 10^{-4} and 10^{-5} mol/L, respectively, mackinawite precipitation rate is 7×10^{-9} mol/(L·s) or 0.22 mol/(L·year).

The formation kinetics of greigite is not well known. The transformation of mackinawite to greigite occurs under a variety of conditions, but is favoured at higher temperature and lower pH (Rickard & Luther 2007).

Pyrite precipitation frequently proceeds via prior formation of mackinawite, a reaction that has been extensively studied. Considering together the two pyrite formation pathways (polysulphide and H_2S) gives the overall kinetic rate formulation (Rickard & Morse 2005):

$$R_{FeS2} = \delta cFeS_2/\delta t = k\ H_2S[FeS(m)][H_2S] + [FeS]^2[S_0][H^+] \qquad (2\text{-}4)$$

As noted by Rickard & Luther (2007), pyrite formation depends entirely on the concentrations of mackinawite and H_2S in cases where S(0) is very small. They estimated typical formation rates in marine sediments 10^{-8} – 10^{-3} mol/(L year) or 3×10^{-10} – 3×10^{-5} mol/(g dry sediment year).

The above rate equation is difficult to apply because it requires knowledge of both FeS and S(0) concentrations which are usually not known. It is also only valid for abiotic reaction rates. However, it is well known that microorganisms can have a catalytic effect and increase pyrite precipitation by several orders of magnitude. Canfield et al. (1998) showed that various sulphur-disproportionating bacterial cultures enhanced pyrite formation by a factor of 10^4 to 10^5 relative to inorganic formation reactions. Pyrite in those experiments formed both by the addition of elemental sulphur and H_2S to natural surface sediments. Transformation of FeS to FeS_2 in the presence of in vitro enrichment cultures was shown to occur rapidly by Donald & Southam (1999). Transformation rates were rapid, with more than 80 % of FeS transformed to FeS_2 after 10 days. Part of the sulphur incorporated in the pyrite crystals stemmed from the bacterial cells as indicated from isotopic analysis.

This section clearly shows that sulphide solubility might be controlled by various phases, which all have associated uncertainties. Moreover, the solubility controlling phase is highly dependent on the pH and Eh of the system. These parameters can be estimated, but their exact values might slightly change over the course of the near-field evolution. The modelling cases that are presented in this report investigate this uncertainty by assessing a range of solubility limits from 0.1 M to 10^{-5} M. Nevertheless, the fact that the solubility of sulphide in solution is limited by sulphide-minerals is considered as plausible and considered as a reference condition in the calculation cases. The hypothetical case of no-solubility limit for sulphide is presented to illustrate the difference with more realistic cases with a solubility limit.

2.3 Sulphide-assisted copper corrosion

The sulphide-assisted corrosion of copper under disposal conditions follows a complex mechanism that involves several reactions (King 2013) and has been studied and reviewed extensively by a number of national disposal programmes (Scully & Edwards 2013, Macdonald et al. 2014, King et al. 2012). Electrochemical studies have shown that Cu oxidises in the presence of sulphide. The conceptual model used in this report considers that copper corrosion is proportional to sulphide fluxes to the canister and follows the simplified reaction:

$$2Cu(s) + HS^-(aq) + H^+(aq) \rightleftharpoons Cu_2S(s) + H_2(aq) \quad (2\text{-}5)$$

Because a mechanistic description of the sulphide-enhanced corrosion of copper is beyond the scope of this report, a simplified copper corrosion mechanism is considered, based on the following assumptions:

- Sulphide is the main corrosive species (polysulphide and thiosulphate being neglected as corrosive species).
- Corrosion follows reaction in Eq. 2-5 which is assumed to be instantaneous and thus the overall rate of corrosion is mass transport dependent.
- Copper does not take part in any other reactions or interact with any other species, e.g. Cl^-, apart from the above mentioned reaction with HS^-.
- The formation of solid corrosion products and their potential protective effects are disregarded.
- Potential localised phenomena, such as pitting, are disregarded and uniform corrosion is assumed.
- The canister is assumed to be made of pure copper and any differences in composition, microstructure or other properties with the copper coatings are disregarded.

One should thus bear in mind that in this report the mentioned corrosion depths are only calculated on a mass-balance principle and do not reflect necessarily actual corrosion depths. The calculated corrosion depths in this report only serve as a proxy for the impact of sulphide flux on Cu-coated canisters and provide a simple way to visualise the extent of corrosion damage to be expected in each case. This approach is well-established and used by other modelling teams dealing with the corrosion of Cu by sulphide fluxes (Wersin et al. 2014, King et al. 2008).

However, in the reaction transport model the above reaction is not implemented explicitly, but rather its effect is mimicked by a fast kinetic reaction converting sulphide to a "dummy" species within an outer "reactive layer" of the canister compartment (whereby sulphide is maintained at a low concentration as might be expected due to chalcocite precipitation). The total mass of this "dummy" species within the model domain is monitored during the calculation and, with the help of stoichiometry of the reaction product (two moles of copper consumed per one mole of sulphide to form one mole of chalcocite), is used to evaluate the number of moles of copper consumed by the sulphide. To recast the number of moles of copper consumed into a corrosion depth, a slab-like geometry of the canister is assumed with corrosion proceeding from one side. The effect of hydrogen production due to copper corrosion is ignored (evolved hydrogen is decoupled from the redox system).

2.4 Transport processes

Once the repository is saturated, dissolved species can migrate through the pore spaces external to the canisters by molecular diffusion and, if water flow occurs, by advection. Diffusive transport is expected to dominate in a bentonite buffer, because of its low hydraulic conductivity. Buffer erosion is not expected to occur, as the Opalinus Clay host rock is a non-fractured porous medium. On the other hand, even if the bentonite buffer has a lower emplaced density, or if a more conductive buffer material is used (see Chapter 3, scenarios B and C), diffusion is still expected to dominate in the buffer because of the low hydraulic conductivity of the surrounding Opalinus Clay host rock and potentially also because of the higher conductivity of the EDZ, which may produce a hydraulic cage effect, diverting any (limited) flow from the rock around the repository emplacement tunnels. In the Opalinus Clay, advection may also contribute to solute transport, although diffusion is expected to be the more dominant process because of the low hydraulic conductivity of the rock. Relatively permeable formations (aquifers) lie beneath and above the host rock. The hydraulic head differs between these aquifers, resulting in a broadly vertical groundwater flow.

3 Scenarios and common parameters

Sulphide transport through the buffer towards the canister depends on several processes (e.g. dissolution and precipitation of minerals, microbial activity) and parameters (e.g. backfilling conditions, sulphate mineral inventory, and diffusion coefficient) that are described in the previous chapter (Chapter 2). In order to assess the ability of the buffer to limit corrosion of the copper-coating, three different backfilling scenarios are selected. Each scenario is described in the following sections. The set of commonly used spatial parameters is given in section 3.4.

3.1 Scenario A: well-emplaced bentonite buffer

Description

This scenario represents the near field in the current reference design of the HLW repository (Fig. 3-1). In this scenario, the bentonite buffer is well-emplaced; reaching a high emplacement density that leads to a high swelling pressure and a low free pore space. It is assumed that in this buffer no microbial activity can take place. The only reactive zone in this scenario is the EDZ, where sulphate may be reduced to sulphide by micro-organisms. The EDZ is characterised by small cracks which enlarge the free pore space for the micro-organisms to be active. A shotcrete liner provides support of the cavern during the operational phase.

The main source of sulphate is celestite in the host rock and gypsum in the bentonite. The transport of sulphide from the EDZ towards the canister through the buffer is dominated by diffusion.

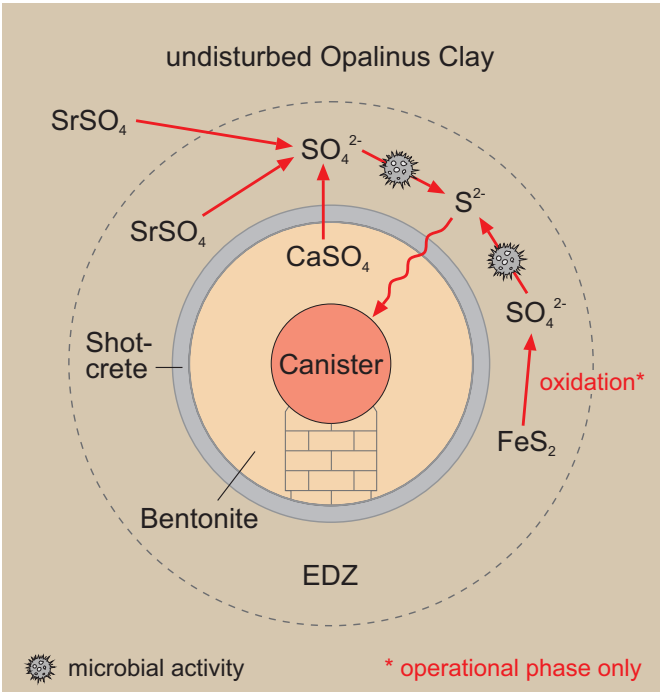

Fig. 3-1: Schematic overview of SF/HLW near field in case of a well-emplaced bentonite buffer.

Abstraction of processes

Both the simplified and reactive transport models estimate the sulphide fluxes in a single emplacement drift with a single canister. The presence of the shotcrete liner is not explicitly modelled. The latter assumption is conservative, as a concrete environment would lead to sulphide precipitation (lower solubility of sulphide at high pH). A dedicated calculation case of the reactive transport model illustrates the impact of a shotcrete liner (see Appendix B). The presence of tunnel support elements made of steel (rock bolts, mesh) is also neglected in the reference case. These elements corrode and produce H_2, which can be used as electron donor by micro-organisms. Ignoring the impact of the tunnel support elements is conservative, as will be illustrated in a dedicated calculation case (Appendix C). The buffer is assumed to be fully saturated and homogenised, thus the period leading to saturation is neglected.

The conceptual basis of the simplified model is that aqueous sulphate ions from minerals present in the repository near field and/or geosphere may be reduced to sulphide ions in regions where sulphate-reducing bacteria are active, which then migrate to the canister surface and cause corrosion. Dissolution of sulphate minerals is fast. In scenario A, the only region where sulphate-reducing bacteria are active is the EDZ around the emplacement drift. No microbial activity can take place within the buffer. The presence of an electron donor (e.g. dissolved organic matter or hydrogen) for microbial activity is not specified (except in the calculation variant in Appendix C) and assumed to be unlimited. It is also assumed that the microbial population remains present and active in the EDZ.

3.2 Scenario B: bentonite buffer with reduced density

Description

The HLW repository is identical to scenario A regarding geometry and choice of materials (shotcrete liner, rock bolts, bentonite buffer) (see Fig. 3-2). Should the emplacement of the bentonite buffer not achieve the targeted values, due to, for example, outbreaks of the shotcrete liner or an inferior bentonite emplacement quality, the swelling pressure might be insufficient and microbial activity could occur. In this case, the buffer and the EDZ would constitute reactive zones in which microbial reduction of sulphate to sulphide may take place[3]. The transport of sulphide and sulphate in the buffer is, however, still dominated by diffusion, due to the low hydraulic conductivity of the surrounding rock.

[3] As a result of a lower swelling pressure in the buffer, it cannot be excluded that biofilms are formed on the canister surface. Modelling biofilm formation and its impact of corrosion is, however, beyond the scope of this report, as a solid conceptual model for biofilm formation is currently unavailable.

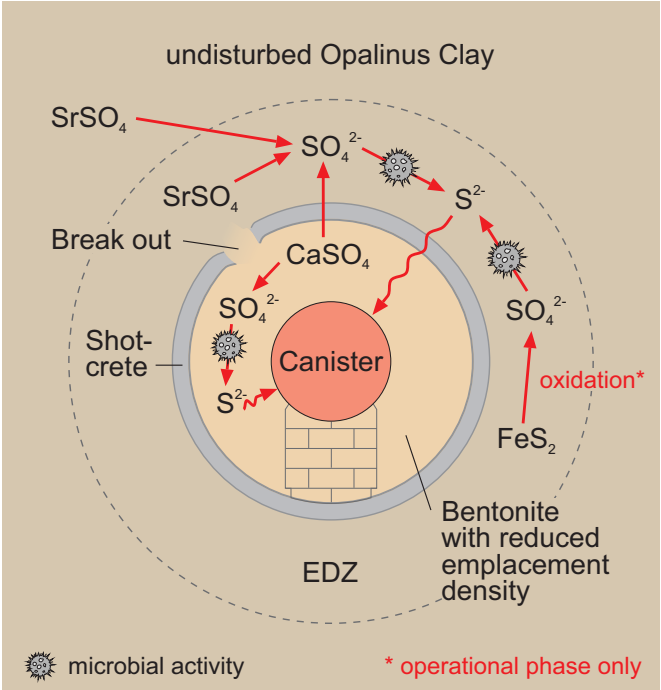

Fig. 3-2: Schematic overview of SF/HLW near field in case of a bentonite buffer with reduced density.

Abstraction of processes

In this scenario, the same assumptions and abstractions are made as in scenario A, with the exception that in scenario B, microbial activity can also take place within the bentonite buffer. This means that the reactive zone is no longer limited to the EDZ, but sulphate reduction may now also take place in the bentonite with reduced density.

3.3 Scenario C: crushed Opalinus Clay buffer

Description

The excavation of the emplacement drifts in the HLW repository will produce a lot of excavated Opalinus Clay. This material could be disposed of after excavation, or – as often suggested – could be used as a buffer material in the emplacement drifts. This scenario would re-use the excavated Opalinus Clay, which has a clay mineral content that could be sufficient to serve as buffer. Based on these arguments, a scenario with a buffer made of crushed Opalinus Clay is considered in this report (Fig. 3-3). Although Opalinus Clay has a high content of clay minerals, the resulting swelling pressure will be lower than in the case of well-emplaced bentonite. The reason for this is the comparatively lower content of swelling clay minerals (smectite) in Opalinus Clay compared with bentonite. Also, higher concentrations of oxidised pyrite due to the preparation of the buffer materials and interim storage can be expected. An increased pore space in the buffer also means sulphide transport through the buffer will take place at a higher mass flow rate, but still diffusion dominated.

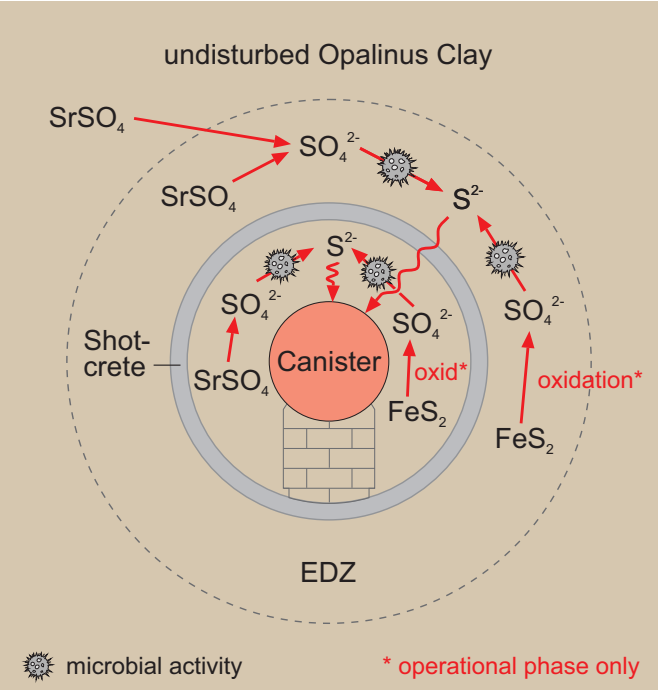

Fig. 3-3: Schematic overview of SF/HLW near field in case of a crushed Opalinus Clay buffer.

Abstraction of processes

Similarly to scenario B, microbial sulphate reduction can take place within a buffer made of crushed Opalinus Clay. The same considerations as in scenario B are therefore valid. Oxidation of pyrite in the crushed Opalinus Clay cannot be prevented, therefore a range of oxidised pyrite content is considered.

3.4 Commonly used parameters

The modelling of all scenarios assumes a single tunnel, containing a Cu-coated canister. All spatial dimensions and other parameter values common to the three scenarios are given in Tab. 3-1. The same parameter values are used in both models wherever appropriate. These parameters include information regarding mineralogy, diffusion coefficients, porosity, and emplacement density.

Tab. 3-1: Parameter values used in all scenarios.

Specific parameter values used in the individual scenarios can be found in Tabs. 5-2, 6-2 and 7-2 for scenarios A, B and C respectively.

General data				
Parameter	**Symbol**	**Units**	**Values**	**Reference**
Tunnel radius	r_0	m	1.25	Nagra (2014b)
Canister radius	r_{can}	m	0.5	Nagra (2014b)
EDZ thickness	$a - r_0$	m	0.7	
Density of copper	ρ_c	kg/m^3	8900	
Molar weight of copper	N_c	g/mol	64	
Formula weight of celestite	f_a, f_c	g/mol	184	
Formula weight of gypsum	f_b	g/mol	172	
Formula weight of pyrite	f_p	g/mol	120	
Stoichiometry factors	n_a, n_b, n_c	-	1	
Data for the undisturbed host rock				
Dry density	ρ_{hr}	kg/m^3	2450	Nagra (2014a)
Hydraulic gradient	i	-	1	
Hydraulic conductivity	K	m/s	2×10^{-14}	Nagra (2014a)
Diffusion distance	L	m	55	Nagra (2014a)
Stoichiometry factor	n_c	-	1	
Celestite solubility	S_c	mol/m^3	16.45	
Celestite concentration		wt.-%	0.02 – 0.06	Wersin et al. (2013)
Pyrite concentration		wt.-%	0.2 – 3.7	Mazurek (2011)
Effective diffusion coefficient (sulphate)	$D_{e,c}$	m^2/s	2×10^{-12}	Nagra (2014b)
Effective diffusion coefficient (sulphide)	$D_{e,sr}$	m^2/s	2×10^{-12}	Nagra (2014b)
Total porosity	ϵ_{OPA}	-	0.11	Nagra (2014a)
Data for the EDZ [1)]				
Total porosity	ϵ_{EDZ}	-	0.14	Gaus et al. (2014)
Dry density	ρ_{EDZ}	kg/m^3	2450	Nagra (2014a)
Stoichiometry factor	n_a	-	1	
Celestite concentration		wt.-%	0.02 – 0.06	Wersin et al. (2013)
Pyrite concentration		wt.-%	0.2 – 3.7	Mazurek (2011)
Data for the buffer				
Gypsum concentration in Wyoming bentonite		wt.-%	0.5 – 0.9	Karnland (2010)
Pyrite concentration in Wyoming bentonite		wt.-%	0.4 – 0.6	Karnland (2010)
Celestite concentration in crushed OPA		wt.-%	0.02 – 0.06	Wersin et al. (2013)
Pyrite concentration in crushed OPA		wt.-%	0.2 – 3.7	Mazurek (2011)

[1)] Mineralogy of the EDZ is identical to the mineralogy of the undisturbed host rock. Only in some calculation cases (see Chapters 5 – 7), a percentage of the pyrite in the Opalinus Clay is assumed to be oxidised in the EDZ (but not in the undisturbed host rock).

4 Description of models

4.1 Assumptions common to both models

The following assumptions are common to both the simplified model and the reactive transport model used to model all three scenarios:

- A 1-D radial geometry is assumed, in a plane normal to the emplacement tunnel axis passing through a canister and with its origin coinciding with the tunnel axis. This simplifying assumption means that the buffer between canisters is disregarded in the calculations.
- Materials external to the canister are represented as porous equivalent compartments (buffer, EDZ and host rock) with homogenous mass transport properties.
- Compartments are fully water-saturated (e.g. no explicit gas phase is present) and conditions are isothermal.
- The main mass transfer mechanism is diffusion in the water-filled pore spaces according to Fick's law. The simplified model also considers advection in the Opalinus Clay (although this is shown to be unimportant). In modelling diffusion, the complex interplay of different diffusion processes (e.g. pore diffusion, surface diffusion) with the pore space geometry (tortuosity, constrictivity) is simplified by using integrated parameters (the pore diffusion coefficient and effective diffusion coefficient).
- In each compartment, a single (physical) porosity is assumed and all aqueous species are assumed to have the same effective diffusion coefficient.
- The impact of precipitation and dissolution of minerals on the porosity and diffusion coefficients in each compartment is disregarded.

Further model-specific assumptions are given in the following sections of this chapter.

4.2 Simplified model

4.2.1 Main processes and cases considered

Two variants of the simplified model are considered in which (i), sulphate-reducing bacteria are active only in the EDZ surrounding the repository emplacement drifts (see Section 4.2.2) and (ii), sulphate-reducing bacteria are also active in the buffer, which may be the case if it is emplaced at relatively low density or if poorly swelling crushed Opalinus Clay is used instead of bentonite (see Section 4.2.3).

For a given sulphide flux F_S [mol m^{-1} a^{-1}] to the canister surface per unit emplacement tunnel length, and noting that 2 moles of copper are corroded per mole of sulphide, the rate of copper corrosion (j_a [m a^{-1}]) is:

$$j_a = \frac{2F_S}{\rho_c} \cdot \frac{N_c}{1000 \cdot 2\pi \cdot r_{can}} \tag{4-1}$$

where ρ_c [kg m^{-3}] is the density of copper, N_c [g mol^{-1}] is the molar weight of copper and r_{can} [m] is the canister radius.

The sulphate minerals from which this sulphide flux ultimately arises may be present:

- in the EDZ itself,
- in the buffer; and
- in the host rock beyond the EDZ.

For simplicity, it is assumed that single, generic sulphate minerals a, b, and c, with formula weights f_a [g mol^{-1}],f_b [g mol^{-1}] and f_c [g mol^{-1}] respectively, are the dominant sulphate minerals in the EDZ the buffer and the host rock. The specific identity of each of these generic minerals varies according to the scenario under consideration, as explained in Chapters 5 to 7. They are assumed to be present in amounts w_a [wt.-%], w_b [wt.-%] and w_c [wt.-%], and other minerals are neglected.

It is assumed that the only source of aqueous sulphide contributing to canister corrosion is from the reduction of sulphate by bacteria. Sulphide may also be initially present in the form of pyrite (FeS_2). However, as noted in Section 1.2, pyrite is very insoluble under anoxic and reducing conditions and so does not contribute directly to corrosion. On the other hand, partial oxidation of pyrite is considered in the model as a potential source of sulphate, which may subsequently be reduced to sulphide and participate in canister corrosion, as described in Section 5.1.1, Eq. 5-1 and associated text.

The main transport process considered for aqueous sulphate and sulphide ions in the near field and geosphere is diffusion; the rate of transport in the host rock by advection in flowing water is also considered, but it is shown later in this report to be of negligible importance compared with diffusion.

4.2.2 Scenario A: Sulphate-reducing bacteria active only in the EDZ

Consider first the model variant in which sulphate-reducing bacteria are active only in the EDZ. This model variant is used to calculate the sulphide flux in scenario A. The main fluxes and processes conceptualised as operating in this case are illustrated schematically in Fig. 4-1.

Aqueous sulphate ions from the dissolution of minerals b and c initially present in the buffer and host rock migrate towards the EDZ by diffusion at rates per unit length denoted by F_{bz} [mol m^{-1} a^{-1}] and F_{czd} [mol m^{-1} a^{-1}], respectively, where they are reduced to sulphide. Sulphate from the rock also reaches the EDZ by advection at a rate per unit length F_{cza} [mol m^{-1} a^{-1}]. The sulphide produced by micro-organisms in the EDZ then diffuses into the buffer and towards the canister at a rate per unit length denoted by F_s (as used in Eq. 4-1), diffuses into the host rock at a rate per unit length denoted by F_{rd} [mol m^{-1} a^{-1}] or is advected into the host rock at a rate denoted by F_{ra} [mol m^{-1} a^{-1}].

Because sulphate concentrations in the buffer and host rock are assumed to be solubility limited, dissolution fronts will develop in these media separating areas depleted in sulphate minerals from the remainder of these media. The dissolution fronts will, over time, migrate away from the interfaces of their respective media with the EDZ, as described further in Appendix A.1.

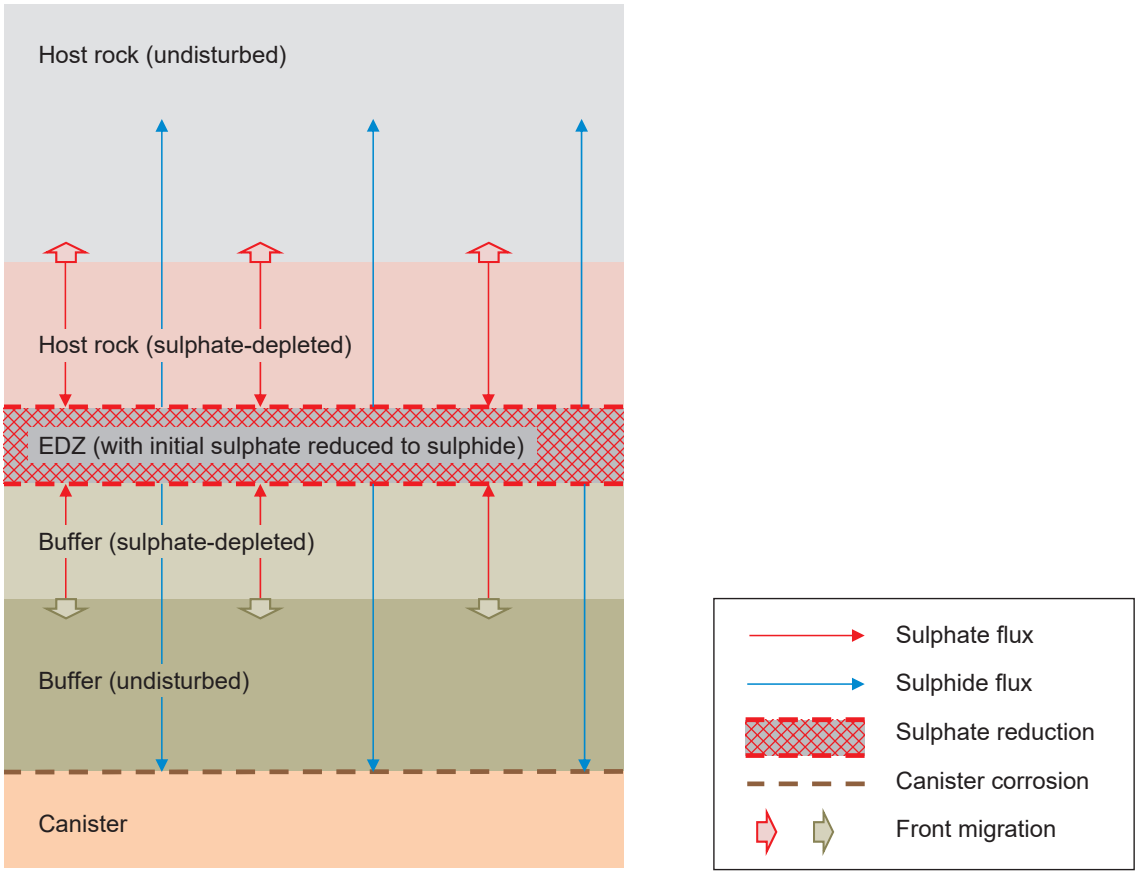

Fig. 4-1: Schematic illustration of fluxes and processes the model variant with sulphate-reducing bacteria active only in the EDZ.

Generic sulphate mineral a, formula weight f_a [g mol^{-1}] is assumed to be initially present at w_a [wt.-%] in the EDZ. It is assumed for simplicity that mineral a dissolves instantaneously at time $t = 0$ and that the sulphate ions released are reduced to sulphide. The mass of sulphide in the EDZ per unit tunnel length at time $t = 0$, M_0 [mol m^{-1}] is thus:

$$M_0 = 10 \cdot n_a \cdot \frac{w_a}{f_a} \cdot \rho_{EDZ} \cdot 2\pi(a^2 - r_0^2) \tag{4-2}$$

where r_0 [m] is the emplacement tunnel radius, a [m] is the outer radius of the EDZ, ρ_{EDZ} [kg m^{-3}] is the dry density of the EDZ and n_a is a stoichiometry factor, i.e. the number of moles of sulphide produced by the reduction of sulphate from one mole of mineral a.

Thereafter, summing and integrating the various fluxes, the mass of sulphide $M(t)$ [mol m^{-1}] in the EDZ at time t will be:

$$M(t) = M_0 + \int_0^t (F_{bz} + F_{czd} + F_{cza} - F_s - F_{rd} - F_{ra})\, dt \tag{4-3}$$

The concentration $C_z(t)$ [mol m^{-1}] of sulphide in the EDZ may also be subject to a solubility limit S_s [mol m^{-3}]:

$$C_z(t) = \begin{cases} \frac{M(t)}{2\pi\epsilon_{EDZ}(a^2-r_0^2)} & \text{if} \quad \frac{M(t)}{2\pi\epsilon_{EDZ}(a^2-r_0^2)} < S_s \\ S_s & \text{otherwise} \end{cases} \tag{4-4}$$

where ϵ_{EDZ} is the EDZ porosity.

Formulae used to calculate the six fluxes F_{bz}, F_{czd}, F_{cza} F_s, F_{rd} and F_{ra} are presented in Appendix A.1. As is shown in that appendix, F_s and F_r are themselves functions of $C_z(t)$. Thus, Eq. 4-4 is solved numerically. The resulting flux F_s is finally substituted in Eq. 4-1 to obtain the rate of copper corrosion.

As described in Appendix A.1, pseudo-steady state concentration distributions of sulphate and sulphide are assumed in calculating the various diffusive fluxes. Sulphate fluxes from the buffer and host rock to the EDZ (F_{bz} and F_{czd}) are calculated with diffusion distances determined by the (transient) positions of the dissolution fronts within these media. Here, the pseudo-steady state assumption leads to an overestimation of the sulphate flux entering the EDZ and thus to an overestimation of the amount of sulphide generated in the EDZ. The diffusive sulphide flux from the EDZ to the canister surface, F_s, is calculated with a fixed diffusion distance equal to the buffer thickness. In this case, the pseudo-steady state assumption leads to an overestimation of the flux of sulphide reaching the canister surface (especially at early times), which is conservative in terms of canister corrosion. Finally, the loss of sulphide generated in the EDZ to the host rock (F_{rd}) is calculated with a fixed diffusion distance equal to the distance to the upper or lower host-rock boundaries. This assumption leads to an underestimation of the loss of sulphide to the host rock, which is also conservative in terms of canister corrosion. The overall degree of conservatism introduced by these assumptions is illustrated in the comparison of results obtained using the simplified model with those obtained with the reactive transport models (in which transient diffusion is modelled) in Section 5.3.

4.2.3 Scenarios B and C: Sulphate-reducing bacteria active in the EDZ and buffer

Consider now the second model variant in which sulphate-reducing bacteria are active in the buffer as well as in the EDZ. This model variant is used to calculate the sulphide fluxes in scenarios B and C. As well as handling a sulphate mineral that is initially present in the buffer, this model variant also handles the case where aqueous sulphide ions are also initially present: in particular, the case of a crushed Opalinus Clay buffer, in which pyrite in the buffer has been partly oxidised prior to, or shortly after, emplacement.

The main fluxes and processes conceptualised as operating in this case are illustrated schematically in Fig. 4-2.

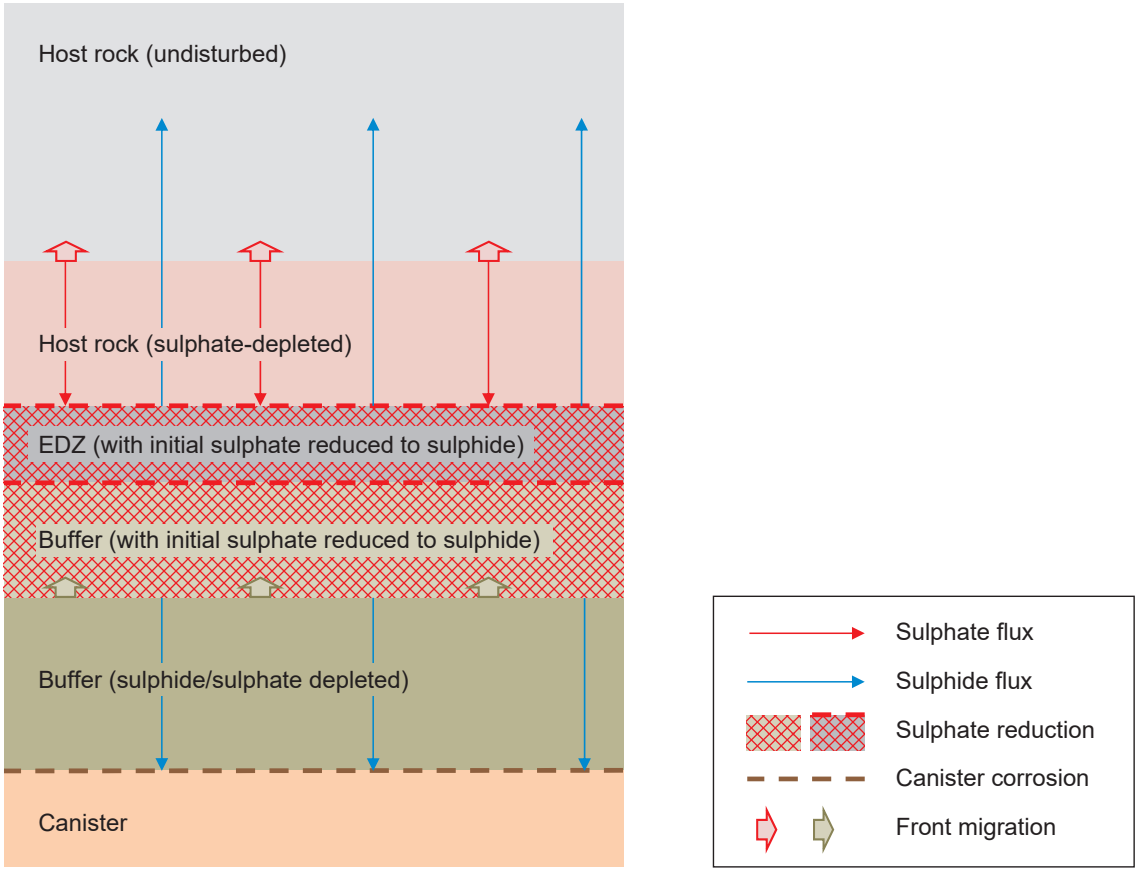

Fig. 4-2: Schematic illustration of fluxes and processes in the model variant with sulphate-reducing bacteria active in the EDZ and buffer.

It is again assumed for simplicity that sulphate mineral a initially present in the EDZ dissolves instantaneously and that the aqueous sulphate ions released are reduced to sulphide ions. Similarly, it is assumed that sulphate mineral b initially present in the buffer dissolves instantaneously and that the resulting aqueous sulphate ions are reduced to sulphide ions, and are combined with any other sulphide ions that are initially present.

As depicted in Fig. 4-2, because sulphide concentrations in the buffer and EDZ are assumed to be solubility limited, a dissolution front will develop separating areas with precipitated sulphide minerals from areas depleted in these minerals. This dissolution front will start at the canister surface and, over time, migrate away from the canister into the buffer and eventually into the EDZ, as described further in Appendix A (in Scanario A, by constrast, the dissolution front starts at the inner and outer boundaries of the EDZ and migrates into the buffer and host rock). As in the variant with sulphide-reducing bacteria present only in the EDZ, a dissolution front will also develop in the host rock separating areas depleted in sulphate minerals from the reminder of the host rock. Aqueous sulphate ions will migrate from this front to the outer boundary of the EDZ, where they will be reduced to sulphide ions and precipitate as sulphide minerals.

Regarding the flux of sulphide F_S to the canister surface required to calculate corrosion via Eq. 4-1, three evolution phases can be distinguished in this model variant:

- the dissolution front separating areas with precipitated sulphide minerals from areas depleted in these minerals resides within the buffer,
- the dissolution front separating areas with precipitated sulphide minerals from areas depleted in these minerals resides within the EDZ, and
- the dissolution front has reached the outer boundary of the EDZ, where sulphide ions originating from the host rock have been precipitated as sulphide minerals (precipitates assumed here to occupy a narrow ring).

The derivation of sulphide fluxes to the canister surface in each of these three phases is described in Appendix A.

4.3 Reactive transport model

Sulphide cycling in the near field of the repository and its potential impact on copper corrosion will be affected by a complex network of coupled microbial, geochemical, transport and hydrologic interactions. The inherent coupling between these processes requires that for a realistic prediction of geochemical evolution of the system a mathematical model capable of representing key processes and their interactions is employed.

Reactive transport modelling explicitly simulates coupled mass transfer and chemical reaction phenomena. The approach permits direct representation and evaluation of the complicated interplay between individual chemical reactions as well as the impact of solute transport on the chemical system (and vice versa).

Reactive transport calculations in this study were carried out using PFLOTRAN (www.pflotran.org), an open source, state-of-the-art massively parallel subsurface flow and reactive transport code. PFLOTRAN executable (along with additional libraries, such as PETSC) was compiled from the source code cloned from https://github.com/petsc/pflotran on 1 November 2016. PFLOTRAN uses the integrated finite difference method to solve a system of generally nonlinear partial differential equations describing reactive flow and transport in porous materials. Spatial discretisation can utilise both structured and unstructured grids. The code allows the implementation of complex bio-geochemical reaction networks including aqueous complexation, mineral, cation exchange and surface complexation reactions using a mixed equilibrium-kinetic approach. The Lawrence Livermore National Laboratory (LLNL) aqueous activity version of the the Thermochimie v. 9b thermodynamic database (https://www.thermochimie-tdb.com/) was used to relate aqueous concentrations and activities.

4.3.1 Concept and key assumptions for geochemical model

Key geochemical processes included in the geochemical model are schematically shown in Fig. 4-3. Sulphate minerals are present in both the buffer (gypsum in the case of bentonite and celestite in the case of crushed Opalinus Clay) and in the surrounding Opalinus Clay (celestite in the EDZ as well as the undisturbed rock). The sulphate minerals dissolve and precipitate in response to changes in the porewater chemistry according to:

$$CaSO_4.2H_2O\ (s) \rightleftharpoons Ca^{2+}(aq) + SO_4^{2-}(aq) + 2H_2O \quad (4\text{-}5)$$

$$SrSO_4(s) \rightleftharpoons Sr^{2+}(aq) + SO_4^{2-}(aq) \quad (4\text{-}6)$$

Solid organic matter (SOM) is present in both Opalinus Clay and in the buffer and can dissolve, releasing dissolved organic matter (DOM) into the porewater (the molecular formula of organic matter is represented simplistically as CH_2O).

$$CH_2O\ (s) \rightarrow CH_2O\ (aq) \qquad (4\text{-}7)$$

Dissolved organic matter is assumed to serve as an electron donor for sulphate-reducing bacteria (although calculations are also carried out for a single case considering hydrogen as the electron donor, see Appendix C). The maximum concentration of dissolved organic matter is 1 mg/L (calculations converting mass to molar concentrations assume pure carbon as the molecular formula of organic matter). All SOM is assumed to be fully biodegradable. It is also assumed that SOM undergoes a fast kinetic reaction to maintain the DOM concentration in the porewater. The entire amount of solid organic matter can dissolve (no residual insoluble fraction), which is a conservative assumption.

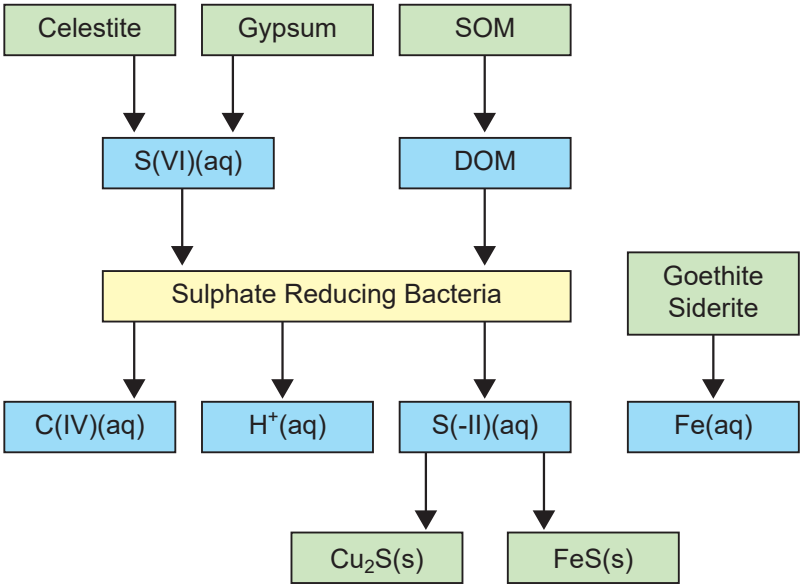

Fig. 4-3: Schematic illustration of main processes considered in the conceptual geochemical model.

Sulphate-reducing bacteria (SRB) are assumed to be active either only in the EDZ (scenario A) or in both the EDZ and in the buffer (scenarios B and C). The sulphate reduction reaction is a fast kinetic reaction (represented using a Monod kinetics model) the rate of which depends on the concentrations of sulphate and DOM. The microbial population is assumed to be constant in time. The micro-organisms utilise sulphate and dissolved organics as the electron acceptor and donor, respectively, and produce sulphide.

In addition, the reaction increases alkalinity and CO_2 according to the reaction:

$$2CH_2O\ (aq) + SO_4^{2-}(aq) \rightleftharpoons HS^-\ (aq) + CO_2(aq) + HCO_3^-(aq) + H_2O \qquad (4\text{-}8)$$

As discussed in Section 2.2, FeS (either amorphous FeS(am) or mono-particulate mackinawite) and pyrite are the likely minerals to control dissolved sulphide concentrations in the near field.

The solubility of FeS(am)/mackinawite and pyrite differ by many orders of magnitude, as do (also considering iron availability) the sulphide solubility limits imposed by these minerals. As available data do not allow it to be decided unequivocally which of the two phases would be solubility limiting for sulphide, we make the pessimistic assumption that the sulphide solubility would be regulated by mackinawite (characterised by relatively high solubility). Although FeS(am) is characterised by a somewhat higher solubility than mackinawite, it is known to convert into mackinawite relatively rapidly (see discussion in Section 2.2). Thus, the generated sulphide may precipitate as mackinawite, which is assumed to be the sole geochemical sink for sulphide. Pyrite is considered to be chemically "inert".

$$Fe^{2+}(aq) + HS^{-}(aq) \rightleftharpoons FeS(s) + H^{+}(aq) \quad (4\text{-}9)$$

Mackinawite precipitation requires availability of sufficient dissolved Fe, which is provided by the dissolution of siderite ($FeCO_3$) and goethite (FeOOH):

$$FeCO_3(s) + H^{+}(aq) \rightleftharpoons Fe^{2+}(aq) + HCO_3^{-}(aq) \quad (4\text{-}10)$$

$$FeOOH(s) + 3H^{+}(aq) \rightleftharpoons Fe^{3+}(aq) + 2H_2O \quad (4\text{-}11)$$

Calcite equilibrium is an important reaction in the model, which helps buffer the carbonate system and pH during microbial sulphide reduction and acidification:

$$CaCO_3(s) + H^{+}(aq) \rightleftharpoons Ca^{2+}(aq) + HCO_3^{-}(aq) \quad (4\text{-}12)$$

Exchange reactions are considered for both the Opalinus Clay and the MX-80 buffer, according to the following generic reaction:

$$AX + B \rightleftharpoons BX + A \quad (4\text{-}13)$$

In the MX-80 buffer, protonation and de-protonation reactions of abundant montmorillonite surfaces *(Ss)* contribute to pH buffering:

$$SsOH \rightleftharpoons SsO^{-} + H^{+} \quad (4\text{-}14)$$

$$SsOH + H^{+} \rightleftharpoons SsOH_2^{+} \quad (4\text{-}15)$$

Dissolved sulphide undergoes diffusive transport due to concentration gradients in the porewater. A proportion of generated sulphide reaches the surface of the canister, where it is instantly consumed by Cu corrosion and immobilised as chalcocite (Cu_2S) according to Eq. 2-5. Sulphide consumption by corrosion of the copper canister is assumed to be instantaneous and controlled by the sulphide flux towards the canister surface. As explained in Section 2.3, sulphide-induced corrosion of the copper canister could be affected by many factors. However, in this assessment we make the simplifying assumption that the corrosion rate is directly proportional to the sulphide flux towards the canister (i.e. every sulphide molecule is instantly consumed to react with the canister surface).

Other assumptions underpinning the geochemical model include:

- All chemical reactions are calculated using the Thermochimie v.9b thermodynamic database (www.thermochimie-tdb.com) at 25° C utilising the Lawrence Livermore National Laboratory (LLNL) aqueous activity model.
- Mineral-porewater reactions follow sufficiently fast kinetics so as to approximate local chemical equilibrium.

4.3.2 Geometry and boundary conditions

1-D radial geometry is considered for reactive transport calculations (Fig. 4-4). The Opalinus Clay end of the domain is held at a constant chemical composition of Opalinus Clay porewater (Dirichlet type boundary). The chemical composition of Opalinus Clay porewater is shown in Tab. 5-6. Calculations indicated that setting the outer boundary of Opalinus Clay at 50 m from the tunnel diameter has a negligible impact on the near-field porewater chemistry at the Opalinus Clay boundary. At the canister end a no-flux boundary is imposed. The domain is variably discretised with a total of 200 cells. The problem is solved for a period of 1'000'000 years using a maximum time step of 1 year.

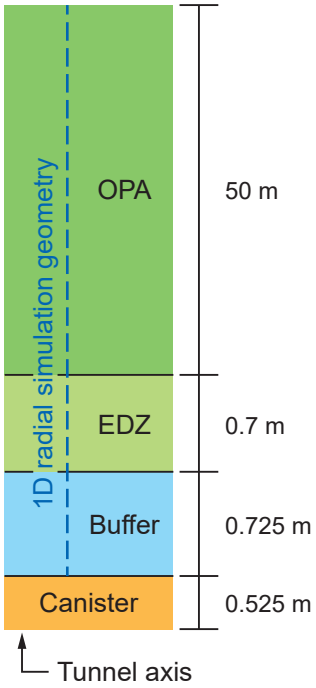

Fig. 4-4: Schematic illustration of the radial geometry of the disposal system with the orientation of 1-D simulation profile used in reactive transport calculations (dashed blue line).

Dimensions not to scale.

4.3.3 Key assumptions for reactive transport model

Specific assumptions underlying the transport model (parameter values) are listed separately for each case considered in the corresponding section of this report. The following general assumptions were made with regard to treatment of mass transport in the reactive transport model:

- Materials are represented as porous equivalent compartments with homogenous properties.
- Compartments are fully water-saturated (e.g. no explicit gas phase is present) and conditions are isothermal. The early phase of elevated temperatures (i.e. first few hundreds of years) was neglected in the calculations, which is deemed justified given the large time scales of interest (i.e. 1 Ma).
- The sole mass transfer mechanism is by diffusion in the water-filled pore space according to Fick's law.
- Single (physical) porosity was assumed for transport and all aqueous species were assumed to have the same diffusion coefficient (within a given compartment).

5 Near field containing well-emplaced bentonite buffer

5.1 Simplified model

5.1.1 Case-specific model set-up

The scenario in which the near field contains a well-emplaced buffer has been analysed using the model variant as described in Section 4.2.2. Mineral a, the dominant soluble sulphate mineral in the EDZ, is taken to be celestite. Celestite is also taken to be the dominant soluble sulphate mineral in the remainder of the host rock, i.e. mineral c. Mineral b, the dominant soluble sulphate mineral in the buffer, is taken to be gypsum. The amount of celestite in the EDZ and host rock is taken to be 0.06 wt.-% and the amount of gypsum in the buffer is taken to be 0.9 wt.-%. These values are taken from the upper ends of the ranges given in Tab. 3-1.

Reduction of sulphate to sulphide occurs in the EDZ only and begins from the start of the modelled period.

23 calculations cases are considered in all for this scenario, including a reference case (A-S-S1) and 22 variant cases that examine the impact of uncertainties related to:

- the amount of gypsum in the buffer and the amount of celestite in the EDZ and in the remainder of the host rock;
- solubility limitation of the concentration of sulphide produced by the action of sulphate-reducing bacteria in the EDZ;
- uncertainty and variability in the diffusion coefficients of sulphate and sulphide ions and in the hydraulic conductivity of the Opalinus Clay host rock;
- uncertainty in the diffusion coefficients of sulphate and sulphide ions in the buffer; and
- the proportion (if any) of pyrite in the EDZ assumed to be oxidised to sulphate[4]; no pyrite oxidation is assumed in the reference case.

The reference and variant cases are summarised in Tab. 5-1.

In practice, the oxidation of an assumed fraction of pyrite is handled by replacing the amount of celestite in the EDZ, w_a [wt.-%], by an effective amount of celestite, w'_a [wt.-%], given by:

$$w'_a = w_a + 2 \cdot w_p \cdot F_{ox} \cdot \frac{f_b}{f_p} \quad (5\text{-}1)$$

where w_p [wt.-%] is the initial amount of pyrite in the EDZ before oxidation (assumed to be 3.7 wt.-%, which is the upper end of the range given in Tab. 3-1), F_{ox} is the fraction oxidised and f_p [g mol^{-1}] is the formula weight of pyrite (f_b is the formula weight of celestite). Here, it is assumed that oxidation of one mole of pyrite gives two moles of sulphate, which is the maximum possible.

[4] Pyrite in the EDZ may be oxidised during the operational phase, which increases the sulphate inventory in the EDZ. This assumption is based on observations in tunnels that were being ventilated for many years (Mont Terri tunnel, Hauenstein tunnel, Col de la Croix; Traber 2004). Gypsum precipitation as a result of pyrite oxidation has only been observed at exposed surfaces and cracks. Experimental observations of pyrite oxidation in Callovian-Oxfordian argillaceous rock at the Meuse/Haute-Marne Underground Rock Laboratory illustrate that oxidation of pyrite preferentially occurs along the excavation-induced fractures (Vinsot et al. 2014). Such local clogging of the open cracks will further restrict the diffusion of oxygen into the rock.

Tab. 5-1: Overview of reference case and variant cases for scenario A calculated with the simplified model.

Main source of uncertainty/variability	**Case**	**Description**
Reference Case	A-S-S1	Solubility limitation of the concentration of sulphide produced by the action of sulphate-reducing bacteria in the EDZ; solubility limit 10^{-4} M
The amount of gypsum in the buffer and the amount of celestite in the EDZ and in the remainder of the host rock	A-S-V1	Lower bound amount of celestite; no sulphide solubility limitation
	A-S-V2	Lower bound amount of gypsum; no sulphide solubility limitation
	A-S-V3	Lower bound amounts of gypsum and celestite; no sulphide solubility limitation
Solubility limitation of the concentration of sulphide produced by the action of sulphate-reducing bacteria in the EDZ	A-S-SX	No solubility limitation
	A-S-S2	10^{-5} M
	A-S-S3	10^{-3} M
	A-S-S4	10^{-2} M
	A-S-S5	10^{-1} M
Diffusion coefficients and hydraulic conductivity of the Opalinus Clay host rock	A-S-SXA	Increased the diffusion coefficient and hydraulic conductivity; no sulphide solubility limitation
	A-S-S1A	Increased the diffusion coefficients and hydraulic conductivity; reference case sulphide solubility limit (10^{-4} M)
Diffusion coefficients in the buffer	A-S-DB	Increased diffusion coefficients in the buffer; no sulphide solubility limitation
	A-S-S1DB	Increased diffusion coefficients in the buffer; reference case sulphide solubility limit (10^{-4} M)
	A-S-S1DBB	Further increased diffusion coefficients in the buffer; reference case sulphide solubility limit (10^{-4} M)
Proportion of pyrite [1)] in the EDZ assumed to be oxidised to sulphate	A-S-C5	5 % pyrite oxidation; no sulphide solubility limitation
	A-S-C10	10 % pyrite oxidation; no sulphide solubility limitation
	A-S-C20	20 % pyrite oxidation; no sulphide solubility limitation
	A-S-C50	50 % pyrite oxidation; no sulphide solubility limitation
	A-S-DBC50	50 % pyrite oxidation; in combination with increased diffusion coefficient in the buffer; no sulphide solubility limitation
	A-S-DBBC50	50 % pyrite oxidation; in combination with further increased diffusion coefficient in the buffer; no sulphide solubility limitation
	A-S-C50A	50 % pyrite oxidation; in combination with increased diffusion coefficient and hydraulic conductivity in the host rock; no sulphide solubility limitation
	A-S-S1C5	5 % pyrite oxidation; in combination with reference case sulphide solubility limit (10^{-4} M)
	A-S-S1C10	10 % pyrite oxidation; in combination with reference case sulphide solubility limit (10^{-4} M)
	A-S-S1C20	20 % pyrite oxidation; in combination with reference case sulphide solubility limit (10^{-4} M)
	A-S-S1C50	50 % pyrite oxidation; in combination with reference case sulphide solubility limit (10^{-4} M)
	A-S-DBS1C50	50 % pyrite oxidation; in combination with reference case sulphide solubility limit (10^{-4} M) and increased diffusion coefficient in the buffer

[1)] Assuming an initial amount of pyrite in the EDZ before oxidation of 3.7 wt.-%, based on the upper end of the range given in Tab. 3-1.

5.1.2 Case-specific parameter values

Case-specific parameter values for the various calculations cases considered for this scenario are given in Tab. 5-2.

Concerning the amounts of gypsum in the bentonite buffer and celestite in the EDZ and in the remainder of the host rock, the reference case cautiously assumes the upper bounding values given in Tab. 3-1, i.e. 0.9 wt.-% and 0.06 wt.-% for gypsum and celestite, respectively. Case A-S-V1 takes the lower bounding value for celestite (0.02 wt.-%), with the amount of gypsum set to its reference case value. Conversely, case A-S-V2 takes the lower bounding value for gypsum (0.5 wt.-%), with the amount of celestite set to its reference case value. Case A-S-V3 combines lower bounding values for both gypsum and celestite.

To illustrate the major impact of solubility limit, some calculation cases with no solubility limit were explored in scenario A only. Concerning solubility limitation of the concentration of sulphide, the reference case (A-S-S1) assumes a sulphide solubility limit of 10^{-4} M, which is supported by the stability of mackinawite. Case A-S-SX is the unrealistic case where no solubility limit is considered. In cases A-S-S2 to A-S-S5, the solubility limit is varied across a wide range, from 10^{-5} M (case A-S-S2) to 0.1 M (case A-S-S5).

Concerning the uncertainty in diffusion and groundwater flow in the host rock, the reference case takes values for the effective diffusion coefficient of anions (sulphide and sulphate) and for hydraulic conductivity that are representative of transport perpendicular to the Opalinus Clay bedding. Values of these parameters representative of transport parallel to the bedding are signify-cantly higher and are considered in case A-S-SXA. The value for hydraulic conductivity used in both of these cases is taken from Nagra (2002, p.79). The effective diffusion coefficients within the host rock are taken from the anion reference values for Cl from Table A3.5-3a in Nagra (2014b). For the diffusion coefficient in the buffer, an arbitrary increase of up to a factor of 10 is considered in the calculation cases, as also assumed in SGT-E2 dose calculations.

There is assumed to be no oxidation of pyrite in the EDZ in the reference case. Calculation cases, however, consider pyrite oxidation from 5 % to 50 %. The corresponding effective celestite concentrations, calculated using Eq. 5-1, are given in Tab. 5-3. Here, upper bound celestite and pyrite amounts in the Opalinus Clay are assumed: 0.06 and 3.7 wt.-%, respectively.

Tab. 5-2: Parameter values used to analyse scenario A of the simplified model.

Reference values are used for all cases unless otherwise stated. General data are shown in Tab. 3-1.

Data for the undisturbed host rock				
Parameter	**Symbol**	**Units**	**Cases**	**Values**
Hydraulic conductivity	K	m/s	All other cases	2×10^{-14}
			A-S-SXA, A-S-S1A, A-S-C50A	10^{-13}
Effective diffusion coefficient (sulphate)	$D_{e,c}$	m^2/s	All other cases	2×10^{-12}
			A-S-SXA, A-S-S1A, A-S-C50A	10^{-11}
Effective diffusion coefficient (sulphide)	$D_{e,sr}$	m^2/s	All other cases	2×10^{-12}
			A-S-SXA, A-S-S1A, A-S-C50A	10^{-11}
Amount of celestite	w_c	wt.-%	All other cases	0.06
			A-S-V1, A-S-V3	0.02
Data for the EDZ				
Amount of celestite (includes effective values, see Tab. 7-3)	w_a	wt.-%	All other cases	0.06
			A-S-V1, A-S-V3	0.02
			A-S-C5, A-S-S1C5	0.63
			A-S-C10, A-S-S1C10	1.19
			A-S-C20, A-S-S1C20	2.33
			A-S-C50, A-S-DBC50, A-S-DBBC50, A-S-C50A, A-S-S1C50, A-S-DBS1C50	5.73
(Molar) solubility limit: sulphide minerals	S_s	mol/m^3	All other cases	No limit
			A-S-S1, A-S-S1A, A-S-S1DB, A-S-S1DBB, A-S-S1C5, A-S-S1C10, A-S-S1C20, A-S-S1C50, A-S-DBS1C50	0.1 (i.e. 10^{-4} M)
			A-S-S2	0.01 (i.e. 10^{-5} M)
			A-S-S3	1 (i.e. 10^{-3} M)
			A-S-S4	10 (i.e. 10^{-2} M)
			A-S-S5	100 (i.e. 10^{-1} M)

Tab. 5-2: (continued)

Data for the buffer				
Parameter	**Symbol**	**Units**	**Cases**	**Values**
Dry density	ρ_b	kg/m^3	All cases	1450
Effective diffusion coefficient (sulphate)	$D_{e,b}$	m^2/s	All other cases	2×10^{-12}
			A-S-DB, A-S-DBC50	5×10^{-12}
			A-S-S1DB, A-S-DBS1C50	2×10^{-11}
			A-S-S1DBB	5×10^{-11}
			A-S-DBBC50	10^{-11}
Effective diffusion coefficient (sulphide)	$D_{e,sb}$	m^2/s	All other cases	2×10^{-12}
			A-S-DB, A-S-DBC50	5×10^{-12}
			A-S-S1DB, A-S-DBS1C50	2×10^{-11}
			A-S-S1DBB	5×10^{-11}
			A-S-DBBC50	10^{-11}
Gypsum solubility	S_b	mol/m^3	All cases	102.7
Amount of gypsum	w_b	wt.-%	All other cases	0.9
			A-S-V2, A-S-V3	0.5

Tab. 5-3: Effective celestite concentrations in the EDZ resulting from potential pyrite oxidation assumed in different calculation cases.

Case	**Fraction of pyrite oxidised** [%]	**Effective celestite conc.** [wt.-%]
All cases except those shown below	0	0.06
A-S-C5, A-S-S1C5	5	0.63
A-S-C10, A-S-S1C10	10	1.19
A-S-C20, A-S-S1C20	20	2.33
A-S-C50, A-S-S1C50	50	5.73

5.1.3 Results

In scenario A dissolution fronts develop in the host rock and in the buffer separating undisturbed areas from areas depleted in sulphate minerals (celestite and gypsum, respectively, in the present scenario). These fronts begin at the inner and outer boundaries of the EDZ and gradually migrate into the adjacent media (i.e. the buffer and host rock, respectively: see Fig. 4-1). The progress of these fronts over time in the reference case A-S-S1 is shown in Fig. 5-1.

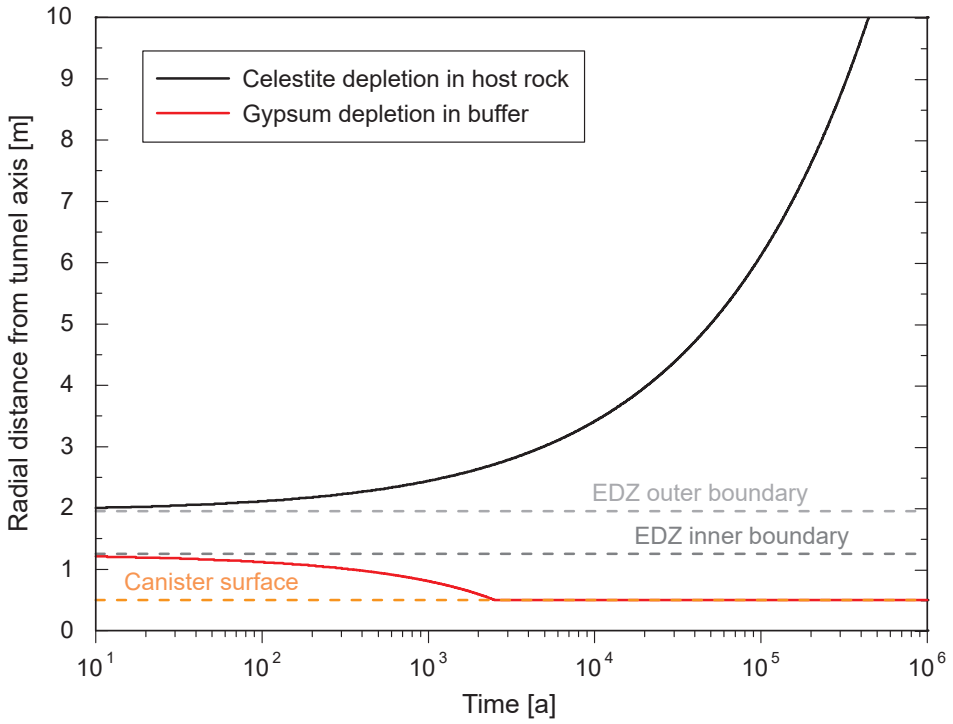

Fig. 5-1: Evolution of celestite and gypsum dissolution fronts in the reference case A-S-S1.

The gypsum dissolution front reaches the canister surface after 2'000 to 3'000 years, at which time all gypsum in the buffer is dissolved. The celestite front extends around 10 m from the tunnel axis after 400'000 years, justifying the assumption that the emplacement drifts, which have a separation of some tens of metres (40 m), can be assumed to evolve independently of one another, at least for the majority of the safety assessment period, which is 1'000'000 years for the HLW repository.

Sulphate ions released by celestite dissolution in the host rock migrate to the EDZ by advection and diffusion, whereas sulphate ions from gypsum dissolution in the buffer are assumed to migrate to the EDZ by diffusion only. Fig. 5-2 shows the sulphate fluxes to the EDZ due to advection and diffusion from the host rock and to diffusion from the buffer. The figure shows that diffusion from the buffer provides the dominant sulphate flux to the EDZ before the gypsum in the buffer is entirely depleted at between 2'000 to 3'000 years. This is in spite of the fact that the effective diffusion coefficient in the buffer is that same as that in the rock. The reason lies in the higher solubility assigned to the gypsum in the buffer (102.7 mol/m^3; see Tab. 5-2) compared with that assigned to the celestite in the rock (16.45 mol/m^3; see Tab. 3-1). Thereafter, diffusion from the host rock provides the dominant flux, with the advective flux from the host rock being relatively minor at all times.

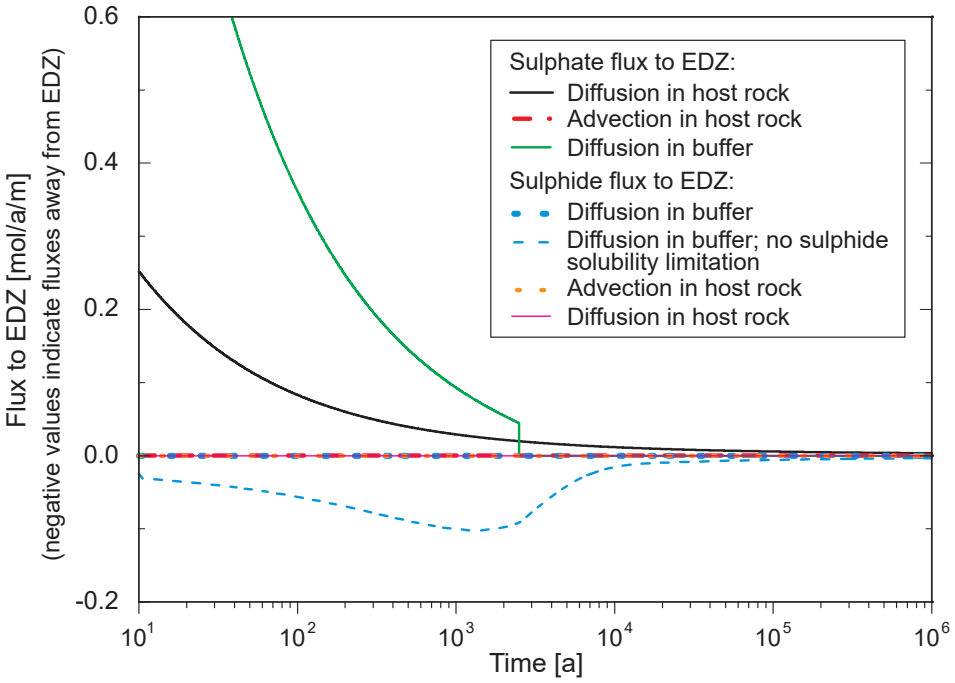

Fig. 5-2: Evolution of sulphate and sulphide fluxes in the reference case A-S-S1.

The sulphide flux to the canister in the case that there is no solubility limitation of sulphide concentration in the EDZ (case A-S-SX) is also shown to illustrate the impact of solubility limitation. The diffusive flux of sulphide to the canister in this case takes a constant value (-4.3×10^{-5} mol/a/m) which is much smaller in magnitide than the flux in the reference case.

On reaching the EDZ, sulphate is assumed to be converted to sulphide by sulphate-reducing bacteria and precipitated if the assumed solubility limit for sulphide (10^{-4} M in the reference case) is exceeded. The sulphide that remains in solution then either diffuses through the buffer to the canister, and reacts with the canister surface, or is lost by diffusion and advection to the host rock. Fig. 5-2 also shows these sulphide fluxes. The figure shows that these sulphide fluxes from the EDZ are vary small in comparison with the sulphate fluxes to the EDZ, implying a build-up of precipitated sulphide (Fig. 5-3 shows that the solubility limit for sulphide in the EDZ is exceeded at all calculated times by a significant margin in the reference case). To further illustrate the impact of solubility limitation of sulphide, the sulphide flux to the canister is also shown for the case where solubility limitation is omitted from the model (case A-S-SX). In this case, the diffusive sulphide flux from the EDZ to the canister is much larger, and is at its greatest shortly before the gypsum in the buffer is entirely depleted.

The amounts of sulphide consumed by canister corrosion, lost to the host rock or present in the EDZ (per metre of tunnel) are shown in Fig. 5-3. In the reference case, most of the sulphide produced within the EDZ remains there as precipitates, with the amounts lost to the rock or consumed by canister corrosion around 2 orders of magnitude or more smaller. Again, for comparison, the results of the case where solubility limitation is omitted from the model (case A-S-SX) are plotted for comparison. For the first thousand years, as in the reference case, most of the sulphide produced within the EDZ remains there. Thereafter, however, most is consumed by canister corrosion, with the amount lost to the host rock being more than an order of magnitude smaller.

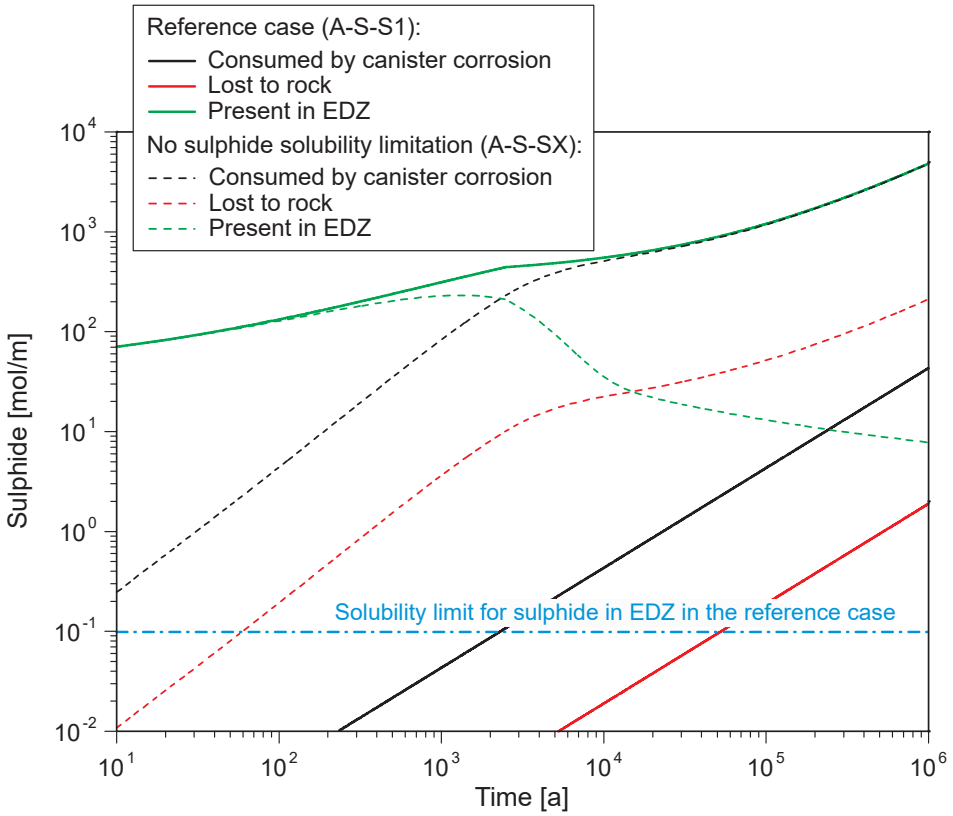

Fig. 5-3: Evolution of amount of sulphide present in the EDZ, compared with the amount consumed by canister corrosion and the amount lost to the host rock in the reference case A-S-S1 and in the case that there is no solubility limitation of sulphide concentration in the EDZ (case A-S-SX).

The sulphide amount required to reach the solubility limit in the EDZ in the reference case is also shown.

The resulting evolution of corrosion depth on the canister surface is shown in Fig. 5-4. Results are shown for the reference case A-S-S1 and for the variant cases for this scenario that examine the impact of solubility limitation for sulphide produced by the action of sulphate-reducing bacteria in the EDZ (cases A-S-SX and A-S2 to A-S-S5). The figure shows that the imposition of solubility limit in the order of 0.01 M or less leads to a marked reduction in the calculated corrosion depths. A solubility limit of 10^{-4} M (0.1 mol/m^3), for example, leads to a corrosion depth after a million years in the order of 0.2 mm, compared with around 2 cm in the unlikely case where the solubility limit is 10^{-2} M or higher.

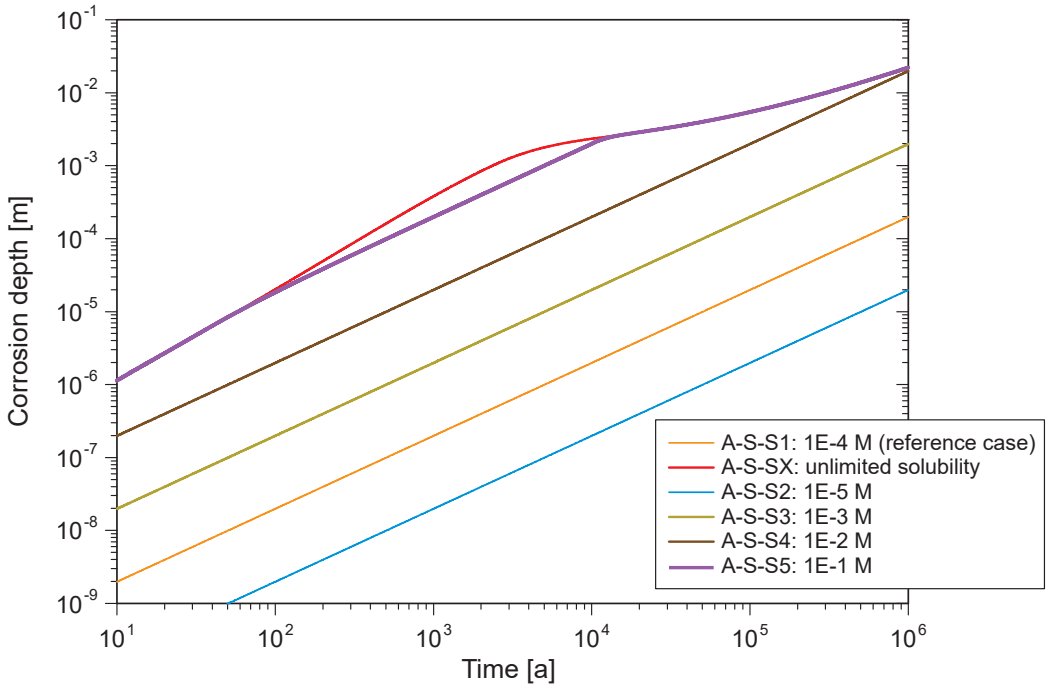

Fig. 5-4: Evolution of corrosion depth in the reference case (A-S-S1), in case A-S-SX, with unlimited sulphide solubility in the EDZ, and in cases A-S-S2 to A-S-S5, in which the solubility limit assigned to sulphide minerals (e.g. mackinawite) in the EDZ is varied.

The assumed amounts of gypsum and celestite have a negligible impact on corrosion depth if sulphide concentration is solubility limited, but a more significant impact if sulphide solubility limitation is omitted. Results are shown in Fig. 5-5 for the case A-S-SX, with no sulphide solubility limitation and reference amounts of gypsum and celestite, and also for the variant cases A-S-V1, A-S-V2 and A-S-V3, which also assume no sulphide solubility limitation, but with varied amounts of gypsum and celestite. However, the assumed amounts of gypsum in the buffer and celestite in the EDZ and in the remainder of the host rock have no impact on corrosion depth in the reference case where a sulphide solubility limit of 10^{-4} M is applied; increasing the amount of sulphate being reduced to sulphide in the EDZ simply results in more sulphide being precipitated there, since the concentation of dissolved sulphide in the EDZ is solubility limited.

The results show that uncertainties in the amount of celestite present in the EDZ and in the host rock are more important in terms of corrosion depth than uncertainties in the amount of gypsum in the buffer, due to the expansion of the host rock region depleted in celestite and due to the depletion of sulphate in the buffer. However, overall, the effects of both these sources of uncertainty are small, with corrosion depths after a million years being around 2.2 cm based on the higher celestite amount (0.06 wt.-%) and around 1.7 cm for the lower amount (0.02 wt.-%).

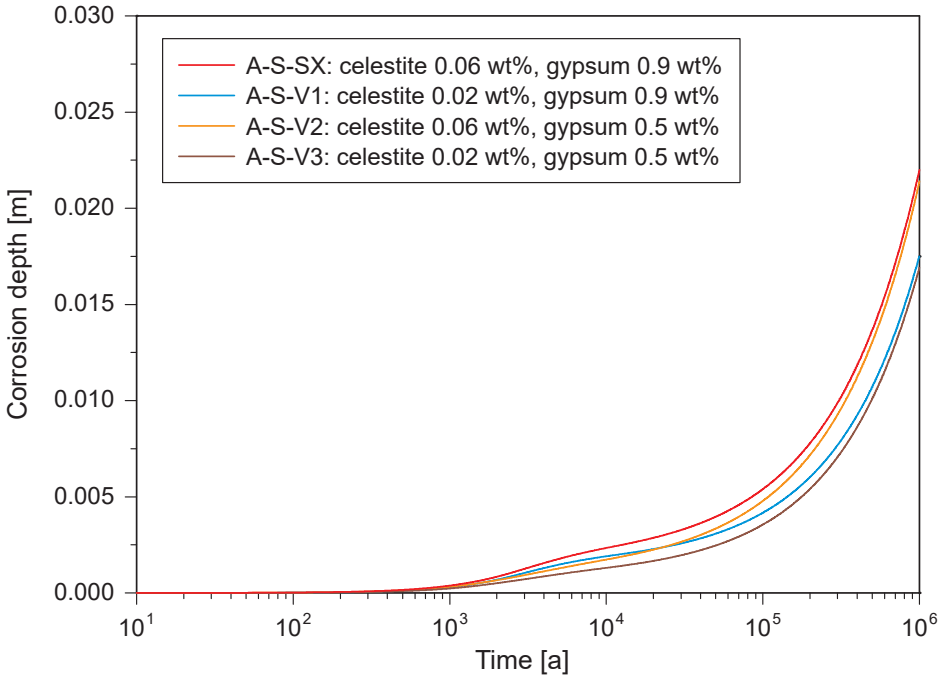

Fig. 5-5: Evolution of corrosion depth in the case A-S-SX, with 0.06 wt.-% celestite and 0.9 wt.-% gypsum (reference amounts), and in the variant cases A-S-V1, A-S-V2 and A-S-V3 in which the amounts of these minerals are varied across their respective ranges of uncertainty.

In all cases, sulphide solubility limitation is omitted.

Tab. 5-4 shows the results of a simple mass balance calculation, in which the limiting corrosion depths are presented assuming all sulphide from a given mineral source is consumed by corrosion. The table shows that, neglecting the possibility of pyrite oxidation to sulphate in the EDZ and its subsequent reduction to sulphide, the most important source of sulphide is the host rock once the dissolution front has progressed a few metres beyond the EDZ. Oxidation of pyrite is, however, a significant source of sulphide, with a potential to produce up to 3 cm of corrosion if all sulphide is consumed by reaction with the canister.

Tab. 5-4: Limiting corrosion depths assuming all sulphide from a given mineral source is consumed by corrosion.

Host rock (4 m, 6 m etc.) indicates an annular region of undisturbed host rock extending from the EDZ to a distance of 4 m, 6 m etc. from the tunnel axis.

Component	**Gypsum** [wt.-%]	**Celestite** [wt.-%]	**Pyrite** [wt.-%]	**Pryite (oxidised fraction)**	**Limiting (mass balance) corrosion depth** [m]
Buffer	0.9	0	0	0	2.86×10^{-3}
	0.5	0	0	0	1.59×10^{-3}
EDZ	0	0.06	0	0	3.05×10^{-4}
	0	0.02	0	0	1.02×10^{-4}
	0	0.02	3.7	50 %	2.89×10^{-2}
Host rock (4 m)	0	0.06	0	0	1.66×10^{-3}
Host rock (6 m)	0	0.06	0	0	4.38×10^{-3}
Host rock (8 m)	0	0.06	0	0	8.19×10^{-3}
Host rock (10 m)	0	0.06	0	0	1.31×10^{-2}

For the same reasons as above, the proportion of pyrite in the EDZ assumed to be oxidised has no impact on corrosion depth in the reference case assuming a sulphide solubility limit of 10^{-4} M. There is, however, some impact if sulphide solubility limitation is omitted. Results are shown in Fig. 5-6 for case A-S-SX, with no pyrite oxidation, and also for the variant cases for this scenario that examine the impact of the proportion of pyrite in the EDZ assumed to be oxidised to sulphate. Also shown is the impact of variations in the transport parameters for sulphate and sulphide, assuming either no pyrite oxidation or 50 % pyrite oxidation. The figure shows that increasing the assumed degree of oxidation increases the corrosion depth significantly. Increasing the diffusion coefficient in the buffer further increases corrosion depths at earlier times (up to a few thousand years) but has little effect at later times. Conversely, increasing the diffusion coefficient and hydraulic conductivity in the host rock increases the corrosion depths mainly at later times.

Finally, Fig. 5-7 shows the results for a group of cases in which no solubility limitation of sulphide concentration is assumed, compared with another group in which the reference 10^{-4} M solubility limit is imposed. The results show that, with no solubility limitation, results are sensitive to all parameters varied, namely the degree of pyrite oxidation and the transport parameters in the buffer and host rock. On the other hand, with a solubility limit constraining the sulphide concentration in the EDZ, the only parameters that affects corrosion depth are the solubility limit itself and the diffusion coefficient in the buffer.

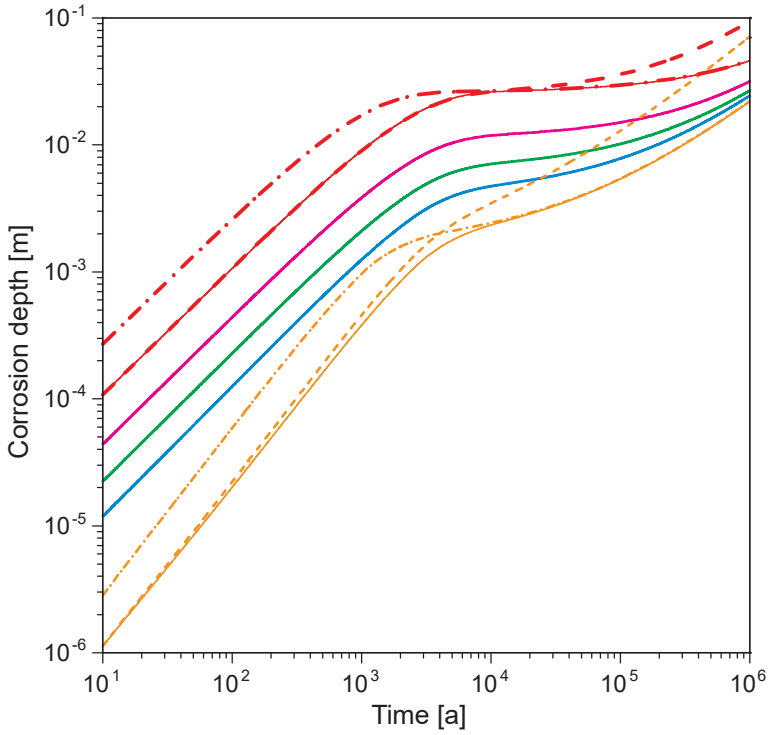

	Case	Pyrite oxidation in EDZ (initial 3.7 wt.-% pyrite assumed)	Effective diffusion coeffiient [m²/s]	
			Buffer	Rock
	A-S-SX	No oxidation	2×10^{-12}	2×10^{-12}
	A-S-C5	5 %		
	A-S-C10	10 %		
	A-S-20	20 %		
	A-S-50	50 %		
	A-S-DB	No oxidation	5×10^{-12}	
	A-S-SXA	No oxidation	2×10^{-12}	10^{-11}
	A-S-DBC50	50 %	5×10^{-12}	2×10^{-12}
	A-S-C50A	50 %	2×10^{-12}	10^{-11}

Fig. 5-6: Evolution of corrosion depth in the case A-S-SX (no pyrite oxidation), in the variant cases A-S-C5 to A-S-C50 in which the extent of pyrite oxidation in the EDZ is varied and in additional cases in which the transport parameters of the buffer and host rock are varied.

Unlimited solubility in the EDZ is assumed in these variant cases.

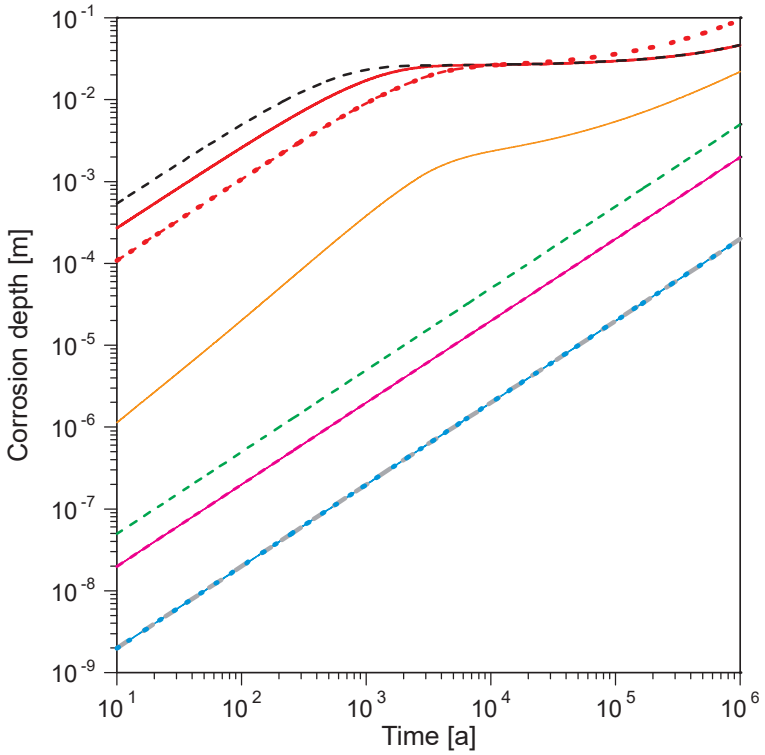

	Case	Solubility limitation in EDZ	Pyrite oxidation in EDZ	Effective diffusion coeffiient [m²/s]	
				Buffer	Rock
	A-S-RC	No limit	No oxidation	2×10^{-12}	2×10^{-12}
	A-S-C50		50 %		
	A-S-DBC50			5×10^{-12}	
	A-S-DBBC50			10^{-11}	
	A-S-C50A			2×10^{-12}	10^{-11}
	A-S-S1	10^{-4}M	No oxidation	2×10^{-12}	2×10^{-12}
	A-S-S1C50		50 %		
	A-S-S1DB		No oxidation	2×10^{-11}	
	A-S-S1DBB			5×10^{-11}	
	A-S-S1A			2×10^{-12}	10^{-11}
	A-S_DBS1C50		50 %	2×10^{-11}	2×10^{-12}

Fig. 5-7: Evolution of corrosion depth in a group of cases in which no solubility limitation of sulphide concentration is assumed, compared with another group in which the reference 10^{-4} M solubility limit is imposed (note that the results of cases A-S-S1C5, A-S-S1C10 and A-S-S1C20 are identical to those of A-S-S1C50, and are therefore not shown in the figure).

5.2 Reactive transport model

5.2.1 Case-specific model setup

Besides the reference case (A-RT-RC), four alternative calculation cases related to the solubility of sulphide are considered for scenario A as shown in Tab. 5-5.

Tab. 5-5: Overview of variant cases for scenario A calculated with the reactive transport model.

Main source of uncertainty/variability	**Case**	**Description**
Mineral constraining sulphide solubility	A-RT-RC	Constrained by mackinawite solubility
	A-RT-SP	Constrained by elemental sulphur
Arbitrary sulphide solubility limit (reduced problem, Section 5.3)	A-RT-S1	10^{-4} M
	A-RT-S2	10^{-5} M
	A-RT-S3	10^{-3} M

5.2.2 Case-specific parameter values

MX-80 buffer

The sulphide and sulphate-containing minerals in the bentonite buffer are taken from Tab. 3-1 (e.g. pyrite and gypsum). Goethite content in the buffer is estimated at 0.64 wt.-% based on Fe mass balance (Kiviranta & Kumpulainen 2011). Solid organic matter is estimated at 0.1 wt.-% based on Wersin et al. (2014). The remaining mineralogical composition of the buffer is simplified after Kiviranta & Kumpulainen (2011) to include: montmorillonite (only included for surface reactions), calcite and quartz. Under the predominantly reducing conditions chemical reactivity of pyrite under anaerobic conditions is assumed to be negligibly small (King & Wersin 2013) and the mineral is not included in the model. For cation exchange and surface protonation in the MX-80 buffer the models and parameterisation of Bradbury & Baeyens (2003), and Bradbury & Baeyens (1997), respectively, are used. Buffer porewater (presented in Tab. 5-6) is calculated by equilibrating the Opalinus Clay porewater reported by Mäder (2009), assuming equilibrium with gypsum, calcite, quartz, goethite at partial pressure of CO_2(g) equal $10^{-2.2}$ bar (corresponding to the partial CO_2 pressure in Opalinus Clay), and assuming exchanger composition reported by Bradbury & Baeyens (2003).

Opalinus Clay

The sulphide and sulphate minerals present in Opalinus Clay are taken from Tab. 3-1 and are the same in all scenarios (e.g. pyrite and celestite). Diffusion coefficients and porosity values are identical to the reference values used in the simplified transport model and can be found in Tab. 5-2. Solid organic matter was taken to be present at 0.6 wt.-% (Nagra 2014a). The remaining mineralogical composition of the Opalinus Clay is simplified after Nagra (2014a) to include: calcite, siderite, dolomite and quartz. A generic exchanger was implemented to represent cation exchange reactions with total CEC and composition reported by Mäder (2009). The Opalinus Clay porewater (shown in Tab. 5-6) was equilibrated with the clay exchanger, calcite, dolomite, quartz, celestite and siderite under CO_2(g) partial pressure of $10^{-2.2}$ bar.

EDZ

It is assumed that the mineral and porewater composition of the EDZ (presented in Tab. 5-6) corresponds to that of the undisturbed Opalinus Clay.

A Monod kinetics model is used to represent sulphate reduction. The model is parameterised using values reported by Grandia et al. (2006) for sulphate reduction using acetate as electron donor: $k_{max} = 3 \times 10^{-10}$ L/s (maximum rate constant), $k_{acetate} = 3 \times 10^{-6}$ mol/L (half-saturation constant for acetate substrate) and $k_{sulphate} = 10^{-6}$ mol/L (half-saturation constant for sulphate substrate).

The initial geochemical conditions for Opalinus Clay, EDZ, and the MX-80 buffer used in reactive transport calculations are presented in Tab. 5-6.

Tab. 5-6: Initial geochemical conditions in the OPA, EDZ, and MX-80 buffer.

	Opalinus Clay and EDZ	**Buffer**
pH	7.27	7.31
Pe	-3.08	-3.24
Eh [mV]	-182	-191
Total aq. components [mol/L]		
Na	1.67×10^{-1}	3.27×10^{-1}
Mg	5.80×10^{-3}	8.13×10^{-3}
Ca	8.08×10^{-3}	1.18×10^{-2}
Sr	3.10×10^{-4}	3.21×10^{-4}
K	1.64×10^{-3}	1.56×10^{-3}
Fe	3.8×10^{-5}	4.71×10^{-5}
Si	1.82×10^{-4}	1.82×10^{-4}
Cl	1.60×10^{-1}	1.60×10^{-1}
C	2.95×10^{-3}	3.44×10^{-3}
S(VI)	1.72×10^{-2}	1.03×10^{-1}
S(-II)	8.70×10^{-10}	8.66×10^{-10}
DOM [1]	8.33×10^{-5}	8.33×10^{-5}
Minerals [volume fraction]		
MX-80_exchanger [2]	0.00	4.74×10^{-1}
OPA_exchanger [3]	4.90×10^{-1}	0.00
Calcite	1.23×10^{-1}	1.07×10^{-3}
Dolomite	5.50×10^{-3}	0.00 [6]
Siderite	3.71×10^{-2}	0.00 [6]
Celestite	3.70×10^{-4}	0.00 [6]
Gypsum	[†]0.00 [6]	5.66×10^{-3}
Quartz	1.84×10^{-1}	2.73×10^{-2}
Goethite	0.00 [6]	2.17×10^{-3}
SOM_MX-80 [4]	0.00	1.21×10^{-4}
SOM_OPA [5]	1.23×10^{-3}	0.00
Mackinawite	0.00 [6]	0.00 [6]

[1] Dissolved organic matter (DOM) is assumed to have the generic molecular formula of CH_2O

[2] Presence of montmorillonite was considered for surface reactions (surface protonation and cation exchange) only

[3] Generic exchanger (with composition reported in Mäder (2009) was considered for Opalinus Clay

[4] Solid organic matter (SOM) in the MX-80 buffer

[5] Solid organic matter (SOM) in the Opalinus Clay and EDZ

[6] Initially absent, but allowed to precipitate if over-saturated.

5.2.3 Results

Sulphide flux [mol/a/m)] towards the canister calculated by the reactive transport model for the reference case (A-RT-RC) is shown in Fig. 5-8. The corresponding corrosion depth (proportional to the time-integrated sulphide flux) of the copper-coated canister is shown in Fig. 5-9. The total corrosion depth calculated at 1'000'000 years is ca. 82 µm.

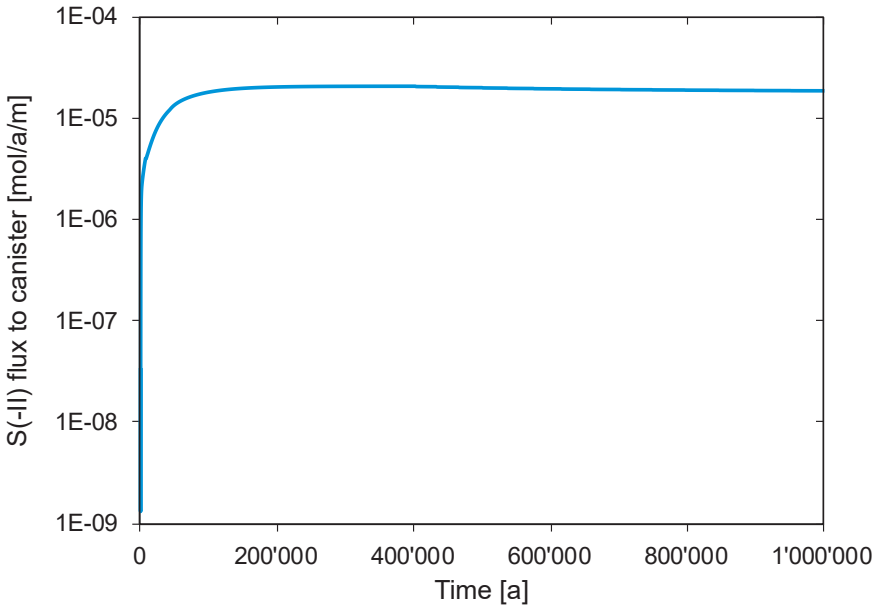

Fig. 5-8: Sulphide flux [mol/a/m] towards the canister predicted by the reactive transport model for a period of 1'000'000 years considering well-emplaced MX-80 buffer for A-RT-RC.

The flux is expressed as per 1 metre tunnel length which corresponds to 3.29 m^2 canister surface.

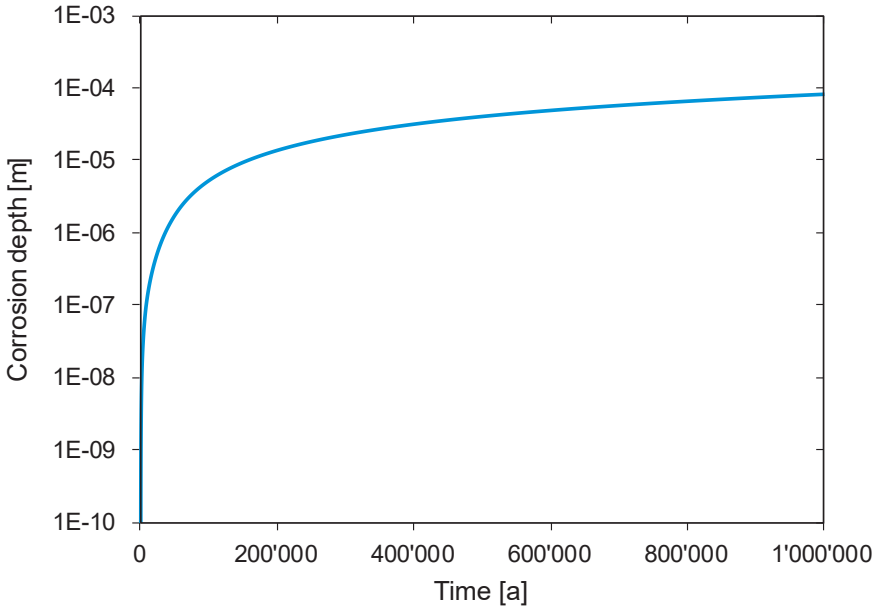

Fig. 5-9: Corrosion depth of copper canister predicted by the reactive transport model for a period of 1'000'000 years considering well-emplaced MX-80 buffer.

Sulphide in the EDZ ("source term")

Sulphide is generated in the EDZ by sulphate-reducing microorganisms. The released sulphide undergoes a fast reaction with Fe to precipitate mackinawite (FeS). Iron required for mackinawite formation is provided by the dissolution of siderite. Acidification associated with microbial activity has an important influence on sulphide solubility due to mackinawite equilibrium. The evolution of total dissolved sulphide, total dissolved Fe(II) and pH at a point located in the middle of the EDZ is shown in Fig. 5-10. The pH correlates negatively with sulphide concentration in agreement with mass action equation for the reaction of mackinawite solubility (see Eq. 4-9). As will be discussed later in Section 5.3, variations in dissolved sulphide in the EDZ (due to mackinawite equilibrium) have a significant influence on sulphide gradients towards the canister, and hence on sulphide fluxes and corrosion rates.

Mackinawite precipitation is enhanced at the EDZ contact with the buffer and Opalinus Clay (Fig. 5-11), where the concentration of dissolved organics is increased due to diffusive transport from the Opalinus Clay and buffer (the concentration of dissolved organics in the EDZ is locally depressed due to microbial activity).

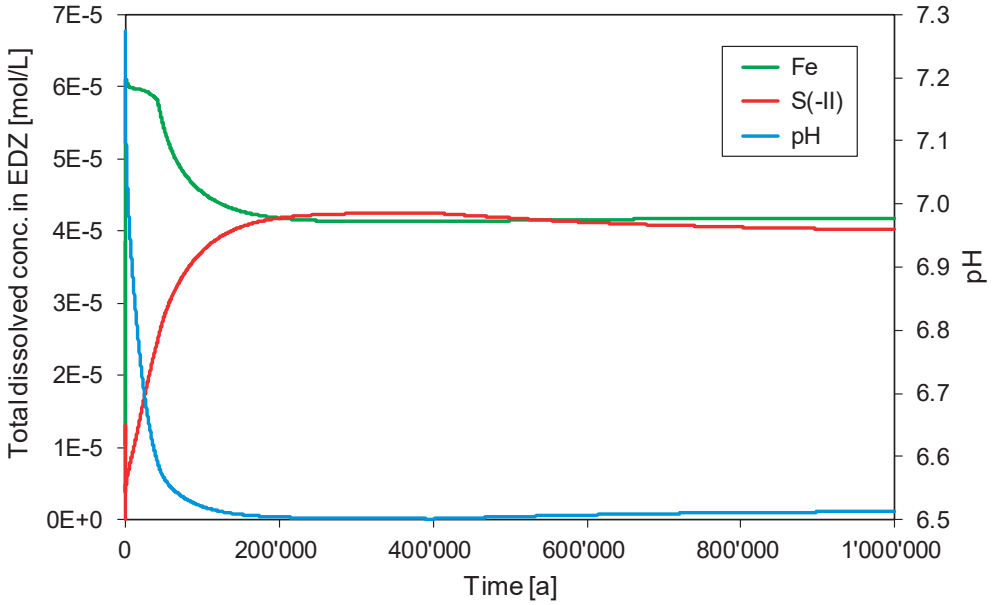

Fig. 5-10: Concentration of total dissolved sulphide S(-II) and total dissolved iron Fe(II) [mol/L], and pH in the EDZ porewater as a function of time calculated by the reactive transport model.

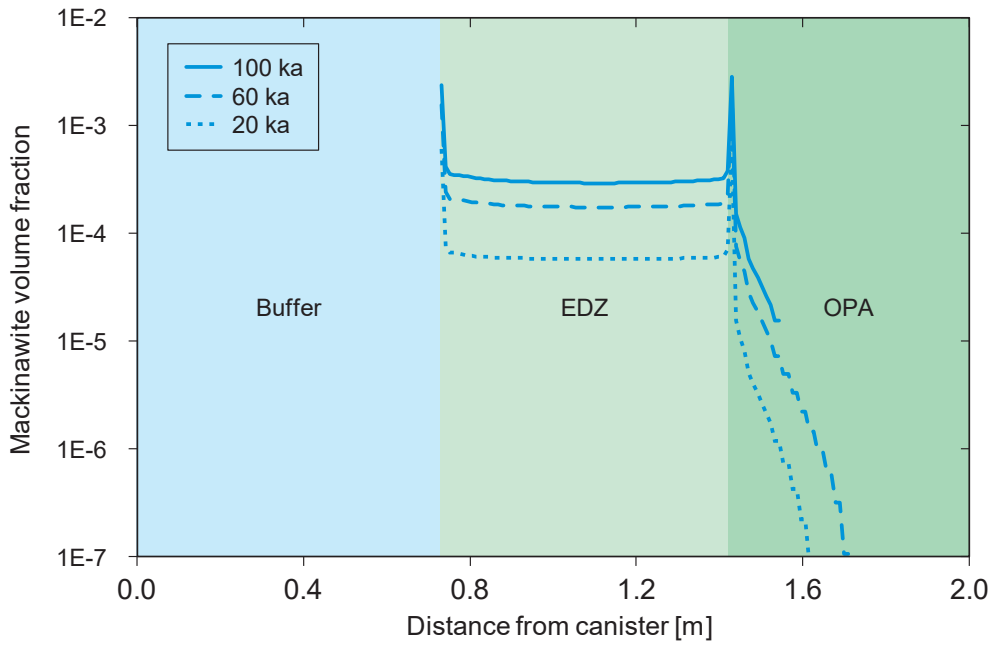

Fig. 5-11: Radial profiles (from canister surface into the Opalinus Clay) of mackinawite mineral volume fractions (-) across the buffer, EDZ and adjacent portions of Opalinus Clay at 20'000, 60'000 and 100'000 years calculated by the reactive transport model.

Sulphide transport and immobilisation

No mackinawite precipitation occurs within the buffer because sulphide is undersaturated with respect to this mineral due to fast sulphide consumption at the canister surface by copper corrosion (Fig. 5-11). Therefore, no sulphide retardation (mackinawite precipitation) process in the buffer is predicted by the model. Consequently there is a direct dependence of the calculated corrosion depth (proportional to the integrated sulphide flux towards the canister) on the dissolved sulphide concentration in the EDZ. This is shown in Fig. 5-12, which demonstrates how the sulphide flux towards the canister correlates with the dissolved sulphide concentration in the EDZ.

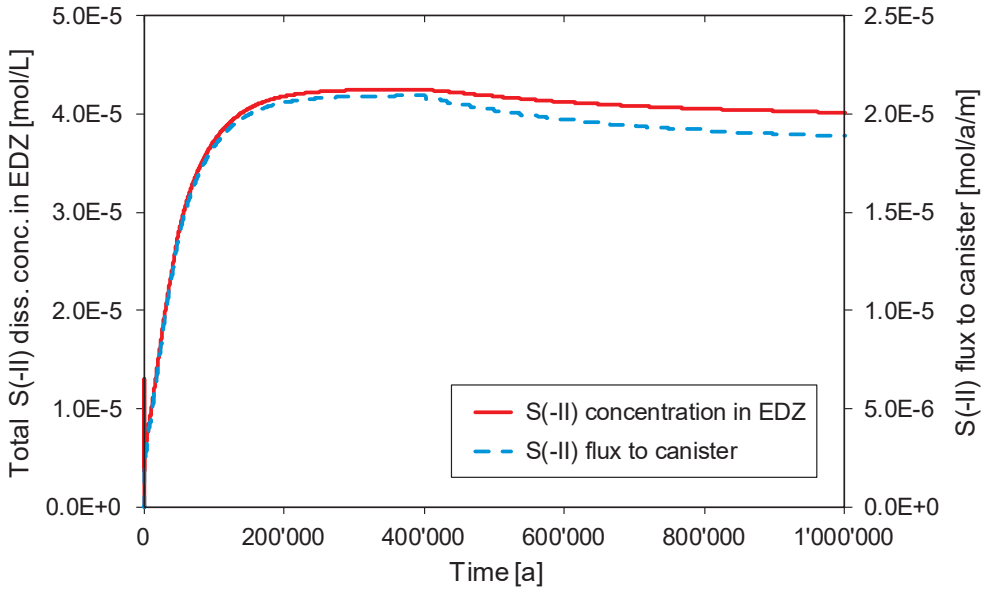

Fig. 5-12: Correlation between the total dissolved sulphide concentration in the EDZ and sulphide flux towards the canister in time.

Elemental sulphur is oversaturated in this model and therefore its precipitation is also possible However, the solubility of elemental sulphur has a stronger dependence on redox potential, than mackinawite solubility. Given the larger uncertainty regarding redox potential in the repository system, it was chosen not to include the precipitation of elemental sulphur in the reference case of the model. To illustrate the impact of the precipitation of elemental sulphur, a calculation case explicitly considering S(0) is compared to the reference case (see Fig. 5-13). The results suggest that the effect of potential sulphur precipitation in the buffer at 1'000'000 years would reduce corrosion by approximately a factor of ten (9 µm considering S(0) precipitation compared to 82 µm when the precipitation of S(0) is neglected).

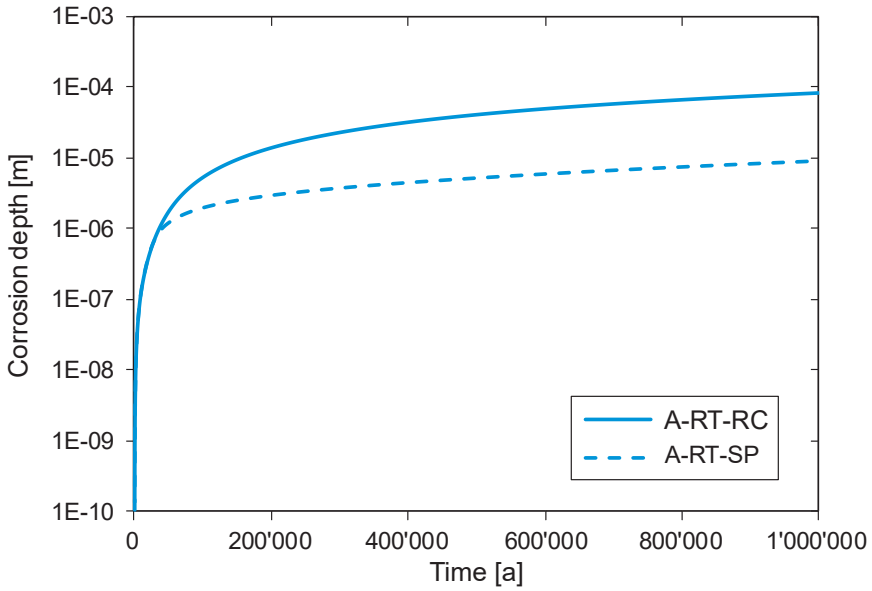

Fig. 5-13: Comparison of copper corrosion depths calculated by the reactive transport without allowing the precipitation of elemental sulphur (Base Case, solid line), and allowing the precipitation (dashed line).

5.3 Comparison of results obtained by the simplified and reactive transport models

Benchmark using a "reduced" problem

Before setting out to compare the results obtained for scenario A by the two modelling approaches let us consider a reduced problem, where in the reactive transport model the solubility of dissolved sulphide in the EDZ is fixed to a maximum value of ca. 10^{-4} M, 10^{-5} M or 10^{-3} M by a single "dummy" mineral phase (cases A-RT-S1, A-RT-S2, A-RT-S3). The sulphide concentrations are therefore decoupled from the Fe concentration and the pH, and the precipitation of mackinawite is excluded from the model. This reactive transport calculation is directly comparable with the results of the simplified model calculated for cases A-S-S1, A-S-S2 and A-S-S3 shown in Fig. 5-6 (sulphide solubility limit of 10^{-4}, 10^{-5} and 10^{-3} mol/L respectively). This exercise allows a better understanding of the conceptual differences between the simplified and reactive transport approaches, which is a necessary prerequisite to quantitatively compare results calculated by the two models.

Fig. 5-14 presents a comparison of results obtained using the simplified model and using the reduced reactive transport models for a period of 1'000'000 years. It can be seen from the figure that the total corrosion depths calculated using the two models closely agree at longer times, but corrosion depths calculated by the reactive transport model lag behind those predicted by the simplified model during the initial several thousands of years. The main reason for the apparent initial discrepancy is the fact that while the reactive transport model solves a time-dependant diffusion equation, the simplified model assumes a steady-state diffusion profile (with a variable position of the mineral dissolution fronts) from the start of the calculation.

The main consequence of this is that at the start of calculations, the simplified model over-estimates sulphide fluxes to the canister and the corresponding corrosion depth, while the reactive transport model explicitly calculates the approach to a steady-state (sulphide fluxes to canister increase gradually). However, the presented benchmark exercise allows us to conclude that this simplification on the part of the simplified model is only noticeable during relatively short initial times, but has no practical significance on longer (than several thousands of years) time scales.

It is noteworthy that in the scenario presented here there is no sulphide immobilisation in the buffer. Should there be significant sulphide or elemental sulphur precipitation in the buffer, the calculated corrosion depths would be generally lower.

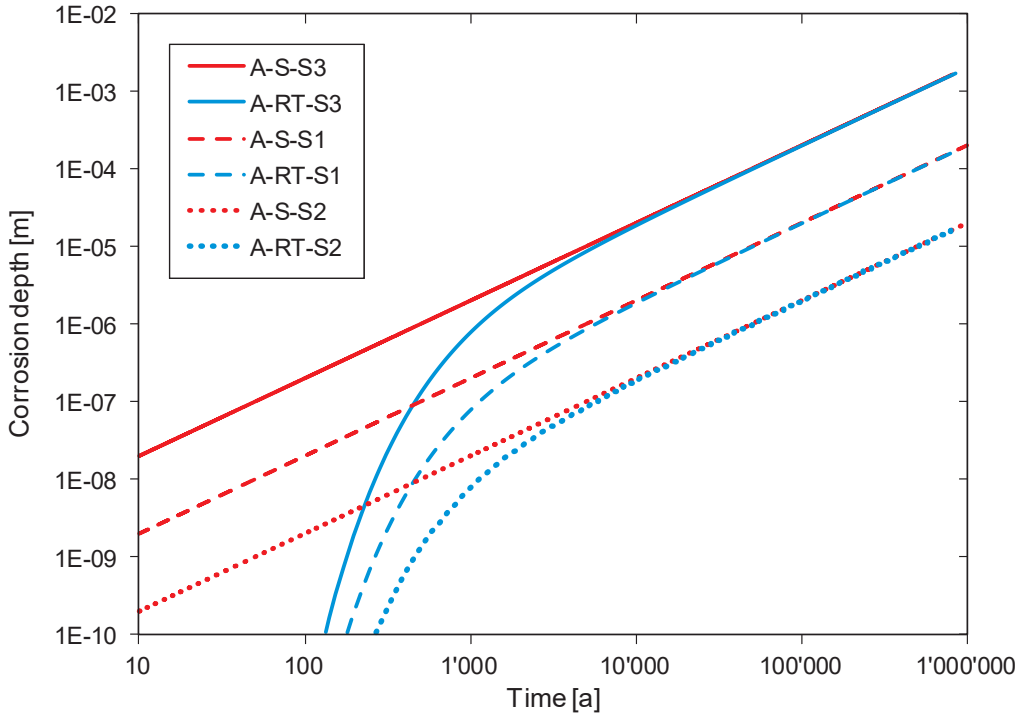

Fig. 5-14: Comparison of results obtained by the simplified model (red lines) and the reactive transport model (blue lines) for a reduced problem, where sulphide solubility is controlled to maximum values of 10^{-3} mol/L (solid lines), 10^{-4} mol/L (dashed lines), and 10^{-5} mol/L (dotted lines).

"Simplified" – simplified model (red lines), "RT" – reactive transport model (blue lines).

Comparison for the "full" problem

Comparison of results on copper corrosion depth predicted by the simplified model (for three different sulphide solubility values: 10^{-3}, 10^{-4} and 10^{-5} mol/L) and calculated using the reactive transport model is shown in Fig. 5-15. It should be noted that, unlike in the reduced problem discussed above, in the full reactive transport model, the concentration of sulphide in the EDZ is controlled by mackinawite, whose solubility is not fixed, but depends on porewater chemistry (mainly pH) as shown in Fig. 5-10.

We have shown (Fig. 5-12) that the calculated corrosion depth is dependent (directly proportional) on sulphide concentration in the EDZ. This is because in both modelling approaches sulphide concentration in the EDZ defines the sulphide concentration gradient (while there is no appreciable sulphide immobilisation in the buffer in both modelling approaches), and therefore sulphide flux, towards the canister. Therefore, the comparison of the calculated corrosion depth shown in Fig. 5-15 is explained primarily in terms of varying sulphide concentration in the EDZ. In addition, during the initial several hundred years, the corrosion depth predicted by the RT model is lower than that calculated by the simplified model due to distinct treatment of diffusion in the two models (steady-state vs. time-dependent diffusion) as explained in the *Benchmark using a "reduced" problem* sub-section above.

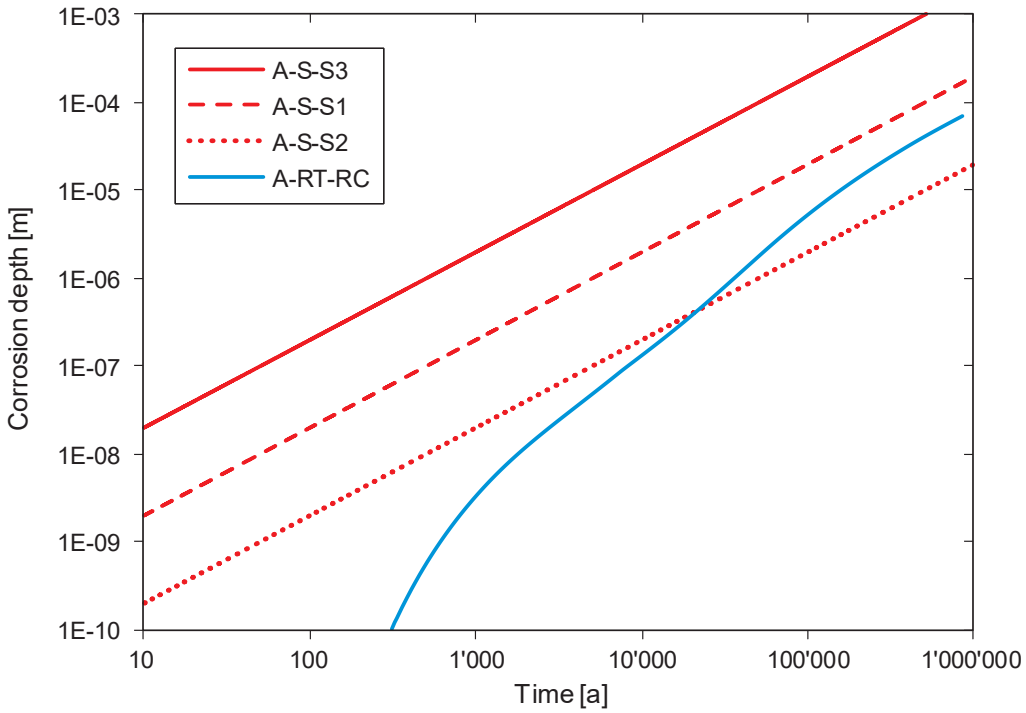

Fig. 5-15: Comparison of copper corrosion depths calculated by the simplified model for three distinct sulphide solubility values: 10^{-3} M (AS-S-S3), 10^{-4} M (AS-S-S1) and 10^{-5} M (AS-S-S2) and calculated using the reactive transport model (A-RT-RC).

6 Near field with a reduced bentonite density

6.1 Simplified model

6.1.1 Case-specific model set-up

The scenario in which the near field contains a buffer with a reduced density (scenario B) has been analysed using the simplified model, as described in Section 4.2.3. Mineral a, the dominant soluble sulphate mineral in the EDZ, is again taken to be celestite. Celestite is also taken to be mineral c, the dominant soluble sulphate mineral in the remainder of the host rock. Mineral b, the dominant soluble sulphate mineral in the buffer, is again taken to be gypsum.

The dry density of the buffer is assumed to be lower than that of the well-emplaced buffer considered in Chapter 5, and the effective diffusion coefficient is assumed to be higher (see Tab. 6-2). Reduction of aqueous sulphate ions to sulphide ions occurs from the beginning of the modelled period in both the bentonite buffer and in the EDZ, where they may precipitate in the form of sulphide minerals.

Four calculation cases are considered for this scenario, including a reference case (B-S-RC) and three variant cases that examine the impact of uncertainties related to:

- solubility limitation of sulphide produced by sulphate-reducing bacteria in the buffer and EDZ (case B-S-S2), and
- sulphide diffusion coefficient in the buffer (cases B-S-DB and B-S-DBS2), the second case in combination with a reduced sulphide solubility.

The reference and variant cases are summarised in Tab. 6-1.

Tab. 6-1: Overview of reference case and variant cases for scenario B calculated with the simplified model.

Main source of uncertainty/variability	**Case**	**Description**
Reference case	B-S-RC	Solubility limit 10^{-4} M, reference diffusion coefficient
Solubility limitation of the concentration of sulphide produced by sulphate-reducing bacteria in the buffer and EDZ (10^{-4} M assumed in reference case B-S-RC)	B-S-S2	10^{-5} M
Diffusion coefficient of sulphide in the buffer	B-S-DB	Increased the diffusion coefficient
	B-S-DBS2	Increased the diffusion coefficient and reduced sulphide solubility (10^{-5} M)

Diffusion is assumed to be the only relevant process in the host rock (as well as elsewhere in the modelled system), since advection was found to be negligible in the analysis of the well-emplaced buffer (Chapter 5).

6.1.2 Case-specific parameter values

Case-specific parameter values for the four variant cases are considered for this scenario are given in Tab. 6-2.

Concerning the solubility limitation of the concentration of sulphide produced by sulphate-reducing bacteria in the EDZ, the reference case in scenario B assumes a solubility limit of 10^{-4} M (see Section 2.2), and the variant cases B-S-DB and B-S-DBS2, a solubility limit of 10^{-5} M.

Tab. 6-2: Parameter values used to analyse scenario B with the simplified model.

Reference values are used for all cases unless otherwise stated. General data are shown in Tab. 3-1.

Data for the undisturbed host rock				
Parameter	**Symbol**	**Units**	**Cases**	**Values**
Effective diffusion coefficient (sulphate)	$D_{e,c}$	m^2/s	All cases	2×10^{-12}
Effective diffusion coefficient (sulphide)	$D_{e,sr}$	m^2/s	All cases	2×10^{-12}
Amount of celestite	w_c	wt.-%	All cases	0.06
Data for the EDZ				
Effective diffusion coefficient (sulphide)	$D_{e,sz}$	m^2/s	All cases	10^{-11}
Amount of celestite (includes effective values, see Tab. 7-3)	w_a	wt.-%	All cases	0.06
(Molar) solubility limit: sulphide minerals	S_s	mol/m^3	All other cases	0.1 (i.e. 10^{-4} M)
			B-S-S2, B-S-DBS2	0.01 (i.e. 10^{-5} M)
Data for the buffer				
Dry density	ρ_b	kg/m^3	All cases	1300
Effective diffusion coefficient (sulphide)	$D_{e,sb}$	m^2/s	All other cases	2.4×10^{-11}
			B-S-DB, B-S-DBS2	10^{-10}
(Molar) solubility limit: sulphide minerals	S_s	mol/m^3	All other cases	0.1 (i.e. 10^{-4} M)
			B-S-S2, B-S-DBS2	0.01 (i.e. 10^{-5} M)
Amount of gypsum	w_b	wt.-%	All cases	0.9

6.1.3 Results

In scenario B, both the buffer and the EDZ constitute reactive zones in which microbial reduction of sulphate to sulphide takes place. It is thus assumed, at the outset of calculations for this scenario, that all gypsum has dissolved and the sulphate reduced to sulphide, which then precipitates as sulphide minerals. These minerals then gradually dissolve and a dissolution front develops in the buffer, starting at the canister surface and moving outwards into the buffer and eventually

into the EDZ. At the same time, a sulphate (celestite) dissolution front develops in the host rock, beginning at the interface with the EDZ and again moving progressively outwards (see Fig. 4-2). The progress of these fronts over time in the reference case (B-S-RC) and in case B-S-S2 for the present scenario is shown in Fig. 6-1.

In the reference case, the sulphide mineral dissolution front reaches the inner boundary of the EDZ at around 300'000 years, and reaches the outer boundary of the EDZ some 200'000 years later. In case B-S-S2, this front remains within the buffer throughout the million year calculation period. As in the case of the well-emplaced buffer, the celestite front extends only 10 m from the tunnel axis after around 400'000 years, justifying the assumption that the emplacement drifts, which have a separation of some tens of metres, can be assumed to evolve largely independently of one another.

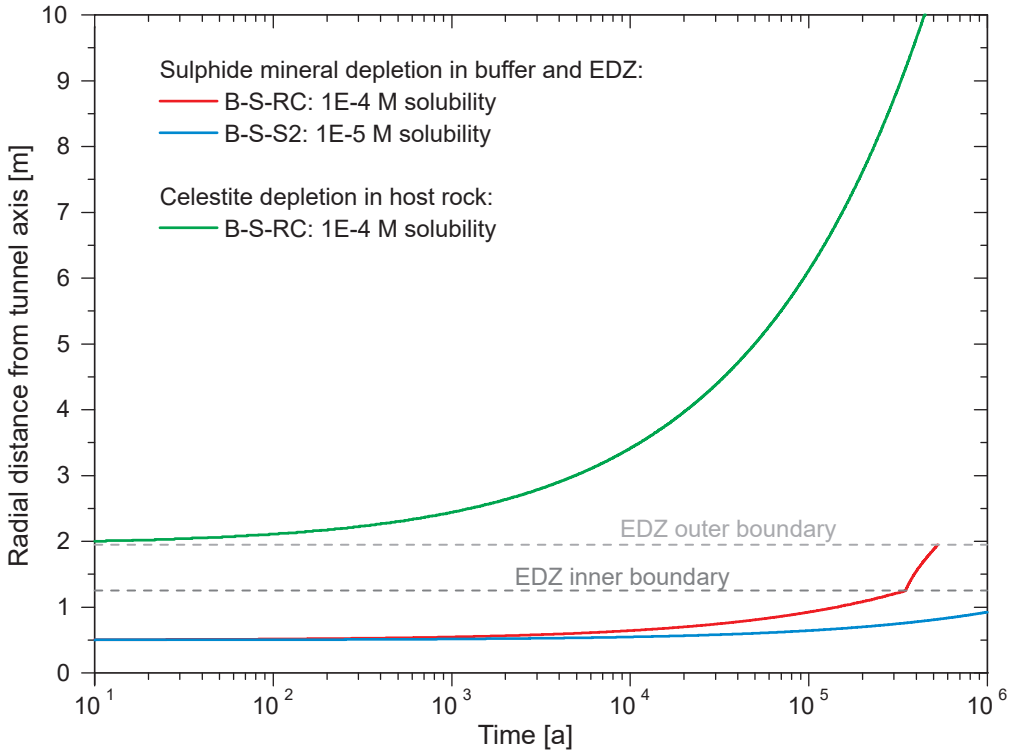

Fig. 6-1: Evolution of celestite and sulphide-mineral dissolution fronts in the reference case B-S-RC and in case B-S-S2 with reduced sulphide solubility.

Note: the celestite depletion fronts in the two cases are identical.

Sulphate from celestite dissolution in the host rock migrates to the EDZ by diffusion, where it is reduced to sulphide. Fig. 6-2 shows this sulphate flux to the EDZ as a function of time, and also the sulphide fluxes to the canister surface and into the rock from the EDZ, in the reference case and in case B-S-S2, which assumes a lower sulphide solubility. In the reference case, the line showing the sulphide flux to the canister surface has an inflection at 300'000 years, which is the time at which the sulphide mineral dissolution front reaches the EDZ, and a further inflection 200'000 years later when the outer boundary of the EDZ is reached. These two inflections separate the three evolution phases that are distinguished in scenario B, as explained in Section 4.2.3. In case B-S-S2, the first phase lasts to the end of the million years modelled period and thus no inflection points are visible.

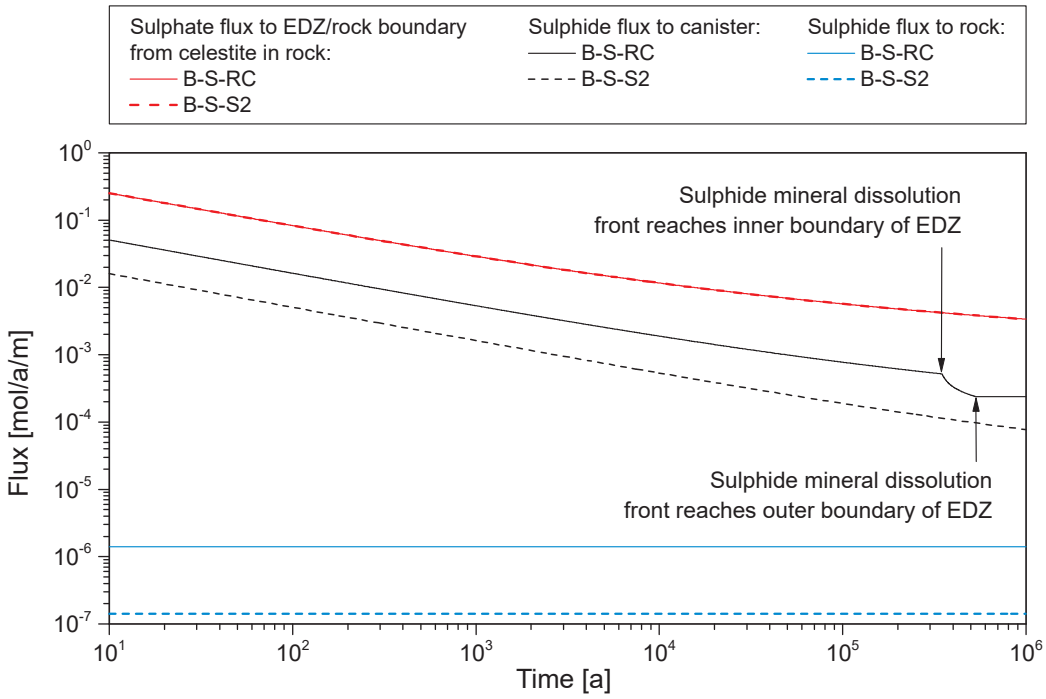

Fig. 6-2: Evolution of sulphate and sulphide fluxes in the reference case B-S-RC and in case B-S-S2 with reduced sulphide mineral solubility.

The figure shows the times at which the sulphide mineral dissolution front reaches the inner and outer boundaries of the EDZ.

Fig. 6-2 shows that the sulphate flux to the EDZ/host-rock boundary due to dissolution of celestite (red curves) exceeds the other fluxes in both calculation cases. This sulphate is then reduced to sulphide at the boundary and either accumulates there as precipitated minerals, or diffuses from there to the canister surface or back into the rock. The figure also shows that the sulphide flux to the rock is small compared with the flux to the canister surface, and that both of these fluxes are reduced in case B-S-S2 compared with the reference case, by a factor of 10 in the case of flux to the rock and around a factor of 3 in the case of the flux to the canister surface. Regarding the flux to the canister surface, the impact of lower dissolved sulphide concentration due to lower solubility in case B-S-S2 comparered with B-S-RC is partly offset by the slower migration of the dissolution front, which results is smaller diffusion distances from the front to the canister, and hence faster diffusion.

Fig. 6-3 shows the same fluxes in the reference case B-S-RC and in cases B-S-DB and B-S-DBS2, where a higher buffer diffusion coefficient for sulphide is assumed. The figure shows, as expected, that increasing the buffer diffusion coefficients increases the sulphide flux to the canister. This increase is offset in B-S-DBS2 by the reduced solubility assigned to sulphide.

The evolution of corrosion depth in the reference case B-S-RC and in case B-S-S2 in the present scenario is shown in Fig. 6-4, along with the corresponding cases with the same solubility limits in the scenario with a well-emplaced buffer (i.e. cases A-S-S1 and A-S-S2). The present scenario is clearly less favourable, giving corrosion depths around an order of magnitude higher than in the scenario with the well-emplaced buffer.

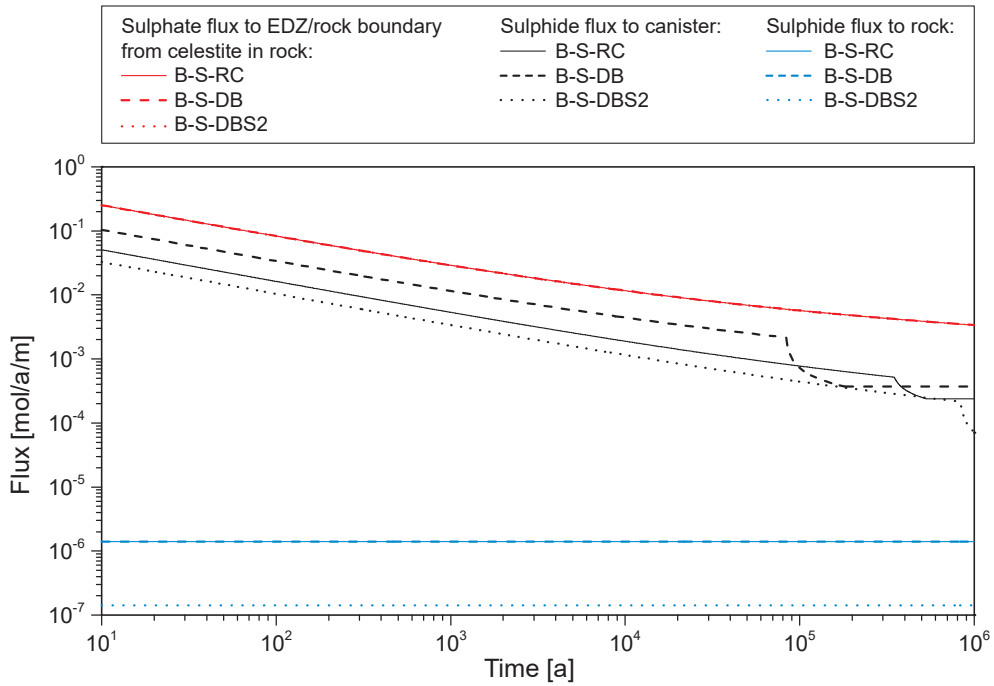

Fig. 6-3: Evolution of sulphate and sulphide fluxes in the reference case results B-S-RC, in case B-S-DB with increased diffusion coefficient for sulphide in the buffer and in case B-S-DBS2 with reduced sulphide mineral solubility and increased diffusion coefficients for sulphide in the buffer.

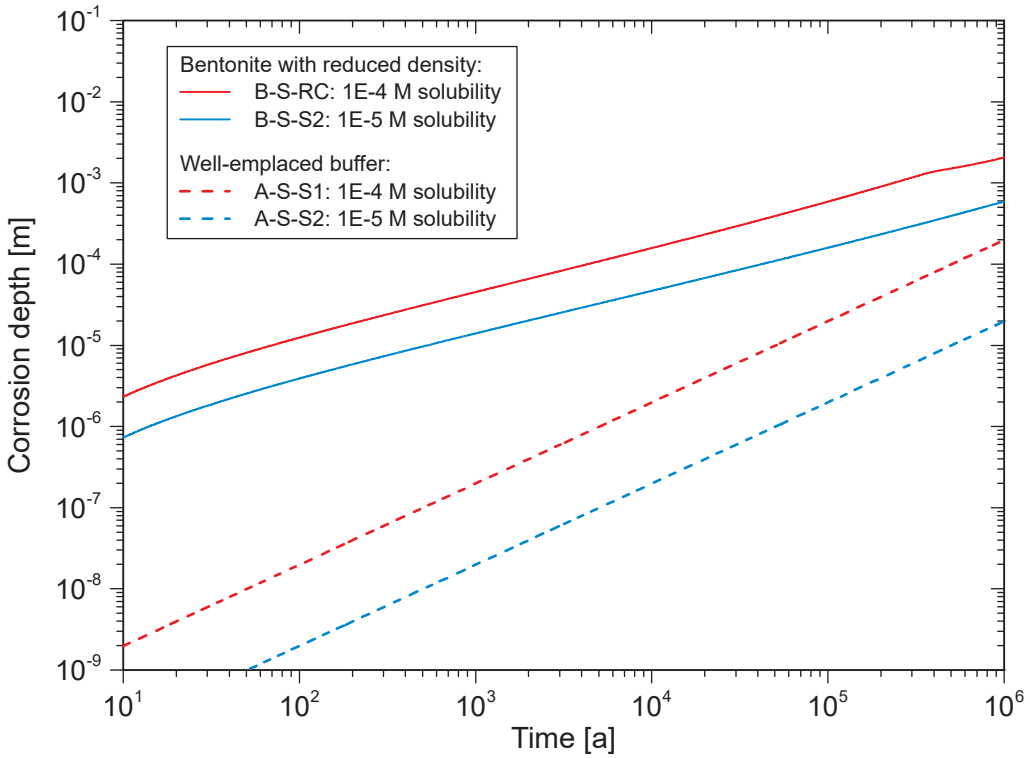

Fig. 6-4: Evolution of corrosion depth in the reference case B-S-RC, in case B-S-S2 and in the corresponding cases with the same solubility limits in the scenario with a well-emplaced buffer (A-S-S1 and A-S-S2).

6.2 Reactive transport model

6.2.1 Case-specific model set-up

Two calculation cases were considered in this scenario:

- Microbial sulphate reduction is absent in the buffer, but present in the EDZ (case B-RT-MA1)
- Microbial sulphate reduction occurs both in the buffer and EDZ (case B-RT-MA2)

Tab. 6-3: Overview of calculation cases for scenario B calculated with the reactive transport model.

Main source of uncertainty/variability	**Case**	**Description**
Location of potential microbial activity	B-RT-MA1	Microbial activity in EDZ only
	B-RT-MA2	Mircobial activity in buffer and EDZ

6.2.2 Case-specific parameter values

The geochemical model (including all parameter values) used in this scenario is the same as that defined for the well-emplaced bentonite buffer (Section 5.2.2). In both scenarios the sulphide solubility is constrained by mackinawite.

Similarly to the simplified transport model, the effective diffusion coefficient of sulphide and sulphate in the buffer (2.4×10^{-11} m^2/s) is enhanced by a factor of approximately ten compared with the well-emplaced MX-80 buffer case (2.0×10^{-12} m^2/s). This value was used in both of the above-mentioned alternative calculation cases. An important result of microbial sulphate reduction taking place in the buffer is that sulphide is generated close to and directly at the canister surface. Consequently, the control of sulphide transport on canister corrosion should be less pronounced than when sulphide generation is restricted to the EDZ only (A-RT-RC).

The initial geochemical conditions for Opalinus Clay, EDZ, and the MX-80 buffer used in reactive transport calculations are presented in Tab. 5-6.

6.2.3 Results

In Figure 6-5, sulphide fluxes [mol/(m·y)] towards the canister calculated using the RT model for a period of 1'000'000 years are shown for the well-emplaced bentonite buffer, for the reduced density buffer with no sulphate-reducing microbial activity in the buffer (only in the EDZ), and for reduced density buffer with sulphate-reducing microbial activity in the buffer.

Corrosion depths of the copper canister (proportional to time-integrated sulphide flux towards the canister) predicted by the RT model during a period of 1'000'000 years for the scenario with a reduced density MX-80 buffer (with and without microbial sulphate reduction in the buffer, but with microbial activity present in the EDZ in both cases) are shown in Fig. 6-6, and compared with the results calculated for the well-emplaced MX-80 buffer. The predicted corrosion depths for the cases without (case B-RT-MA1) and with (case B-RT-MA2) sulphate-reducing microbial activity in buffer are ca. 1 mm and 1.3 mm, respectively, at 1'000'000 years. On the other hand, the sole difference between the calculations for a well-emplaced MX-80 buffer (case A-RT-RC)

and those for the reduced density MX-80 buffer without sulphate-reducing microbial activity in the buffer (B-RT-MA1) is the value of the effective diffusion coefficient in the buffer (2.0×10^{-12} m^2/s and 2.4×10^{-11} m^2/s, respectively). This is reflected in the difference in corrosion depth between these two cases, which is about one order of magnitude. Notably, sulphide fluxes in the case with the reduced density MX-80 buffer with microbial activity in the buffer (B-RT-MA2) decrease after ca. 380'000 years – this is predicted due to complete solid sulphate (celestite formed by earlier dissolution of gypsum) consumption in the buffer.

Fig. 6-7, which is a zoom-in of Fig. 6-6 in the early period, indicates that with microbial activity in the buffer (sulphide generation occurs directly at the canister surface) corrosion proceeds at an approximately constant rate from early times of the calculation, with no appreciable lag in the onset of corrosion due to diffusive transport of sulphide across the buffer as is the case when microbial activity is restricted to the EDZ.

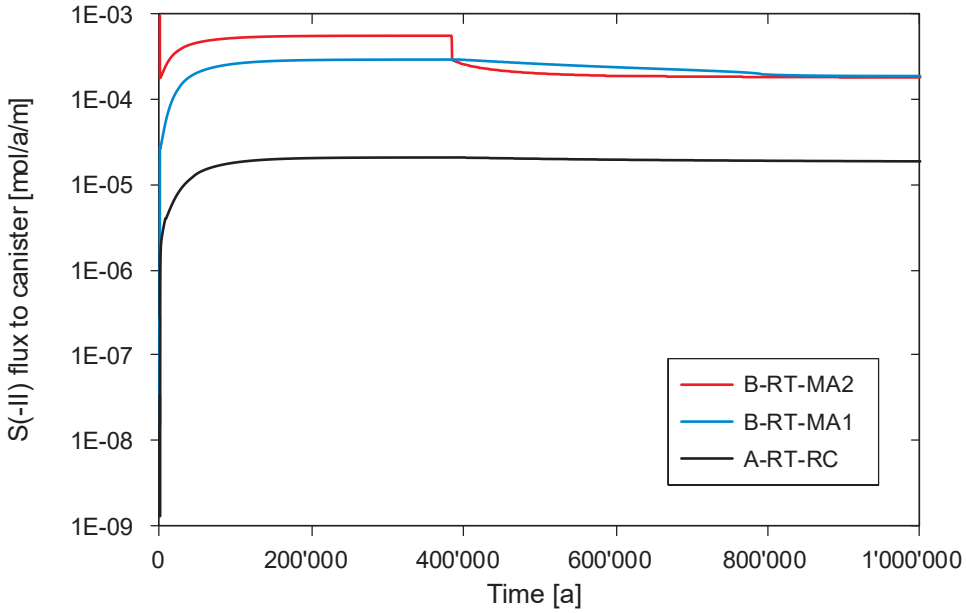

Fig. 6-5: Comparison of sulphide fluxes towards the canister predicted by the reactive transport model during a period of 1'000'000 years for three calculation cases (reference case A-RT-RC and two calculation cases with the presence and absence of microbial activity in the buffer: B-RT-MA2 and B-RT-MA1).

The flux is expressed as per 1 metre tunnel length which corresponds to 3.29 m^2 canister surface.

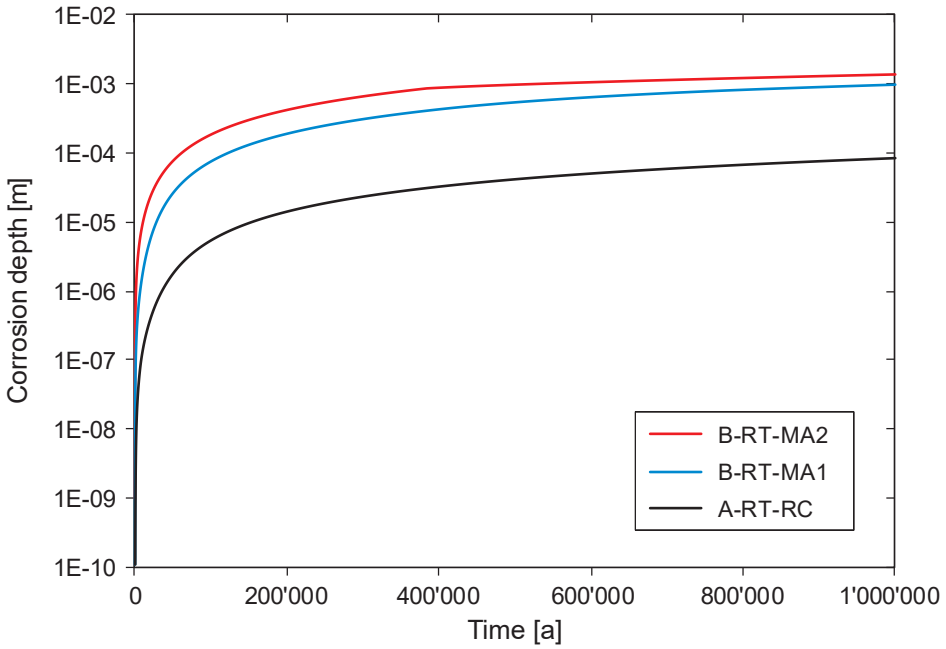

Fig. 6-6: Comparison of copper corrosion depths predicted by the reactive transport model during a period of 1'000'000 years for three calculation cases (reference case A-RT-RC and two calculation cases with the presence and absence of microbial activity in the buffer: B-RT-MA2 and B-RT-MA1).

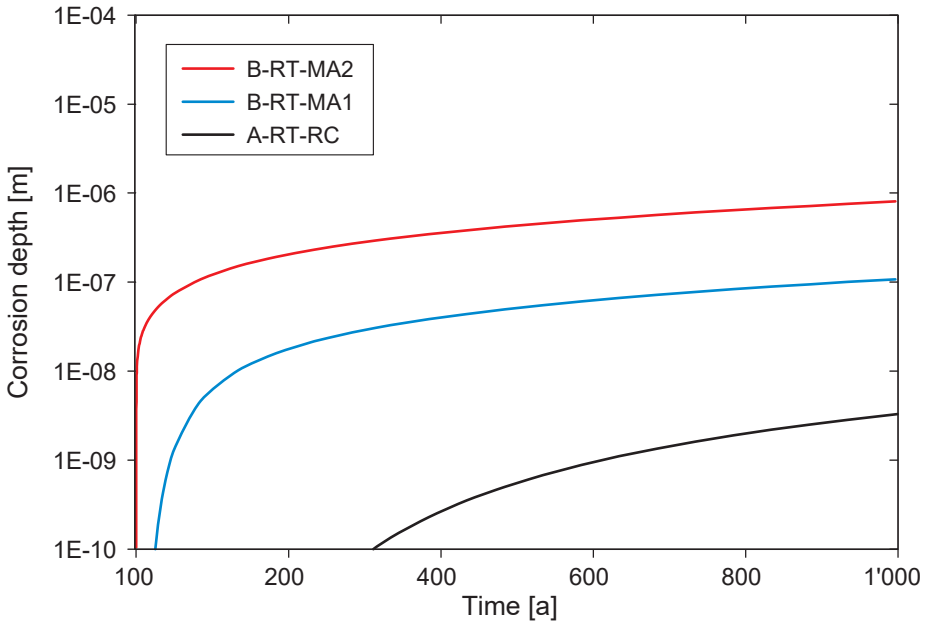

Fig. 6-7: Comparison of copper corrosion depths predicted by the reactive transport model during a period of 1'000 years (zoom-in of Fig. 6-6).

See caption of Fig. 6-6 for additional details.

6.3 Comparison of results obtained by the simplified and reactive transport models

Fig. 6-8 shows a comparison of copper corrosion depths for scenario B calculated using the simplified model (for two distinct sulphide solubility values: 10^{-4} and 10^{-5} mol/L) and calculated using the reactive transport model, assuming mackinawite as solubility limiting phase. All shown cases consider activity of sulphate-reducing bacteria both in the buffer and EDZ. Similarly to scenario A, the reactive transport model predicts lower corrosion depths than the simplified model, because of the difference of steady state vs time-dependent diffusion. At 1'000'000 years, however, the difference between both models becomes negligible. The corrosion depth is, however, one order of magnitude larger than the corrosion depth in scenario A (not shown in Fig. 6-8).

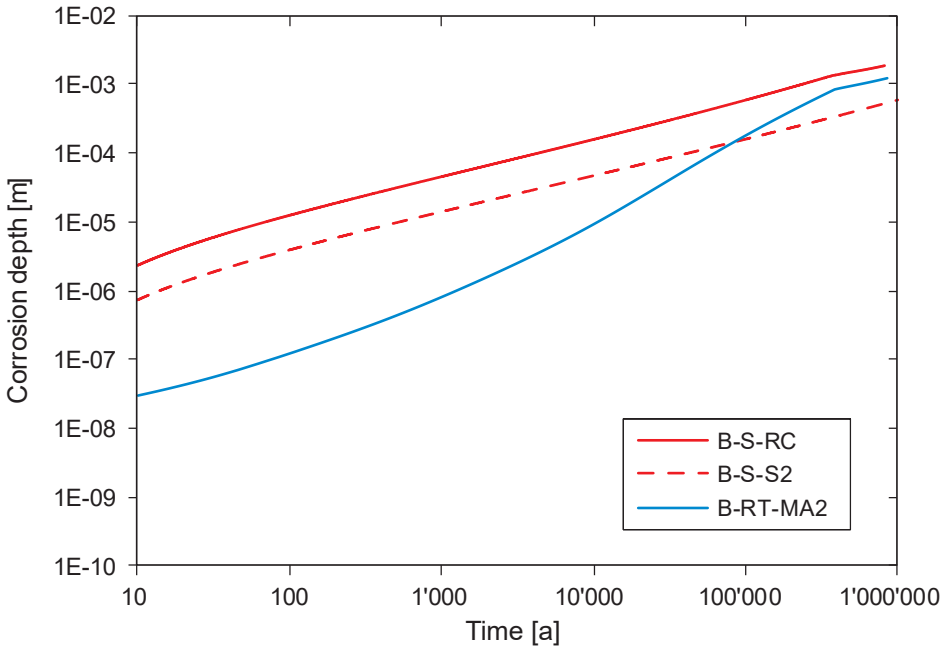

Fig. 6-8: Comparison of copper corrosion depths calculated by the simplified model cases B-S-RC (sulphide solubility limit of 10^{-4} M) and B-S-S2 (sulphide solubility limit of 10^{-5} M), and calculated by the reactive transport model (B-RT-MA2).

7 Near field containing crushed Opalinus Clay buffer

7.1 Simplified model

7.1.1 Case-specific model set-up

The scenario in which the near field contains crushed Opalinus Clay (scenario C) has also been analysed using the simplified model, as described in Section 4.2.3. Mineral a, the dominant soluble sulphate mineral in the EDZ, is again taken to be celestite. Celestite is also taken to be mineral c, the dominant soluble sulphate mineral in the remainder of the host rock. Mineral b, the dominant soluble sulphate mineral in the buffer, is taken to be celestite in the reference case. In addition, however, alternative calculation cases are considered in which a fraction of the pyrite in the crushed Opalinus Clay is assumed to be oxidised during the handling, crushing or emplacement operations to sulphate.

Reduction of sulphate to sulphide occurs before the beginning of the modelled period in both the crushed Opalinus Clay and in the EDZ, where it may precipitate in the form of sulphide minerals.

Seven calculation cases are considered for this scenario, including a reference case (C-S-RC). Variant calculation cases are defined that examine the impact of uncertainties related to:

- the solubility limitation of concentration of sulphide produced by sulphate-reducing bacteria in the buffer and EDZ (case C-S-S2), and
- the proportion (if any) of pyrite in the crushed Opalinus Clay assumed to be oxidised to sulphate (cases C-S-C5 to C-S-C100)

The reference and variant cases are summarised in Tab. 7-1.

Tab. 7-1: Overview of reference and variant cases for scenario C calculated with the simplified model.

Main source of uncertainty/variability	**Case**	**Description**
Reference case	C-S-RC	Solubility limit 10^{-4} M, no pyrite oxidation
Solubility limitation of the concentration of sulphide produced by sulphate-reducing bacteria in the buffer and EDZ	C-S-S2	10^{-5} M
Proportion of pyrite in crushed Opalinus Clay assumed to be oxidised to sulphate (initial 3.7 wt.-% pyrite assumed)	C-S-C5	5 % pyrite oxidation, solubility limit 10^{-4} M,
	C-S-C10	10 % pyrite oxidation, solubility limit 10^{-4} M,
	C-S-C20	20 % pyrite oxidation, solubility limit 10^{-4} M,
	C-S-C50	50 % pyrite oxidation, solubility limit 10^{-4} M,
	C-S-C100	100 % pyrite oxidation, solubility limit 10^{-4} M,

In practice, the oxidation of an assumed fraction of pyrite is handled by replacing the amount of celestite in the crushed Opalinus Clay, w_b [wt.-%], by an effective amount of celestite, w'_b [wt.-%], given by:

$$w'_b = w_b + 2 \cdot w_p \cdot F_{ox} \cdot \frac{f_b}{f_p} \quad (7\text{-}1)$$

where w_p [wt.-%] is the amount of pyrite in crushed Opalinus Clay, F_{ox} is the fraction oxidised and f_p [g mol^{-1}] is the formula weight of pyrite. Here, it is assumed that oxidation of one mole of pyrite gives two moles of sulphate, which is the maximum possible.

Diffusion is again assumed to be the only relevant process in the host rock (as well as elsewhere in the modelled system), since advection was found to be negligible in the analysis of the well-emplaced buffer (Chapter 5).

7.1.2 Case-specific parameter values

Case-specific parameter values for the seven calculations cases are considered for this scenario and are given in Tab. 7-2.

Concerning the solubility limitation of the concentration of sulphide produced by the action of sulphate-reducing bacteria in the EDZ, the reference case assumes a solubility limit of 10^{-4} M and the alternative calculation case (C-S-S2) a solubility limit if 10^{-5} M.

Concerning the proportion of pyrite in the crushed Opalinus Clay assumed to be oxidised to sulphate, oxidation is assumed not to occur in the reference case. Alternative calculation cases consider oxidation from 5 % to 100 %. The corresponding effective celestite concentrations, calculated using Eq. 7-1, are given in Tab. 7-3. Here, upper bound pyrite and celestite amounts in the crushed Opalinus Clay are assumed: 0.06 and 3.7 wt.-%, respectively (see Tab. 3-1).

Tab. 7-2: Parameter values used to analyse scenario C with the simplified model.

Reference values are used for all cases unless otherwise stated. General data are shown in Tab.3-1.

Data for the EDZ				
Parameter	**Symbol**	**Units**	**Cases**	**Values**
Effective diffusion coefficient (sulphide)	$D_{e,sz}$	m^2/s	All cases	10^{-11}
Amount of celestite (includes effective values, see Tab. 7-3)	w_a	wt.-%	All cases	0.06
(Molar) solubility limit: sulphide minerals	S_s	mol/m^3	All other cases	0.1 (i.e. 10^{-4} M)
			C-S-S2	0.01 (i.e. 10^{-5} M)
Data for the buffer				
Dry density	ρ_b	kg/m^3	All cases	1632
Effective diffusion coefficient (sulphide)	$D_{e,sb}$	m^2/s	All cases	4.44×10^{-11}
(Molar) solubility limit: sulphide minerals	S_s	mol/m^3	All other cases	0.1 (i.e. 10^{-4} M)
			C-S-S2	0.01 (i.e. 10^{-5} M)
Amount of celestite (effective values, see Tab. 7-3)	w_b	wt.-%	All other cases	0.06
			C-S-C5	0.63
			C-S-C10	1.19
			C-S-C20	2.33
			C-S-C50	5.73
			C-S-C100	11.41

Tab. 7-3: Effective celestite concentrations in the crushed Opalinus Clay buffer resulting from potential pyrite oxidation assumed in different calculation cases.

Case	**Fraction of pyrite oxidised** [%]	**Effective celestite conc.** [wt.-%]
C-S-RC	0	0.06
C-S-C5	5	0.63
C-S-C10	10	1.19
C-S-C20	20	2.33
C-S-C50	50	5.73
C-S-C100	100	11.41

7.1.3 Results

In scenario C, following the reduction of sulphate ions by micro-organisms and the precipitation of sulphide minerals, a dissolution front of these sulphide minerals develops in the crushed Opalinus Clay, starting at the canister surface and moving outwards into the buffer and eventually into the EDZ. At the same time, a sulphate (celestite) dissolution front develops in the host rock, beginning at the interface with the EDZ and again moving progressively outwards (see Fig. 4-2). The progress of these fronts over time in the reference case (C-S-RC) and in case C-S-S2 for the present scenario is shown in Fig. 7-1.

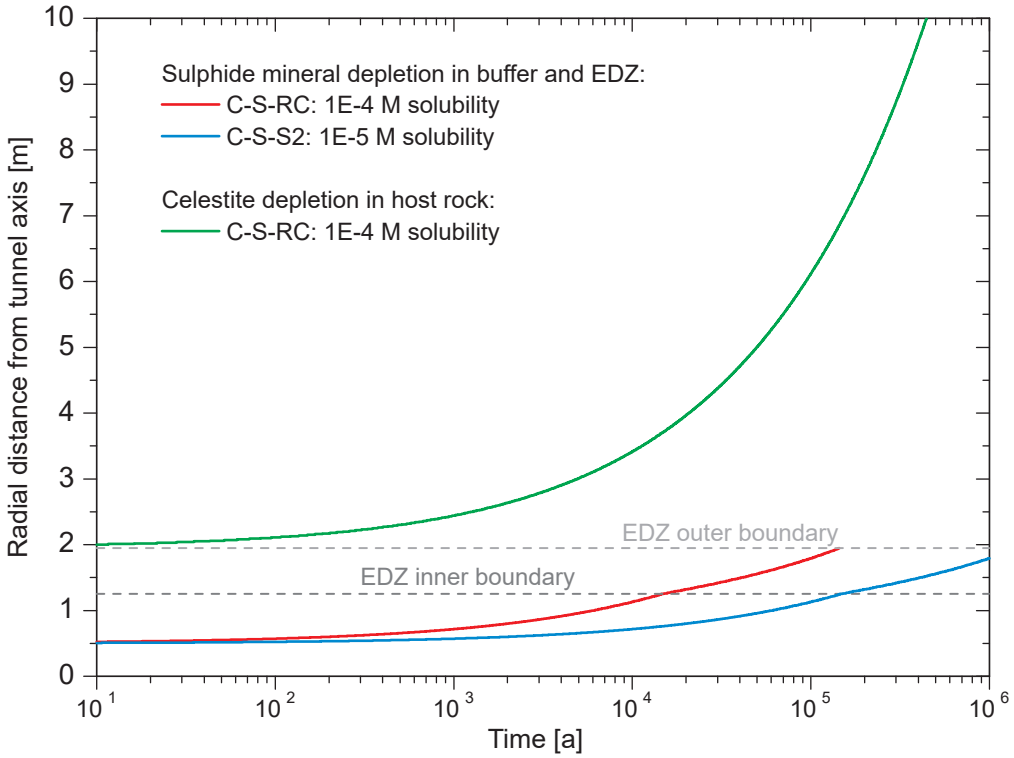

Fig. 7-1: Evolution of celestite depletion fronts in the host rock and in buffer for the reference case C-S-RC and in case C-S-S2 with reduced sulphide solubility in the buffer and EDZ.

In the reference case, the sulphide mineral dissolution front reaches the inner boundary of the EDZ at a little after 10'000 years, but requires over 100'000 years to reach the outer boundary of the EDZ. In case C-S-S2, the front reaches the inner boundary of the EDZ after about 100'000 years and then remains within the EDZ for the rest of the million year-long calculation period. As in the case of the well-emplaced buffer, the celestite front in the host rock extends only 10 m from the tunnel axis after around 400'000 years, justifying the assumption that the emplacement drifts, which have a separation of some tens of metres, can be assumed to evolve largely independently of one another.

Sulphate from celestite dissolution in the host rock migrates to the EDZ by diffusion, where it is reduced to sulphide. Fig. 7-2 shows the sulphate flux to the EDZ as a function of time, and also the sulphide fluxes to the canister surface and into the rock, in the reference case C-S-RC and in case C-S-S2, which assumes a lower sulphide solubility. In the reference case, the line showing the sulphide flux to the canister surface has an inflection a little over 10'000 years, which is the

time at which the sulphide mineral dissolution front reaches the EDZ, and a further inflection around 100'000 years later when the outer boundary of the EDZ is reached. These two inflections separate the three evolution phases that are distinguished in scenario C, as explained in Section 4.2.3. In case C-S-S2, the first phase lasts for a little over 100'000 years and the second phase for the rest of the million year calculation period.

Fig. 7-2 shows that the sulphate flux to the EDZ/host-rock boundary due to dissolution of celestite exceeds the other fluxes in both calculation cases. The flux decreases with time as the celestite dissolution front retreats away from the tunnel, increasing the diffusion distance. This sulphate is then reduced to sulphide at the boundary and accumulates there as precipitated minerals. The figure also shows that the sulphide flux to the rock is small compared with the flux to the canister surface, and that both of these fluxes are reduced in case C-S-S2.

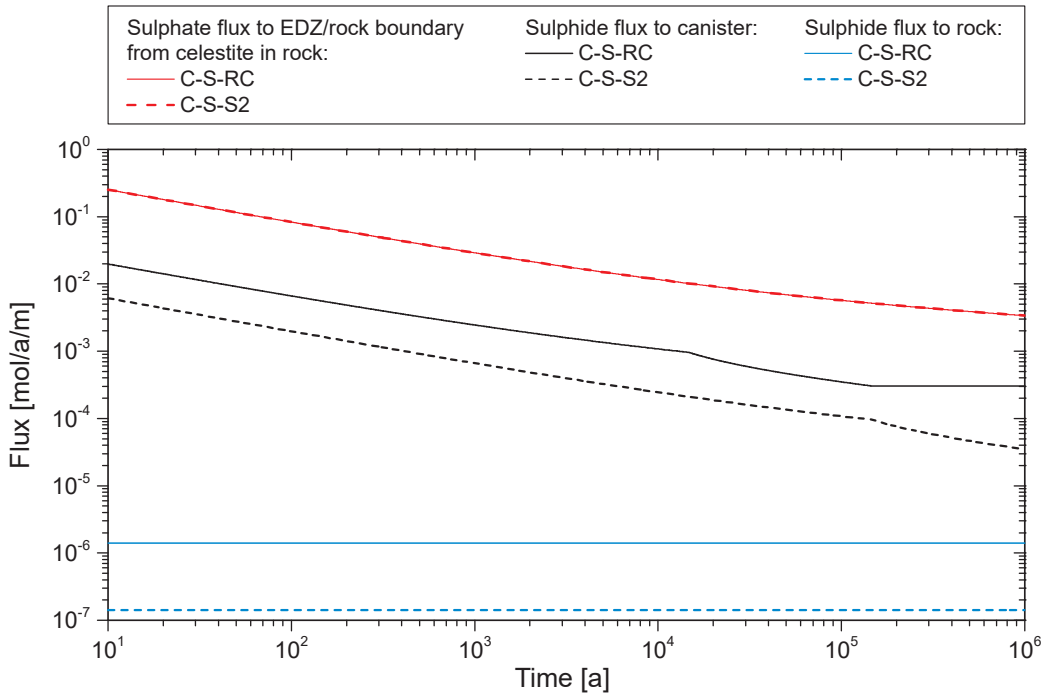

Fig. 7-2: Evolution of sulphate and sulphide fluxes in the reference case C-S-RC and in case C-S-S2 with reduced sulphide mineral solubility.

The evolution of corrosion depth in the reference case C-S-RC and in case C-S-S2 in the present scenario is shown in Fig. 7-3, along with the corresponding cases with the same sulphide solubility limits in the scenario with a well-emplaced bentonite buffer (i.e. cases A-S-S1 and A-S-S2) and in the scenario with a reduced density bentonite buffer (i.e. cases B-S-RC and B-S-S2). For these cases, the present scenario C is clearly less favourable than a well-emplaced bentonite buffer, but somewhat more favourable than a reduced density bentonite buffer. In the analysis of scenario A, it was shown that, with a solubility limit constraining the sulphide concentration in the EDZ, the only parameters that affects corrosion depth are the solubility limit itself and the diffusion coefficient in the buffer (with reference value of 2×10^{-12} m^2 s^{-1}). It is these parameters, along with the buffer thickness, that determine the diffusive sulphide flux across the buffer to the canister surface. In scenarios B and C, the sulphide flux to the canister surface is not only determined by the solubility limit and diffusion coefficient in the buffer, but also by the location of the dissolution front in the buffer separating areas with precipitated sulphide minerals from areas depleted in these minerals (see Fig. 4-2). This front starts at the canister surface and migrates

through the buffer towards the EDZ and, as it migrates, the sulphide concentration gradient and hence the diffusive flux will start very large and gradually diminish. This is the reason why the curves in Fig. 7-3 have different shapes for scenarios B and C compared with scenario A, with a high rate of increase in corrosion depth early on, which then diminishes with time. The reference value of the diffusion coeffient in the buffer is 2.4×10^{-11} m^2 s^{-1} in scenario B, but 4.44×10^{-11} m^2 s^{-1} in scenario C, favouring higher corrosion rates in scenario C if the amounts of sulphide in the two scenarios were the same. On the other hand, the amount of sulphide produced by the reduction of sulphate in the crushed Opalinus Clay buffer in scenario C (reference value: 0.06 wt.-% as celestite) is much less than the amount produced by the reduction of sulphate in bentonite in scenario B (reference value 0.9 wt.-% gypsum). This means that, in scenario C, the dissolution front migrates away from the canister faster than in scenario B. Hence, the sulphide concentration gradient at any given time is lower in scenario C than scenario B, and the sulphide flux to the surface is also lower, in spite of the higher diffusion coefficient in scenario C. This explains why scenario C is somewhat more favourable than scenario B.

The present scenario, however, becomes significantly less favourable than a reduced density bentonite buffer if pyrite oxidation is taken into account, as shown in Fig. 7-4. The figure shows the evolution of corrosion depth in the reference case C-S-RC and in cases C-S-C5 to C-S-C100, in which the amount of pyrite assumed oxidised is varied, along with the corresponding cases with the same sulphide solubility limit in the scenario with a well-emplaced bentonite buffer (i.e. case A-S-S1) and in the scenario with a reduced density bentonite buffer (i.e. cases B-S-RC). According to these results, as little as 5 % pyrite oxidation, implies a crushed Opalinus Clay buffer is less favourable than a reduced density bentonite buffer.

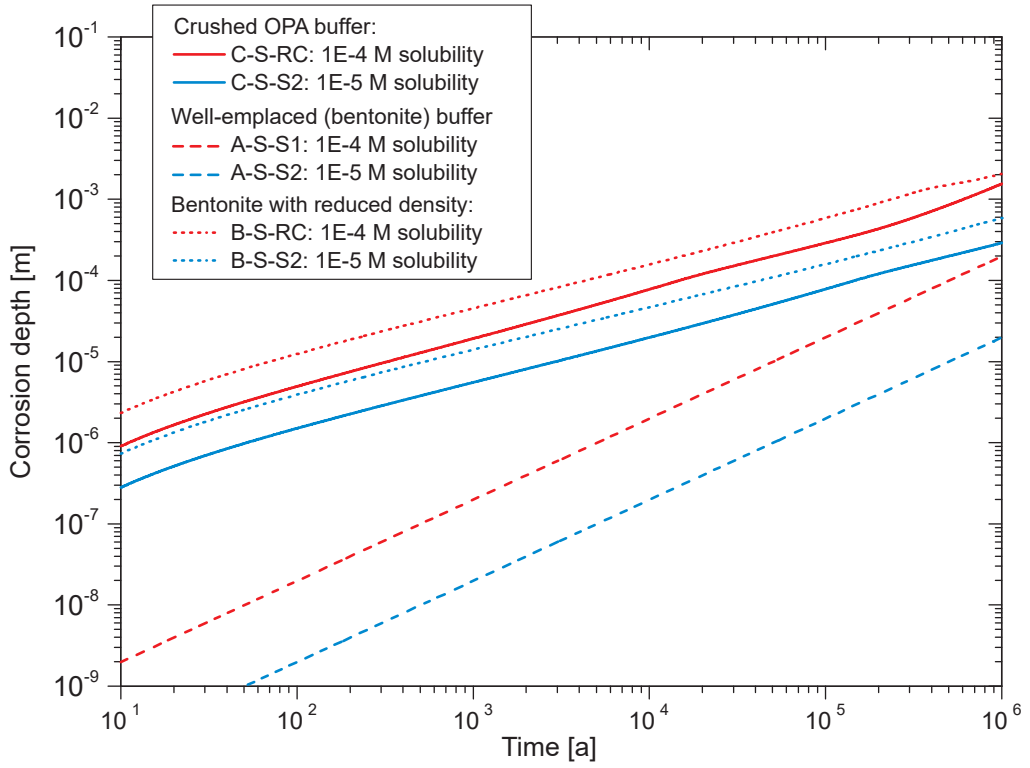

Fig. 7-3: Evolution of corrosion depth in the reference case C-S-RC, in case C-S-S2 and in the corresponding cases with the same solubility limits in the scenario with a well-emplaced buffer (A-S-S1 and A-S-S2) and in the scenario with a reduced density bentonite buffer (cases B-S-RC and B-S-S2).

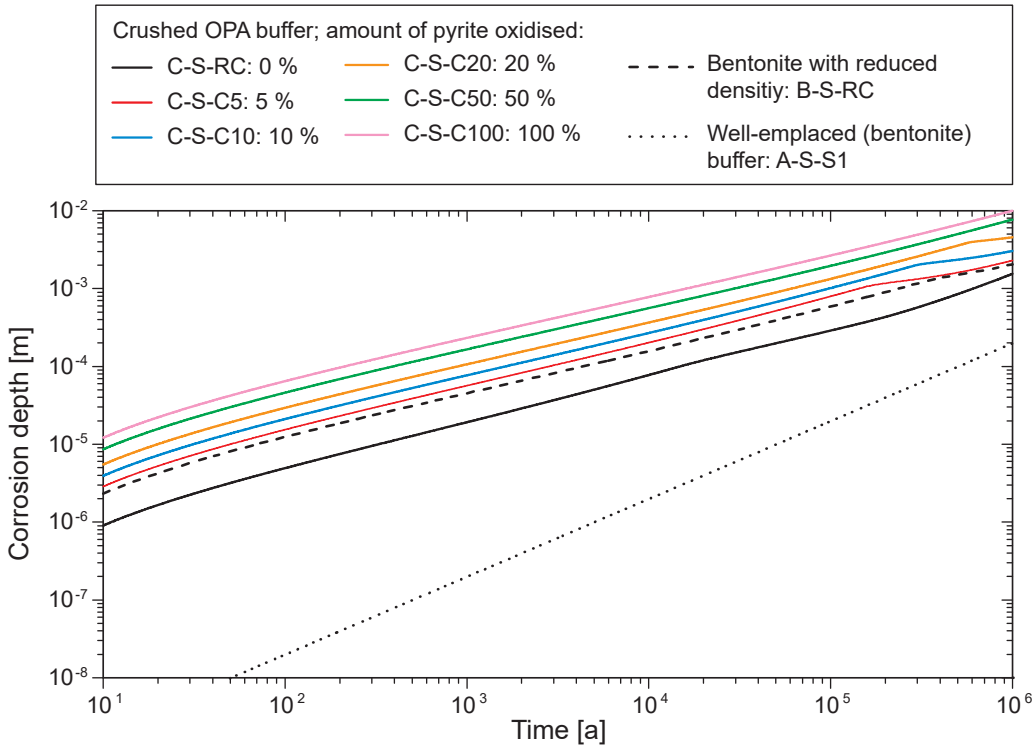

Fig. 7-4: Evolution of corrosion depth in the reference case C-S-RC, in cases C-S-C5 to C-S-C100 in which the amount of pyrite assumed oxidised is varied, and in the corresponding cases with the same solubility limit in the scenario with a well-emplaced buffer (A-S-S1) and in the scenario with a reduced bentonite bentonite buffer (cases B-S-RC).

7.2 Reactive transport model

7.2.1 Case-specific model set-up

Reactive transport calculations were performed for two calculation cases:

- Microbial sulphate reduction is absent in the buffer, but present in the EDZ (C-RT-MA1)
- Microbial sulphate reduction occurs both in the buffer and EDZ (C-RT-MA2)

Tab. 7-4: Overview of calculation cases for scenario C calculated with the reactive transport model.

Main source of uncertainty/variability	Case	Description
Location of potential microbial activity	C-RT-MA1	Microbial activity in EDZ only
	C-RT-MA2	Mircobial activity in buffer and EDZ

In both of the above calculation cases the effective diffusion coefficient in the buffer (4.44×10^{-11} m^2/s) is enhanced by a factor of ca. 22 compared with the well-emplaced case (2.0×10^{-12} m^2/s). The important consequence of microbial sulphate reduction taking place in the

buffer is that sulphide is generated close to and directly at the canister surface. Consequently, the control of sulphide transport on canister corrosion is less pronounced than when sulphide generation is restricted to the EDZ only (well-emplaced MX-80 buffer).

Both calculation cases consider that 10 % of the pyrite initially present in the Opalinus Clay (3.7 wt.-% was used as the upper limit) is oxidised as a result of storage and manipulation between tunnel excavation and backfilling. In the model, the effect of pyrite oxidation is simplistically represented by converting that amount of pyrite into the equivalent amount of gypsum and ferrihydrite (one mole of ferrihydrite, $Fe(OH)_3$, and two moles of gypsum produced per one mole of pyrite oxidised), according to the overall reaction stoichiometry:

$$FeS_2(s) + 7.5H_2O + 3.75O_2(aq) + 2Ca^{2+}(aq) \Rightarrow Fe(OH)_3(s) + 2CaSO_4 \cdot 2H_2O + 4H^+ \quad (7\text{-}2)$$

7.2.2 Case-specific parameter values

Crushed Opalinus Clay as buffer material

The mineralogical composition of the crushed Opalinus Clay is assumed to contain gypsum and ferrihydrite due to partial oxidation of initially present pyrite (molar equivalents to 10 % of the initial pyrite content of 3.7 wt.-%). The resulting quantities of gypsum and ferrihydrite are 1.1 and 3.3 wt.-%, respectively. Otherwise the crushed Opalinus Clay composition is identical to that of the intact rock described in Section 5.2.2. The porewater composition of the crushed Opalinus Clay buffer (shown in Tab. 7-5) is calculated assuming equilibrium with a generic cation-exchanger, calcite, dolomite, quartz, celestite, siderite, ferrihydrite and gypsum under CO_2(g) partial pressure of $10^{-2.2}$ bar.

Opalinus Clay

Parameter values for transport, mineralogical and porewater composition of the Opalinus Clay used in reactive transport calculations are reported in Section 5.2.2.

EDZ

Parameter values for transport, mineralogical and porewater composition of the Opalinus Clay used in reactive transport calculations are reported in Section 5.2.2.

The initial geochemical conditions in the buffer assuming crushed Opalinus Clay as buffering material are presented in Tab. 7-5. The initial conditions in the EDZ and Opalinus Clay are shown in Tab. 5-6.

Tab. 7-5: Initial geochemical conditions in the buffer assuming crushed Opalinus Clay as buffering material.

	Crushed Opalinus Clay as buffer
pH	7.18
pe	-2.42
Eh [mV]	-143
Total aq. components [mol/L]	
Na	2.02×10^{-1}
Mg	1.13×10^{-2}
Ca	1.64×10^{-2}
Sr	1.65×10^{-4}
K	1.98×10^{-3}
Fe	7.50×10^{-5}
Si	1.82×10^{-4}
Cl	1.60×10^{-1}
C	2.52×10^{-3}
S(VI)	4.91×10^{-2}
S(-II)	1.76×10^{-10}
DOM [1)]	8.33×10^{-5}
Minerals [volume fraction]	
OPA_exchanger [2)]	3.26×10^{-1}
Calcite	8.19×10^{-2}
Dolomite	3.66×10^{-3}
Siderite	2.47×10^{-2}
Celestite	2.47×10^{-4}
Gypsum [3)]	2.44×10^{-3}
Ferrihydrite [4)]	4.60×10^{-4}
Quartz	1.23×10^{-1}
SOM_OPA [5)]	8.16×10^{-4}
Mackinawite	0.00 [6)]

1) Dissolved organic matter (DOM) was assumed to have the generic molecular formula of CH_2O

2) Generic exchanger (with composition reported in Mäder (2009) was considered for Opalinus Clay

3) Gypsum assumed present due to 10 wt.-% oxidation of initial pyrite

4) Ferrihydrite ($Fe(OH)_3$) assumed present due to 10°wt.-% oxidation of initial pyrite

5) Solid organic matter (SOM) in the Opalinus Clay and EDZ

6) Initially absent, but allowed to precipitate if over-saturated

7.2.3 Results

Sulphide fluxes towards the canister predicted by the reactive transport model during a period of 1'000'000 years for three cases: (i) well-emplaced MX-80 buffer (A-RT-RC), (ii) crushed Opalinus Clay as buffer material without microbial activity in the buffer (C-RT-MA1), and (iii) crushed Opalinus Clay as buffer material with microbial activity in the buffer and in the EDZ (C-RT-MA2) are shown in Fig. 7-5. The corresponding corrosion depths for these calculation cases are shown in Fig. 7-6. The predicted corrosion depths for the crushed Opalinus Clay buffer cases without and with sulphate-reducing microbial activity in the buffer are ca. 2 mm and 3.1 mm, respectively, at 1'000'000 years.

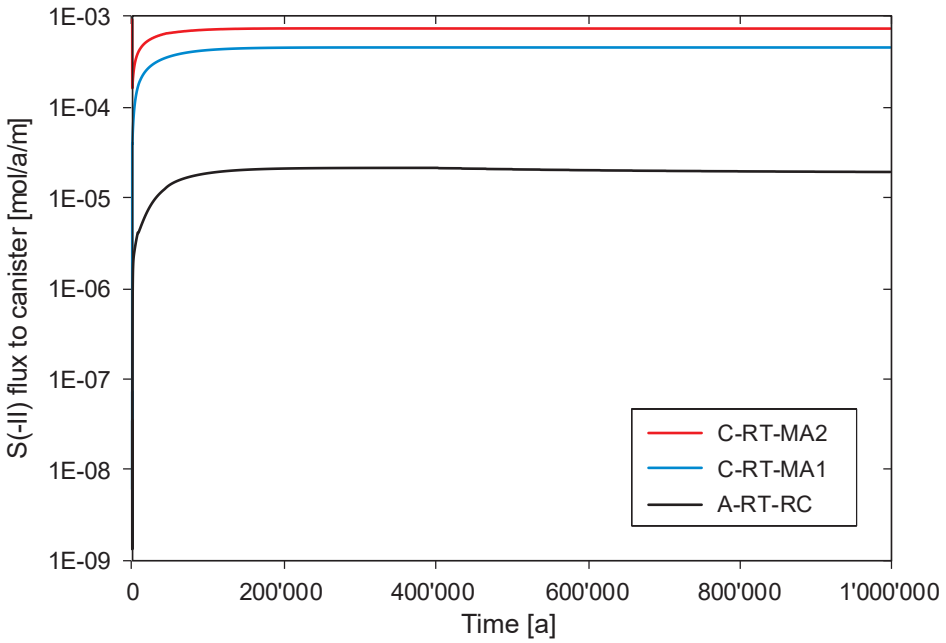

Fig. 7-5: Comparison of sulphide fluxes towards the canister predicted by the reactive transport model during a period of 1'000'000 years for three cases: A-RT-RC, C-RT-MA1 and C-RT-MA2.

The flux is expressed as per 1 metre tunnel length which corresponds to 3.29 m^2 canister surface.

In both the well-emplaced MX-80 case and in the crushed Opalinus Clay as buffering material cases (with and without microbial sulphate reduction in the buffer), sulphide concentration in the EDZ is controlled by mackinawite. Although ferrihydrite is assumed to be present in crushed Opalinus Clay, the concentration of dissolved Fe in the buffer is controlled by the more stable siderite. In the well-emplaced MX-80 buffer, the dissolved Fe in the buffer is assumed to be controlled by goethite, which is close to siderite saturation. Consequently, in both cases, dissolved Fe concentrations are quite similar, i.e. in the order of 10^{-5} and 10^{-4} mol/L. In the reduced density bentonite buffer, the dissolved sulphide and iron concentrations in the EDZ are also broadly comparable. Consequently, copper corrosion depths at 1'000'000 years for all three scenarios are very similar. The only parameter that makes a slight difference is the effective diffusivity of the buffer, which is highest in crushed Opalinus Clay, followed by the reduced density bentonite and the well-emplaced bentonite.

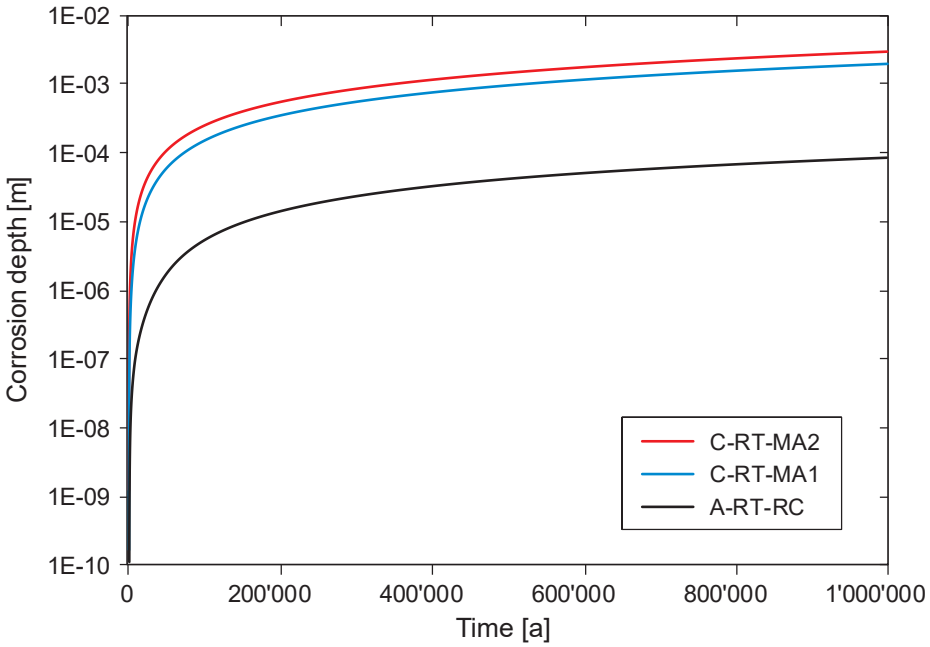

Fig. 7-6: Comparison of copper corrosion depths predicted by the reactive transport model during a period of 1'000'000 years for three cases (A-RT-RC, C-RT-MA1 and C-RT-MA2).

The difference between corrosion depths calculated for the well-emplaced MX-80 case and for the case considering crushed Opalinus Clay as buffering material (without microbial sulphate reduction activity in the buffer) seen in Fig. 7-7 is also explained in terms of significantly higher buffer diffusivity in the latter case. When microbial sulphate reduction activity takes place in both the buffer and EDZ, sulphide is generated close to and right at the canister surface. As a result, no delay in corrosion is observed due to transport during initial times (see Fig. 7-7).

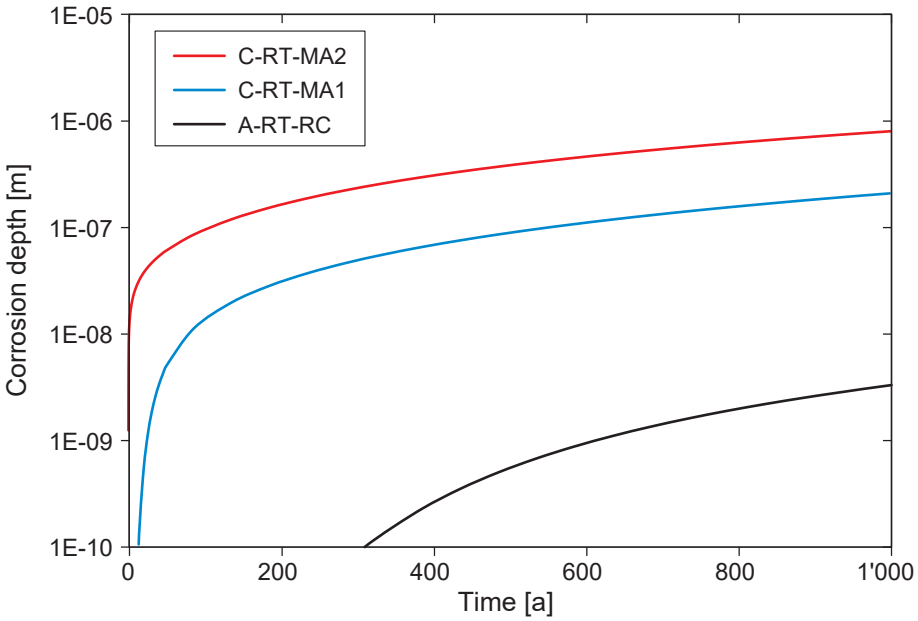

Fig. 7-7: Comparison of copper corrosion depths predicted by the reactive transport model during a period of 1'000 years (zoom-in of Fig. 7-6).

See caption of Fig. 7-6 for additional details.

7.3 Comparison of results obtained by the simplified and reactive transport models

Comparison of copper corrosion depths calculated using the simplified model (assuming sulphide solubility limit at 10^{-4} mol/L and 10^{-5} mol/L and considering microbial sulphate-reducing activity in the buffer and EDZ), and using the reactive transport model with microbial sulphate reduction occurring in the buffer during a period of 1'000'000 years is shown in Fig. 7-8.

Initially, the reactive transport model predicts a lower corrosion rate than the simplified model, which was also observed in the two other scenarios. In contrast to the other two scenarios, the corrosion depth calculated by the reactive transport model approaches the corrosion depth calculated by the simplified model at 1'000'000 years. Part of the reason for this is that the simplified model did not assume any oxidised pyrite in the Opalinus Clay, while the reactive transport model did assume 10 % oxidised pyrite in the buffer. For an exact comparison with an identical assumption regarding pyrite oxidation, cases C-S-C10 should be compared with C-RT-MA2 (see Fig. 7-9). This comparison shows that the sulphide flux calculated by the reactive transport model is lower than the one calculated by the simplified model, as was observed in the previous two scenarios. However, in general the simplified transport model shows declining corrosion rates towards later times. The explanation for this is that the front, in which sulphate availability limits the sulphide production, moves further and further away from the canister, thus slowing down the sulphide flux. This is in contrast to the reactive transport model, where the availability of sulphate is not the limiting factor for sulphide production, but rather the availability of dissolved organic matter. This also makes the reactive transport model less dependent on the sulphate concentration (or amount of oxidised pyrite) and the sulphide flux is less variable in time. In addition, at later times sulphide concentration in the buffer slightly increases (from about 1×10^{-5} M to 4×10^{-5} M), due to mackinawite equilibrium and gradual pH drop. Consequently, sulphide fluxes are as shown in Fig. 7-5: they tend to slightly increase at later times.

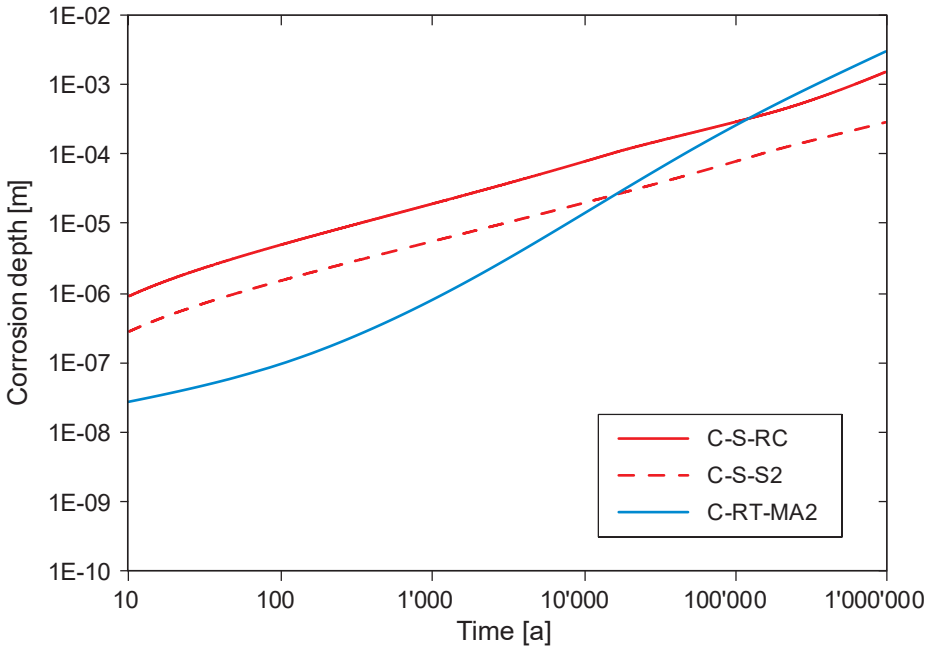

Fig. 7-8: Comparison of copper corrosion depths calculated by the simplified model (C-S-RC and C-S-S2) and by the reactive transport model (C-RT-MA2).

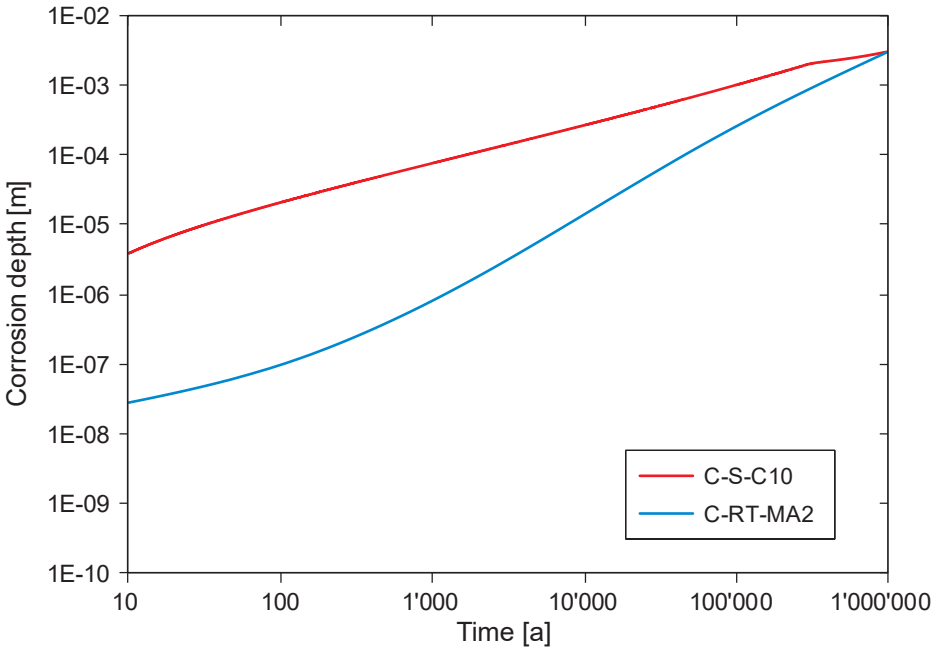

Fig. 7-9: Comparison of copper corrosion depths calculated by the simplified model (C-S-C10) and by the reactive transport model (C-RT-MA2).

8 Discussion and conclusions

Three different scenarios are calculated; scenario A describes a well-emplaced bentonite buffer, scenario B a bentonite buffer with a reduced density and scenario C a buffer made of crushed Opalinus Clay. In each scenario a number of calculation cases are used to illustrate the sensitivity to certain parameters (e.g. concentration of gypsum, celesite, pyrite, diffusion coefficient, solubility limit). Two different models are applied for the calculation of all these cases: a simplified model and a reactive transport model. While the simplified model is instrumental in varying parameters in sensitivity studies, the reactive transport model provides a more realistic view on the geochemical evolution of the near field. The results of both models were systematically compared in each scenario.

Transport models

The simplified and reactive transport models give comparable results where similar conditions are considered (e.g. sulphide solubility). Initial differences between corrosion depth calculated by the two models are due to their respective conceptual simplifications (e.g. the assumption of steady state diffusion profiles for sulphide for the simplified transport model vs. transient transport regime for the reactive transport model), but these differences vanish within several thousands of years – a short period of time compared with the total assessment time. The simplified model allows for a relatively rapid calculation and therefore lends itself to an extensive sensitivity analysis of the different parameters that are relevant (diffusion coefficient, concentration of celestite, pyrite, etc.). On the other hand, the reactive transport model provides unique insights into the nature and magnitude of key system-controlling processes. The use of this model provides insight in a more realistic evolution of the near field. Mineral precipitation and dissolution function as a mechanism to delay the sulphide transport towards the canister. Once a geochemical equilibrium has been reached, the sulphide flux is again governed by its diffusion, as in the simplified model. For this reason, the sulphide fluxes calculated by the two models approach each other after several thousand years.

Critical model parameters, assumptions and remaining uncertainties

Within the different scenarios, the sensitivity to model parameters is assessed by both the simplified and the reactive transport models. The calculation cases have shown that the following parameters have a significant impact on the corrosion depth:

1. Solubility limit: Given the likelihood that at some point during the near-field evolution (at the right pH and Eh) sulphide will precipitate as insoluble sulphide-minerals (mackinawite, greigite, pyrite) or as elemental sulphur, it is safe to assume that the solubility of sulphide is limited (see Chapter 2). As demonstrated in scenario A, the use of a sulphide solubility limit (by assuming formation of FeS(am) or mackinawite only) in the simplified model has a large impact on the sulphide flux in the near field and is assumed as the most likely situation to occur (10^{-4} M). The no-solubility calculation case thus illustrates an unrealistic case that can only be considered as an extremely conservative calculation case. The applicability of mackinawite as the solubility limiting mineral also requires a system with sufficiently available iron. In the bentonite system, goethite (FeOOH) provides sufficient iron, whereas in the crushed Opalinus Clay siderite ($FeCO_3$) is available (see Tab. 5-6). Additional iron will be available in the EDZ from the corrosion of steel tunnel support. However, this is not taken into account in the current calculations.

2. The diffusion coefficient of sulphide in the host rock and buffer influences the sulphide flux. When considering no solubility limit, the effect of the diffusion coefficient in the buffer is more pronounced up to 10'000 years, whereas the diffusion coefficient in the host rock defines the corrosion depth towards later times (see Fig. 5-6). For the cases with a sulphide solubility limit, only the diffusion coefficient in the buffer influences the corrosion depth over the entire period (compare cases A-S-S1, A-S-S1DB and A-S-S1DBB in Fig. 5-7).

3. Pyrite oxidation in the EDZ: as long as the concentration of sulphide in the EDZ is assumed to be controlled by its solubility, the amount of oxidised pyrite has no effect on the sulphide flux towards the canister (see case A-S-S1 and A-S-S1C50 in Fig. 5-7). On the other hand, if solubility limitation is disregarded, the amount of pyrite oxidised in the EDZ as calculated in scenario A contributes significantly to the sulphide flux (cases A-S-SX to A-S-C50 in Fig. 5-6). Based on experimental observations in the Meuse/Haute-Marne URL in Bure (France) only 10 % pyrite oxidation is expected in the EDZ (Vinsot et al. 2014) which would lead to a corrosion depth of about 2.5 cm if no solubility limitation is assumed.

4. Pyrite oxidation in the crushed Opalinus Clay buffer greatly affects the sulphide flux, even if solubility limitation of sulphide is assumed (cases C-S-C5 to C-S-C100 in Fig. 7-4). However, there is a significant uncertainty on the extent of pyrite oxidation in crushed Opalinus Clay. In order to identify a likely sulphide flux towards the canister when using a crushed Opalinus Clay buffer, an exact value for the amount of oxidised pyrite would be required. In the upper bounding case that 100 % pyrite is oxidised, the corrosion depth could increase up to 1 cm. Unless this value is better bound and can be controlled during future production of crushed Opalinus Clay, it renders a crushed Opalinus Clay backfill much less favourable than a bentonite backfill.

5. pH evolution in the near field: both the activity of micro-organisms and the corrosion of steel may affect the local pH value. The degradation of organic material by micro-organisms forms CO_2, which will reduce the pH (see Appendix D). As a result of corrosion, the pH could, however, locally increase (see Appendix C). As shown by the calculations with the reactive transport model, the pH decrease simultaneously leads to the dissolution of siderite in the Opalinus Clay, thus releasing Fe for the formation of mackinawite. In this way, the sulphide fluxes down to pH 6 will not increase much above 10^{-4} M and limited corrosion depth is expected. The opposite effect, increasing pH, leads to further sulphide solubility reduction and thus to lower corrosion depths and is thus not considered a critical development.

6. One of the major factors affecting the evolution of the near field is the presence of microbial populations and their activity throughout the considered time period. It is well-known that micro-organisms are dependent on the presence of trace elements that form critical nutrients (e.g. phosphorous). The assumption employed in our approach that microbial activity is not limited by the availability of nutrients is thus conservative. However, our approach is not conservative in assuming that microbial activity is uniformly distributed within the buffer. Should the conditions (water, pore space, electron donor and electron acceptor) allow microbial activity for 1'000'000 years, micro-organisms could preferentially be active in biofilms at the canister surface. In such a case the corrosion depth might be higher because of biofilm formation. It is well known that conditions within a biofilm can be more corrosive than under regular conditions. It seems therefore valuable to bound microbial activity and biofilm formation (e.g. by defining bio-availability of DOM, temperature or pore space dependency of microbial life, limiting nutrients).

Corrosion depths in the different scenarios

In order to make a comparison, a selection of representative calculation cases of the expected near-field evolution is made in this summary. In all three scenarios these were the cases investigated by the simplified model: A-S-S1, B-S-RC, C-S-C10 and their equivalents (as far as possible) by the reactive transport model: A-RT-RC, B-RT-MA2 and C-RT-MA2 as summarised in Tab. 8-1. For the calculated corrosion depths of additional cases generated during the sensitivity analysis, we refer the reader to the respective chapters. The corrosion depths were calculated from the sulphide fluxes assuming uniform corrosion of the copper surface.

Of the three studied scenarios, the well-emplaced bentonite case leads to the least corrosion depth. Significantly larger corrosion depths are calculated for both crushed Opalinus Clay and for the bentonite with reduced density. When comparing the corrosion depths after 1'000'000 years generated by both models (simplified and reactive transport), one could consider that the simplified model provides the upper boundary of the expected corrosion depth, while the reactive transport model provides a more realistic corrosion depth. This means that for scenario A, the more realistic corrosion depth after 1'000'000 years in a well-emplaced bentonite buffer is 0.08 mm (A-RT-RC) and the upper corrosion depth 0.2 mm (A-S-S1). In the reduced density buffer the more realistic corrosion depth after 1'000'000 years is 1.3 mm (as calculated by B-RT-MA2), and the upper corrosion depth is 2 mm (B-S-RC). For the buffer made of crushed Opalinus Clay, the more realistic corrosion depth at 1'000'000 years is 3.1 mm (C-RT-MA2) whereas the upper bound is 3.4 mm (C-S-C10). The corrosion depth values at 100 ka 1 Ma are displayed in Tab. 8-1.

Tab. 8-1: Overview of copper corrosion depths for different cases and scenarios calculated by the simplified and by the reactive transport models.

Case description	**Simplified model**			**Case description**	**Reactive transport model**		
	Case	**Corrosion depth 100'000 years** [mm]	**Corrosion depth 1'000'000 years** [mm]		**Case**	**Corrosion depth 100'000 years** [mm]	**Corrosion depth 1'000'000 years** [mm]
Well emplaced bentonite, solubility limit 10^{-4} M, microbial activity in EDZ only, no oxidation of pyrite in EDZ, reference values for diffusion coefficient	A-S-S1	0.02	0.2	Well-emplaced bentonite, solubility controlled by mackinawite, microbial activity in EDZ only, no oxidation of pyrite in EDZ, reference values for diffusion coefficient	A-RT-RC	0.005	0.08
Poorly emplaced bentonite, solubility limit 10^{-4} M, microbial activity in EDZ and bentonite buffer, reference values for diffusion coefficient	B-S-RC	0.5	2.0	Poorly emplaced bentonite, solubility limit controlled by mackinawite, microbial activity in EDZ and bentonite buffer, reference values for diffusion coefficient	B-RT-MA2	0.18	1.3
Crushed Opalinus Clay buffer, solubility limit 10^{-4} M, microbial activity in EDZ and buffer, 10 % pyrite (or 0.37 wt.-%) oxidised in buffer, reference values for diffusion coefficient	C-S-C10	1	3.40	Crushed Opalinus Clay buffer, solubility limit controlled by mackinawite, microbial activity in EDZ and buffer, 10 % pyrite (or 0.37 wt.-%) oxidised in buffer, reference values for diffusion coefficient	C-RT-MA2	0.26	3.1

Conclusions

This report assesses the sulphide flux towards a Cu-coated canister under consideration of three different scenarios. Scenario A considers a well-emplaced bentonite buffer in which microbial activity does not take place; sulphide in this scenario is formed in the EDZ and diffuses towards the canister. In scenario B the bentonite buffer exhibits a reduced density, which leads to the possibility of microbial activity within the buffer and leads also to higher diffusion coefficients for sulphide. The use of crushed Opalinus Clay buffer was evaluated in scenario C. This scenario is comparable with the scenario B, but also has an additional sulphide source within the buffer (pyrite content in Opalinus Clay is higher than in bentonite, see Tab. 3-1). In each scenario, selected calculation cases were made to illustrate the importance of certain parameters.

Two models are used to assess the sulphide flux: the simplified model, which does not take into account chemical reactions within the system which could reduce the sulphide concentration, except for the solubility limits in some calculation cases. In contrast to this, the reactive transport model provides a more detailed insight into the processes at play during near-field evolution. The fluxes obtained by the reactive transport model are therefore considered to be more realistic, whereas the fluxes calculated by the simplified transport model function as an upper limit. In general, the reactive transport model highlighted the crucial role of sulphide immobilisation via iron sulphide and sulphide mineral solubility.

It was shown in this study that the use of a sulphide solubility limit in the buffer plays a major role in the sulphide flux towards the canister. The solubility limit was set to a fixed value in the simplified model, whereas in the reactive transport model, the sulphide solubility was controlled by a mineral and dependent on pH-Eh range of the buffer (FeS(am) or mackinawite). The presence of Fe-rich minerals in both the bentonite (goethite) and the crushed Opalinus Clay (siderite) buffer enables the formation of these sulphide-rich minerals and limits the sulphide flux towards the canister. The formation of minerals that control the free sulphide concentration is a very robust mechanism, which applies within a broad enough range of pH and Eh (see Appendices B – D) that is found in the near field.

In the reference calculation cases of the three studied scenarios, the well-emplaced bentonite clearly shows the lowest sulphide fluxes towards the canister, followed by comparable fluxes for both crushed Opalinus Clay and for the bentonite with reduced density. In the scenario of a well-emplaced bentonite buffer the sulphide flux to the canister leads to a calculated uniform corrosion depth of 0.08 mm after 1'000'000 years (assuming sulphide mineral solubility), while the upper bound corrosion depth is 0.2 mm (assuming solubility limit 10^{-4} M). In a bentonite buffer with reduced density, a significantly larger corrosion depth of approximately 1.3 mm when assuming sulphide mineral solubility (upper bound 2 mm, assuming solubility limit 10^{-4} M) is expected after 1'000'000 years. For the buffer made of crushed Opalinus Clay, the corrosion depth for the same time period is between 3.1 mm (sulphide mineral solubility) and 3.4 mm (solubility limit 10^{-4} M).

Important processes and parameters that should be further explored to increase confidence in this model are the extent of microbial activity, oxidation of pyrite in the EDZ, the extent of oxidised pyrite in crushed Opalinus Clay and the diffusion coefficients of sulphide in the buffer with low emplacement densities. However, based on the models and data currently available, the sulphide flux towards the canister remains low in all calculation cases. Moreover, this appraisal of the sulphide flux is strongly based on the principle of sulphide solubility limitation, which is well-understood and is largely independent of buffer engineering. It thus increases the reliability of the presented calculated sulphide fluxes. Furthermore, the impact of temperature and potentially reduced transport across the shotcrete-clay interface were in this report neglected. In future assessments, these effects could also be incorporated into the models, to get a more realistic sulphide flux towards the canister.

9 References

Allen, C.M., Cater, S., Andrews, R.E., Kumar, V., Punshon, C.S., Bono, D. de, Bastid, P., Johnson, L.H. & Diomidis, N. (2016): Development of design concepts for a copper-coated SF/HLW disposal canister – evaluation of welding methods. Nagra Arbeitsber. NAB 16-55.

Bagnoud, A., Leupin, O., Schwyn, B. & Bernier-Latmani, R. (2016): Rates of microbial hydrogen oxidation and sulfate reduction in Opalinus Clay rock. Applied Geochemistry 72, 42-50.

Bard, A.J., Parson, R. & Jordan, J. (1985): Standard Potentials in Aqueous Solution. Marcell Dekker, New York.

Bastid, P., Blackwell, S. & Punshon, C.S. (2015): Finite element stress analyses of copper-coated Nagra BWR spent fuel canister with partially penetrating weld detail under circumferentially variable welling pressure. Nagra Arbeitsber. NAB 15-18.

Benning, L.G., Wilkin, R.T. & Barnes, H. (2000): Reaction pathways in the Fe-S system below 100°C. Chemical Geology 167/1-2, 25-51.

Berner, R.A. (1967): Thermodynamic stability of sedimentary iron sulfides. American Journal of Science 265/9, 773-785.

Bradbury, M.H. & Baeyens, B. (1997): A mechanistic description of Ni and Zn sorption on Na-montmorillonite Part II. Journal of Contaminant Hydrology 27/3-4, 223-248.

Bradbury, M.H. & Baeyens, B. (2003): Porewater chemistry in compacted re-saturated MX-80 bentonite. Journal of Contaminant Hydrology 61/1-4, 329-338.

Briggs, S., McKelvie, J., Keech, P., Sleep, B. & Krol, M. (2016): Transient modelling of sulphide diffusion under conditions typical of a deep geological repository. Corrosion Engineering, Science and Technology 52 suppl. 1, 200-203.

Briggs, S., McKelvie, J. & Krol, M. (2017a): Temperature dependent sulphide transport in highly compacted bentonite. International High Level Radioactive Waste Management Conference, Charlotte, USA, 9-13 Apr. 2017, 317-321.

Briggs, S., McKelvie, J., Sleep, B. & Krol, M. (2017b): Multi-dimensional transport modelling of corrosive agents through a bentonite buffer in a Canadian deep geological repository. Science of The Total Environment 599-600, 348-354.

Canfield, D.E., Thamdrup, B. & Fleischer, S. (1998): Isotope fractionation and sulfur metabolism by pure and enrichment cultures of elemental sulfur-disproportionating bacteria. Limnology and Oceanography 43/2, 253-264.

Chen, S., Wang, P. & Zhang, D. (2014): Corrosion behavior of copper under biofilm of sulfate-reducing bacteria. Corrosion Science 87, 407-415.

Courdouan, A., Christl, I., Meylan, W., Wersin, P. & Kretzschmar, R. (2007): Isolation and characterization of dissolved organic matter from the Callovo-Oxfordian formation. Applied Geochemistry 22, 1537-1548.

Csákberényi-Malasics, D., Rodriguez-Blanco, J.D., Kis, V.K., Recnik, A., Benning, L.G. & Posfai, M. (2012): Structural properties and transformations of precipitated FeS. Chemical Geology 294-295, 249-258.

Davison, W. (1991): The solubility of iron sulphides in synthetic and natural waters at ambient temperature. Aquatic Sciences 53/4, 309-329.

Davison, W., Phillips, N. & Tabner, B.J. (1999): Soluble iron sulfide species in natural waters: Reappraisal of their stoichiometry and stability constants. Aquatic Sciences 61/1, 23-43.

Diomidis, N. (2014): Scientific basis for the production of gas due to corrosion in a deep geological repository. Nagra Arbeitsber. NAB 14-21.

Donald, R. & Southam, G. (1999): Low temperature anaerobic bacterial diagenesis of ferrous monosulfide to pyrite. Geochim. Cosmochim. Acta 63/13-14, 2019-2023.

Elie, M. & Mazurek, M. (2008): Biomarker transformations as constraints for the depositional environment and for maximum temperatures during burial of Opalinus Clay and Posidonia Shale in Northern Switzerland. Applied Geochemistry 23, 3337-3354.

Gaus, I., Garitte, B., Senger, R.K., Gens, A., Vasconcelos, R., Garcia-Sineriz Martinez, J.L., Trick, T., Wieczorek, K., Czaikowski, O., Schuster, K., Mayor, J.C., Velasco, M., Kuhlmann, U. & Villar, M.V. (2014): HE-E Experiment: Lay-out, interpretation and THM modelling. Nagra Arbeitsber. NAB 14-53.

Grandia, F., Domenech, C. & Arcos, D. (2006): Porewater chemistry (PC) experiment: Results of the geochemical modeling. Unpubl. Mont Terri Technical Note. Mont Terri Project, Switzerland.

Grass, G., Rensing, C. & Solioz, M. (2011): Metallic copper as an antimicrobial surface. Applied and Environmental Microbiology 77/5, 1541-1547.

Harmandas, N.G., Navarro Fernandez, E. & Koutsoukos, P.G. (1998): Crystal growth of pyrite in aqueous solutions. Inhibition by organophosphorus compounds. Langmuir 14/5, 1250-1255.

Holdsworth, S.R., Graule, T. & Mazza, E. (2014): Feasibility evaluation study of candidate canister solutions for the disposal of spent nuclear fuel and high level waste. A status review. Nagra Working Report NAB 14-90.

Hummel, W., Berner, U., Curti, E., Pearson, J.F. & Thoenen, T. (2002): Nagra/PSI Chemical Thermodynamic Data Basel 01/01. Nagra Technical Report NTB 02-16.

Hunger, S. & Benning, L.G. (2007): Greigite: a true intermediate on the polysulfide pathway to pyrite. Geochemical Transactions 8/1, 1-20.

Karnland, O. (2010): Chemical and mineralogical characterization of the bentonite buffer for the acceptance control procedure in a KBS-3 repository. SKB Technical Report TR-10-60. Svensk Kärnbränslehantering AB, Stockholm, Sweden.

KBS (1978): Copper as canister material for unreprocessed nuclear waste – evaluation with respect to corrosion. Final Report 1978-03-31, KBS TR-90, Swedish Corrosion Institute. Kärn-Bränsle-Säkerhet, Stockholm, Sweden.

Keech, P.G., Vo, P., Ramamurthy, S., Chen, J., Jacklin, R. & Shoesmith, D.W. (2014): Design and development of copper coatings for long term storage of used nuclear fuel. Corrosion Engineering, Science and Technology 49/6, 425-430.

King, F. (2009): Microbiologically influenced corrosion of nuclear waste containers. Corrosion 65/4, 233-251.

King, F. (2013): A review of the properties of pyrite and the implications for corrosion of the copper canister. SKB Technical Report TR 13-19. Svensk Kärnbränslehantering AB, Stockholm, Sweden.

King, F., Kolar, M. & Maak, P. (2008): Reactive-transport model for the prediction of the uniform corrosion behaviour of copper used fuel containers. Journal of Nuclear Materials 379/1-3, 133-141.

King, F., Lilja, C., Pitkänen, P. & Vähänen, M. (2012): An update of the state-of-the-art report on the corrosion of copper under expected conditions in a deep geologic repository. Posiva Report 2011-01. Posiva Oy, Helsinki, Finland.

King, F., Lilja, C. & Vähänen, M. (2013): Progress in the understanding of the long-term corrosion behaviour of copper canisters. Journal of Nuclear Materials 438/1-3, 228-237.

King, F. & Wersin, P. (2013): Review of supercontainer copper shell-bentonite interactions and possible effects on buffer performance for the KBS-3H design. Posiva Working Report 2013-03. Posiva Oy, Helsinki, Finland.

Kiviranta, L. & Kumpulainen, S. (2011): Quality control and characterization of bentonite materials. Posiva Working Report 2011-84. Posiva Oy, Olkiluoto, Finland.

Lerouge, C., Grangeon, S., Claret, F., Gaucher, E., Blanc, P., Guerrot, C., Flehoc, C., Wille, G. & Mazurek, M. (2014): Mineralogical and Isotopic Record of Diagenesis from the Opalinus Clay Formation at Benken, Switzerland. Clays and Clay Minerals 62/4, 286-312.

Lerouge, C., Grangeon, S., Gaucher, E.C., Tournassat, C., Agrinier, P., Guerrot, C., Widory, D., Fléhoc, C., Wille, G., Ramboz, C., Vinsot, A. & Buschaert, S. (2011): Mineralogical and isotopic record of biotic and abiotic diagenesis of the Callovian–Oxfordian clayey formation of Bure (France). Geochim. Cosmochim. Acta 75/10, 2633-2663.

Leupin, O., Smith, P., Marschall, P., Johnson, L.H., Savage, D., Cloet, V., Schneider, J. & Senger, R.K. (2016): High-level waste repository-induced effects. Nagra Tech. Report NTB 14-13.

Macdonald, D.D., Sharifi-Asl, S. & Engelhardt, G.R. (2014): Issues in the corrosion of copper in a Swedish high level nuclear waste repository: Phase III. Role of sulphide ion in anodic and cathodic processes. SSM Technical Note 2014/57, Stockholm, Sweden.

Mäder, U.K. (2009): Reference pore waters for the Opalinus Clay and 'Brown Dogger' for the provisional safety-analysis in the framework of sectoral plan – interim results (SGT-ZE). Nagra Arbeitsber. NAB 09-14.

Masurat, P., Eriksson, S. & Pedersen, K. (2010): Microbial sulphide production in compacted Wyoming bentonite MX-80 under in situ conditions relevant to a repository for high-level radioactive waste. Applied Clay Science 47/1-2, 58-64.

Mazurek, M. (2011): Aufbau und Auswertung der Gesteinsparameter-Datenbank für Opalinuston, den 'Braunen Dogger', Effinger Schichten und Mergel-Formationen des Helvetikums. Nagra Arbeitsber. NAB 11-20.

Mazurek, M. & Haller, A. de (2017): Pore-water evolution and solute-transport mechanisms in Opalinus Clay at Mont Terri and Mont Russelin (Canton Jura, Switzerland). Swiss Journal of Geosciences 110, 1, 129-149.

Müller, H.R., Garitte, B., Vogt, T., Köhler, S., Sakaki, T., Weber, H., Spillmann, T., Hertrich, M., Becker, J.K., Giroud, N., Cloet, V., Diomidis, N. & Vietor, T. (2017): Implementation of the full-scale emplacement (FE) experiment at the Mont Terri rock laboratory. Swiss Journal of Geosciences 110/1, 287-306.

Nagra (2002): Project Opalinus Clay. Safety report. Demonstration of disposal feasibility for spent fuel, vitrified high-level waste and long-lived intermediate-level waste (Entsorgungsnachweis). Nagra Tech. Report NTB 02-05.

Nagra (2014a): SGT Etappe 2: Vorschlag weiter zu untersuchender geologischer Standortgebiete mit zugehörigen Standortarealen für die Oberflächenanlage: Geologische Grundlagen. Dossier VI: Barriereneigenschaften der Wirt- und Rahmengesteine. Nagra Tech. Report NTB 14-02 Dossier VI.

Nagra (2014b): SGT-Etappe 2: Vorschlag weiter zu untersuchender geologischer Standortgebiete mit zugehörigen Standortarealen für die Oberflächenanlage: Charakteristische Dosisintervalle und Unterlagen zur Bewertung der Barrierensysteme. Nagra Tech. Report NTB 14-03.

Nagra (2016): Entsorgungsprogramm 2016 der Entsorgungspflichtigen. Nagra Tech. Report NTB 16-01.

Ottosson, M., Boman, M., Berastegui, P., Andersson, Y., Hahlin, M., Korvela, M. & Berger, R. (2016): Copper in ultrapure water. SKB Technical Report TR-16-01. Svensk Kärnbränslehantering AB, Stockholm, Sweden.

Parkhurst, D.L. & Appelo, C. (2013): Description of input and examples for PHREEQC version 3 – A computer program for speciation, batch-reaction, one-dimensional transport, and inverse geochemical calculations. US Geological Survey Techniques and Methods, Book 6, Chapter A43.

Pedersen, K. (2010): Analysis of copper corrosion in compacted bentonite clay as a function of clay density and growth conditions for sulfate-reducing bacteria. Journal of Applied Microbiology 108/3, 1094-1104.

Posiva (2012): Safety case for the disposal of spent nuclear fuel at Olkiluoto- design basis 2012. Posiva report 2012-03. Posiva Oy, Olkiluoto, Finland.

Raiko, H. (2005): Disposal canister for spent nuclear fuel - design report. Posiva report 2005-02. Posiva Oy, Olkiuoto, Finland.

Rickard, D. (2006): The solubility of FeS. Geochim. Cosmochim. Acta 70/23, 5779-5789.

Rickard, D., Butler, I.B. & Oldroyd, A. (2001): A novel iron mineral switch and its implications for earth and planetary science. Earth and Planetary Science Letters 189, 85-91.

Rickard, D. & Luther, G.W. (1997): Kinetics of pyrite formation by the H_2S oxidation of iron(III)monosulphide in aqueous solution between 25 and 125°C: the mechanism. Geochim. Cosmochim. Acta 61, 135-147.

Rickard, D. & Luther, G.W. (2007): Chemistry of iron sulfides. Chemical Reviews 107/2, 514-562.

Rickard, D. & Morse, J.W. (2005): Acid volatile sulfide (AVS). Marine Chemistry 97/3-4, 141-197.

Robie, R.A. & Waldbaum, D.R. (1968): Thermodynamic properties of minerals and related substances at 298.15 K (25° C) and one atmosphere (1.013 bars) pressure and at higher temperatures. Geological Survey Bulletin 1259.

Sato, T., Fujimori, Y., Nakayama, T., Gotoh, Y., Sunaga, Y., Nemoto, M., Matsunaga, T. & Tanaka, T. (2012): Assessment of the anti-biofouling potentials of a copper iodide-doped nylon mesh. Applied Microbiology and Biotechnology 95/4, 1043-1050.

Scully, J.R. & Edwards, M. (2013): Review of the NWMO copper corrosion allowance. TR-2013-04. NWMO, Toronto, Canada.

SKB (2010a): Corrosion calculations report for the safety assessment SR-Site. SKB Technical Report TR 10-66. Svensk Kärnbränslehantering AB, Stockholm, Sweden.

SKB (2010b): Design, production and initial state of the canister. SKB Technical Report TR-10-14. Svensk Kärnbränslehantering AB, Stockholm, Sweden.

Stroes-Gascoyne, S., Haveman, S.A. & Vilks, P. (1997): The change in bioavailability of organic matter associated with clay-based buffer materials as a result of heat and radiation treatment. MRS Proceedings 465, 987-994.

Stroes-Gascoyne, S., Sergeant, C., Schippers, A., Hamon, C.J., Nèble, S., Vesvres, M.-H., Barsotti, V., Poulain, S. & Le Marrec, C. (2011): Biogeochemical processes in a clay formation in situ experiment. Part D – Microbial analyses – Synthesis of results. Applied Geochemistry 26/6, 980-989.

Traber, D. (2004): Studies on weathered Opalinus Clay in a 130 year old railway tunnel (Col de La Croix). Part lll: Geochemical investigations of drillcore BBC3. Unpubl. Mont Terri Technical Note. Mont Terri Project, Switzerland.

Vinsot, A., Appelo, C.A.J., Lundy, M., Wechner, S., Cailteau-Fischbach, C., Donato, P. de, Pironon, J., Lettry, Y., Lerouge, C. & Cannière, P. de (2017): Natural gas extraction and artificial gas injection experiments in Opalinus Clay, Mont Terri rock laboratory (Switzerland). Swiss Journal of Geosciences 110/1, 375-390.

Vinsot, A., Leveau, F., Bouchet, A. & Arnould, A. (2014): Oxidation front and oxygen transfer in the fractured zone surrounding the Meuse/Haute-Marne URL drifts in the Callovian–Oxfordian argillaceous rock. Geological Society, London, Special Publications 400/1, 207-220.

Wersin, P., Alt-Epping, P., Pitkänen, P., Román-Ross, G., Trinchero, P., Molinero, J., Smith, P., Snellman, M., Filby, A. & Kiczka, M. (2014): Sulphide fluxes and concentrations in the spent nuclear fuel repository at Olkiluoto. Posiva report 2014-01. Posiva Oy, Olkiluoto, Finland.

Wersin, P., Mazurek, M., Waber, N., Mäder, U.K., Gimmi, T., Rufer, D. & de Haller, A. (2013): Rock and porewater characterisation on drillcores from the Schlattingen borehole. Nagra Arbeitsbericht NAB 12-54.

Wersin, P., Stroes-Gascoyne, S., Pearson, F.J., Tournassat, C., Leupin, O.X. & Schwyn, B. (2011): Biogeochemical processes in a clay formation in situ experiment. Part G – Key interpretations and conclusions. Implications for repository safety. Applied Geochemistry 26/6, 1023-1034.

A Sulphate and sulphide fluxes in the simplified model

A.1 Scenario A: Sulphate-reducing bacteria active only in the EDZ

In the description of scenario A with the simplified model, which is described in overview in Section 4.2.2, sulphate ions from the dissolution of minerals b and c initially present in the buffer and host rock migrate towards the EDZ by diffusion, at rates denoted by F_{bz} and F_{czd}, respectively, where they are reduced to sulphide ions. Sulphate ions from the rock also reach the EDZ by advection at a rate F_{cza}, where they are again reduced to sulphide. The sulphide so-produced then diffuses into the buffer and towards the canister at a rate denoted by F_s, diffuses into the host rock at a rate denoted by F_{rd} [mol m^{-1} a^{-1}] or is advected back into the host rock at a rate denoted by F_{ra}. In the following, formulae are derived to calculate the six fluxes F_{bz}, F_{czd}, F_{cza} F_s, F_{rd} and F_{ra}.

A.1.1 Diffusive sulphate flux from the buffer to the EDZ

The approach used to determine F_{bz}, the diffusive sulphate flux from the buffer to the EDZ, is shown in Fig. A-1. It is assumed that the concentration $C_b(r,t)$ [mol m^{-3}] of sulphate in the buffer is subject to a solubility limit S_b [mol m^{-3}]. This concentration is maintained wherever mineral b is present. However, as sulphate diffuses through the buffer to the EDZ and is converted there (instantaneously and completely) to sulphide, the buffer is gradually depleted in mineral b. The depleted buffer region starting as a narrow band where the buffer contacts the EDZ, and gradually broadens until the whole of the buffer is depleted. Shrinkage of the un-depleted buffer "core" gradually reduces the concentration gradient across the depleted region, so the sulphate flux F_{bz} also decreases with time.

It is assumed that the time scale for diffusion across the depleted region is small compared with the rate of shrinkage of the core, so, in calculating diffusion, a pseudo-steady state sulphate concentration distribution is assumed across the depleted region. This distribution is the steady-state solution to the diffusion equation in cylindrical polar coordinates, with a fixed concentration boundary condition at the inner edge of the depleted region (or outer edge of the core) and a zero concentration boundary condition at the inner boundary of the EDZ:

$$C_b(r,t) = S_b \cdot \begin{cases} \dfrac{ln\left(\frac{r}{r_o}\right)}{ln\left(\frac{r_b}{r_o}\right)} & r > r_b \\ 1 & r_{can} \le r \le r_b \end{cases} \qquad \text{(A-1)}$$

where r_b [m] is the core radius. The sulphate flux across the depleted region, per unit tunnel length, is:

$$F_{bz} = \begin{cases} -2\pi r D_{e,b} \dfrac{dC_b}{dr} = -2\pi D_{e,b} S_b / ln\left(\frac{r_b}{r_o}\right) & \text{if} \quad r_b > r_{can} \\ 0 & \text{otherwise} \end{cases} \qquad \text{(A-2)}$$

where $D_{e,b}$ [m^2 a^{-1}] is the effective diffusion coefficient of sulphate in the buffer. Note that the value assigned to the effective diffusion coefficient should, in principle, take account of any possible effect of the dissolution of mineral b on diffusion, but this has not been considered in the present study.

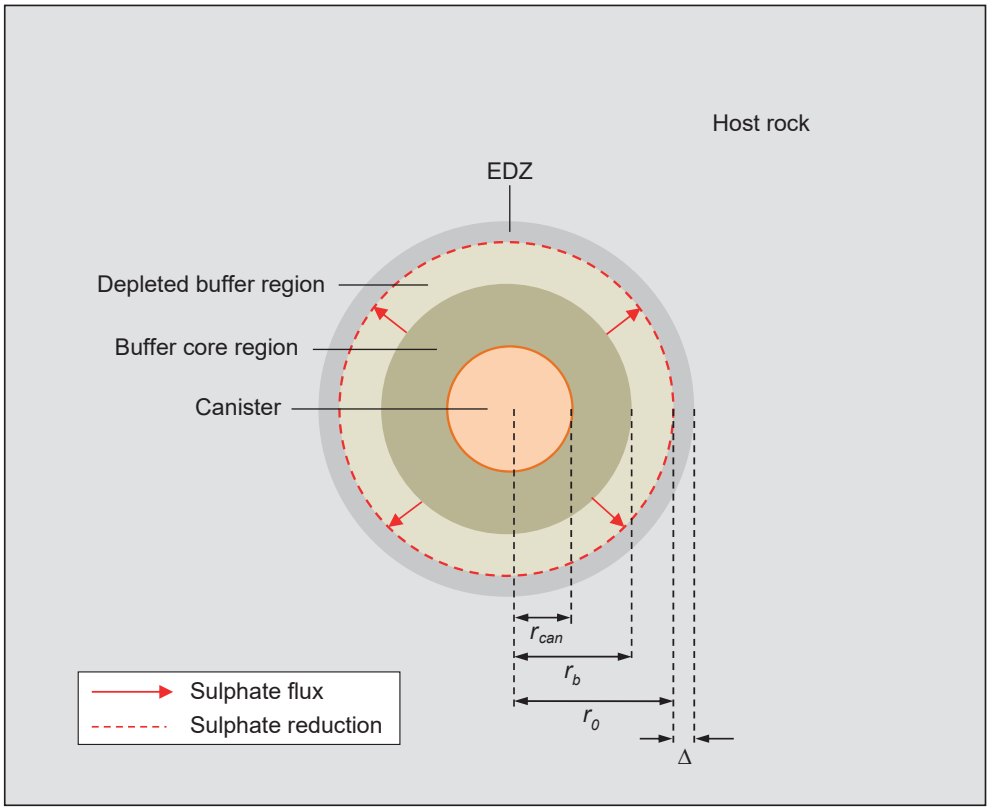

Fig. A-1: Model to determine the sulphate flux from the buffer to the EDZ.

This sulphate flux can also be expressed in terms of the rate of change of the core radius, since this determines the amount of sulphate released per unit time:

$$F_{bz} = -10 \cdot n_b \cdot \rho_B . \frac{w_b}{f_b} \cdot 2\pi \cdot r_b \cdot \frac{dr_b}{dt} \tag{A-3}$$

where ρ_b [kg m^{-3}] is the dry density of the buffer, and n_b is a stoichiometry factor , i.e. the number of moles of sulphate (and hence sulphide) produced by the dissolution of one mole of mineral b.

From Eqs. (A-2) and (A-3):

$$r_b \cdot \frac{dr_b}{dt} \cdot \ln\left(\frac{r_f}{r_o}\right) = \frac{D_{eb} S_b t}{10 \cdot n_b \cdot \rho_B . \frac{w_b}{f_b}} \qquad r_b > r_{can} \tag{A-4}$$

The radius of the core region is obtained by integrating this equation:

$$\int_{r_o}^{r_b} r_b' ln\left(\frac{r_b'}{r_o}\right) dr_b' = \frac{D_{eb} S_b t}{10 \cdot n_b \cdot \rho_B . \frac{w_b}{f_b}} \qquad r_b > r_{can} \tag{A-5}$$

$$r_0^2 \int_{r_r'=r_o}^{r_f} \left[\frac{1}{2}\left(\frac{r_b'}{r_o}\right)^2 ln\left(\frac{r_b'}{r_o}\right) - \frac{1}{4}\left(\frac{r_b'}{r_o}\right)^2\right] = \frac{D_e S_b t}{10 \cdot n_b \cdot \rho_B . \frac{w_b}{f_b}} \qquad r_b > r_{can} \tag{A-6}$$

$$\frac{r_f^2}{2}\left[ln\left(\frac{r_f}{r_o}\right) + \frac{1}{2}\left(\frac{r_0^2 - r_b^2}{r_b^2}\right)\right] = \frac{D_e S_b t}{10 \cdot n_b \cdot \rho_B . \frac{w_b}{f_b}} \qquad r_b > r_{can} \tag{A-7}$$

r_b is obtained by solving Eq. A-7 iteratively.

Having determined r_b as a function of time, the sulphate flux F_{bz} to the EDZ (per unit length of EDZ) is obtained using Eq. A-2.

A.1.2 Diffusive sulphate flux from the host rock to the EDZ

The approach used to determine F_{czd}, the diffusive sulphate flux from the host rock to the EDZ, is shown in Fig. A-2. It is analogous to that used to determine the flux from the buffer to the EDZ, and involves an expanding region of the host rock adjacent to the EDZ that is depleted in mineral c.

It is assumed that the concentration $C_c(r,t)$ [mol m^{-1}] of sulphate in the host rock is subject to a solubility limit S_c [mol m^{-3}]. This concentration is maintained wherever mineral c is present.

This concentration distribution across the depleted region is again the steady-state solution to the diffusion equation in cylindrical polar coordinates, with a fixed concentration boundary condition at the outer edge of the depleted region and a zero concentration boundary condition where the undisturbed host rock contacts the EDZ:

$$C_c(r,t) = S_c \cdot \begin{cases} \dfrac{ln\left(\frac{r}{a}\right)}{ln\left(\frac{r_f}{a}\right)} & r < r_c \\ 1 & r \geq r_c \end{cases} \tag{A-8}$$

where r_c [m] is in this instance the outer radius of the depleted region and a [m] is the outer radius of the EDZ. The (inwardly directed) sulphate flux diffusing across the depleted region, per unit tunnel length, is:

$$F_{czd} = \frac{2\pi r D_{e,c} \frac{dC_c}{dr} = 2\pi D_{e,c} S_c}{ln\left(\frac{r_c}{a}\right)} \tag{A-9}$$

where $D_{e,c}$ [$m^2 a^{-1}$] is the effective diffusion coefficient of sulphate in the host rock. Note again that the value assigned to the effective diffusion coefficient should, in principle, take account of any possible effect of the dissolution of mineral c on diffusion, but this has not been considered in the present study.

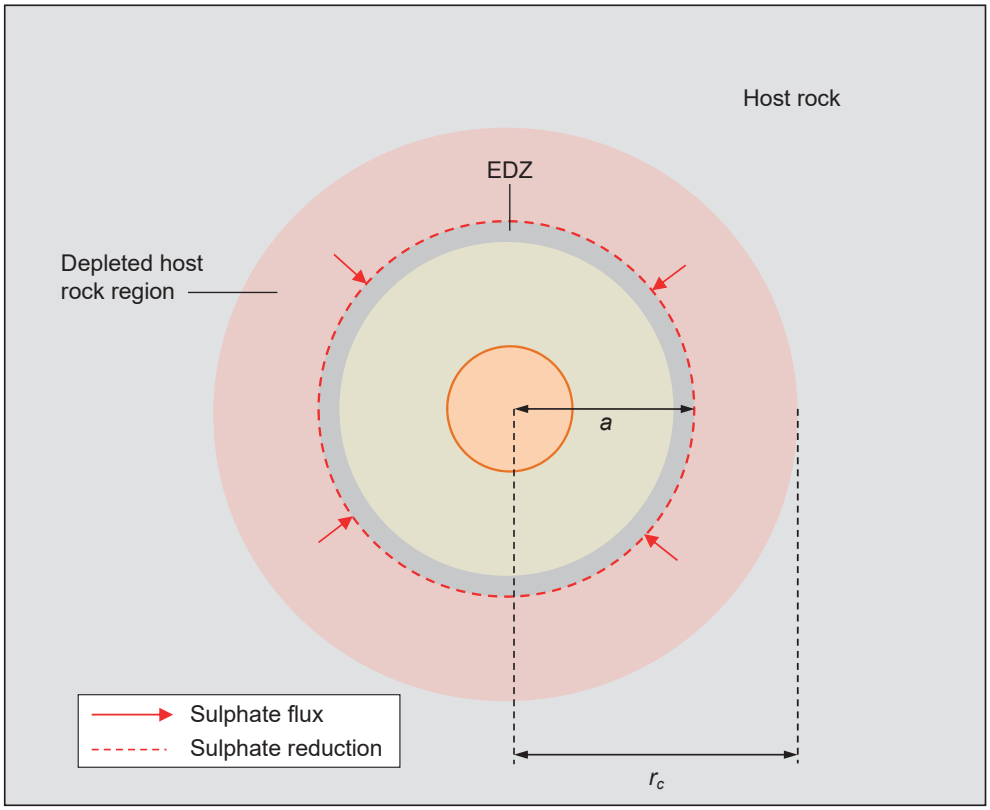

Fig. A-2: Model to determine the diffusive sulphate flux from the host rock to the EDZ.

This sulphate flux can also be expressed in terms of the rate of change of the depleted region radius, since this determines the amount of sulphate released per unit time:

$$F_{czd} = 10 \cdot n_c \cdot \rho_{hr} \cdot \frac{w_c}{f_c} \cdot 2\pi \cdot r_f \cdot \frac{dr_c}{dt} \quad \text{(A-10)}$$

where ρ_{hr} [kg m^{-3}] is the dry density of the host rock, and n_c is a stoichiometry factor , i.e. the number of moles of sulphate (and hence sulphide) produced by the dissolution of one mole of mineral c.

From Eq. (A-9) and (A-10):

$$r_c \cdot \frac{dr_c}{dt} \cdot \ln\left(\frac{r_c}{r_o}\right) = \frac{D_{ec} S_c t}{10 \cdot n_c \cdot \rho_{hr} \cdot \frac{w_c}{f_c}} \quad \text{(A-11)}$$

The radius of the core region of obtained by integrating this equation:

$$\int_a^{r_c} r_c' ln\left(\frac{r_c'}{a}\right) dr_c' = \frac{D_{ec} S_c t}{10 \cdot n_c \cdot \rho_{hr} \cdot \frac{w_c}{f_c}} \tag{A-12}$$

$$a^2 \Big|_{r_c'=a}^{r_c} \left[\frac{1}{2}\left(\frac{r_c'}{a}\right)^2 ln\left(\frac{r_c'}{a}\right) - \frac{1}{4}\left(\frac{r_c'}{a}\right)^2\right] = \frac{D_{ec} S_c t}{10 \cdot n_c \cdot \rho_{hr} \cdot \frac{w_c}{f_c}} \tag{A-13}$$

$$\frac{r_c^2}{2}\left[ln\left(\frac{r_c}{a}\right) + \frac{1}{2}\left(\frac{a - r_c^2}{r_c^2}\right)\right] = \frac{D_{ec} S_c t}{10 \cdot n_c \cdot \rho_{hr} \cdot \frac{w_c}{f_c}} \tag{A-14}$$

r_c is obtained by solving Eq. A-14 iteratively.

Having determined r_c as a function of time, the sulphate flux F_{czd} to the EDZ (per unit length of EDZ) is obtained using Eq. A-9.

A.1.3 Advective sulphate flux from the host rock to the EDZ

The approach used to determine F_{cza}, the advective sulphate flux from the host rock to the EDZ, is shown in Fig. A-3. In reality, diffusion and advection transport in the host rock are not independent processes, since both depend on the sulphate concentration distribution and its evolution. At early times, the supply of sulphate to the EDZ will be predominantly by diffusion. At later times, advection could become more important. However, for the purpose of the present simplified model, this coupling is disregarded. Furthermore, it is assumed that advection is a relatively fast process compared with sulphate mineral depletion in the host rock, such that depletion can be neglected when calculating advective fluxes. This approach is conservative, in that it will tend to over-estimate sulphate fluxes.

In the Nagra safety studies, it is generally assumed that the hydraulic conductivity of the EDZ around the emplacement drifts is much larger than that of the undisturbed host rock. As a result, the ambient flow within the host rock will converge upstream of these features, pass through them, and then diverge again downstream, as shown in the figure. The flow capture width is the term used for the width of a stream tube that passes into and out of the EDZ, before convergence or after divergence, since it can be used to express the amount of water that passes through (or is "captured" by) the EDZ for a known ambient flow. In Poller et al. (2014), the capture width for a circular emplacement drift with an EDZ in a homogeneous and isotropic rock is shown to be twice the tunnel diameter (including EDZ), i.e. equal to $4a$.

If the hydraulic conductivity of the host rock is K [m a^{-1}], the hydraulic gradient is i and the undisturbed concentration of sulphate in the Opalinus Clay porewater fixed by the solubility limit of mineral c, i.e. S_c, the advective sulphate flux F_A to the outer boundary of the EDZ is given by:

$$F_{cza} = 4a \cdot K \cdot i \cdot S_c \tag{A-15}$$

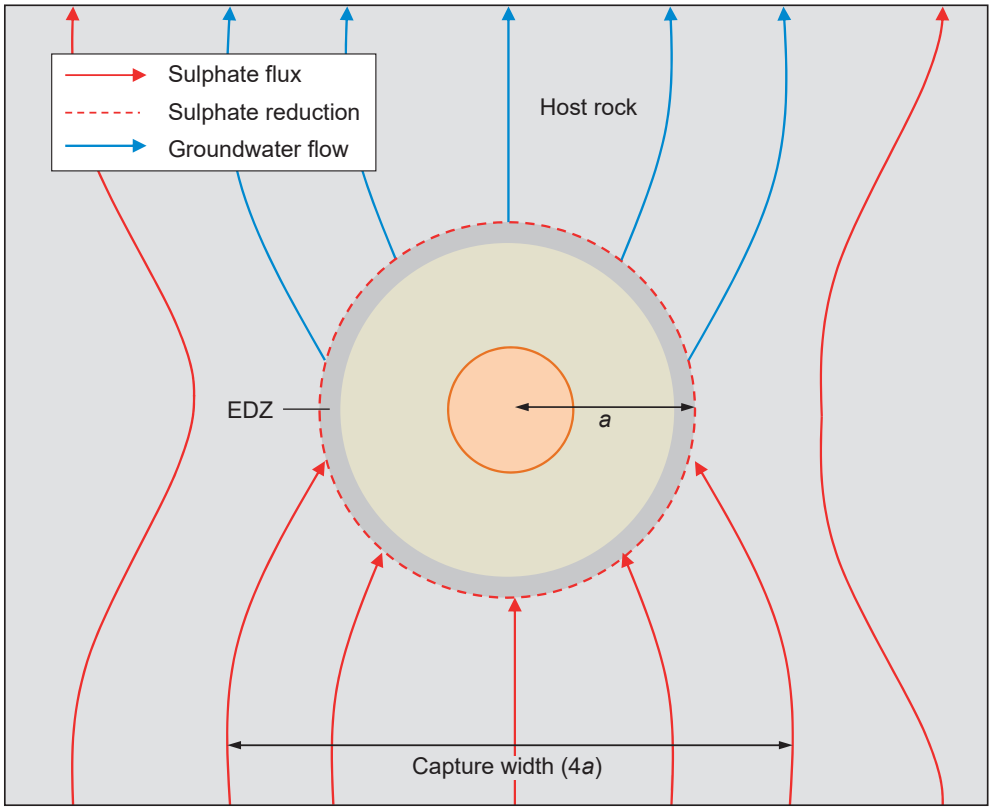

Fig. A-3: Model to determine the advective sulphate flux from the host rock to the EDZ.

A.1.4 Diffusive sulphide flux from the EDZ to the canister surface

The approach used to determine F_s, the diffusive sulphate flux from the EDZ to the canister surface, is shown in Fig. A-4.

As in the case of sulphate, a pseudo-steady state sulphide concentration distribution is assumed in the buffer, whereby the sulphide concentration $C_{sb}(r,t)$ [mol m^{-1}] at any given time and location in the buffer is approximated by the steady-state solution to the diffusion equation, with boundary conditions $C_z(t)$, the time-dependent concentration of sulphide (see Eq. 4-4), imposed at the inner boundary of the EDZ (i.e. the outer boundary of the buffer), and zero concentration imposed at the canister surface, due to the consumption of sulphide by canister corrosion:

$$C_{sb} = C_z(t) \cdot \frac{\ln\left(\frac{r}{r_{can}}\right)}{\ln\left(\frac{r_0}{r_{can}}\right)} \qquad \text{(A-16)}$$

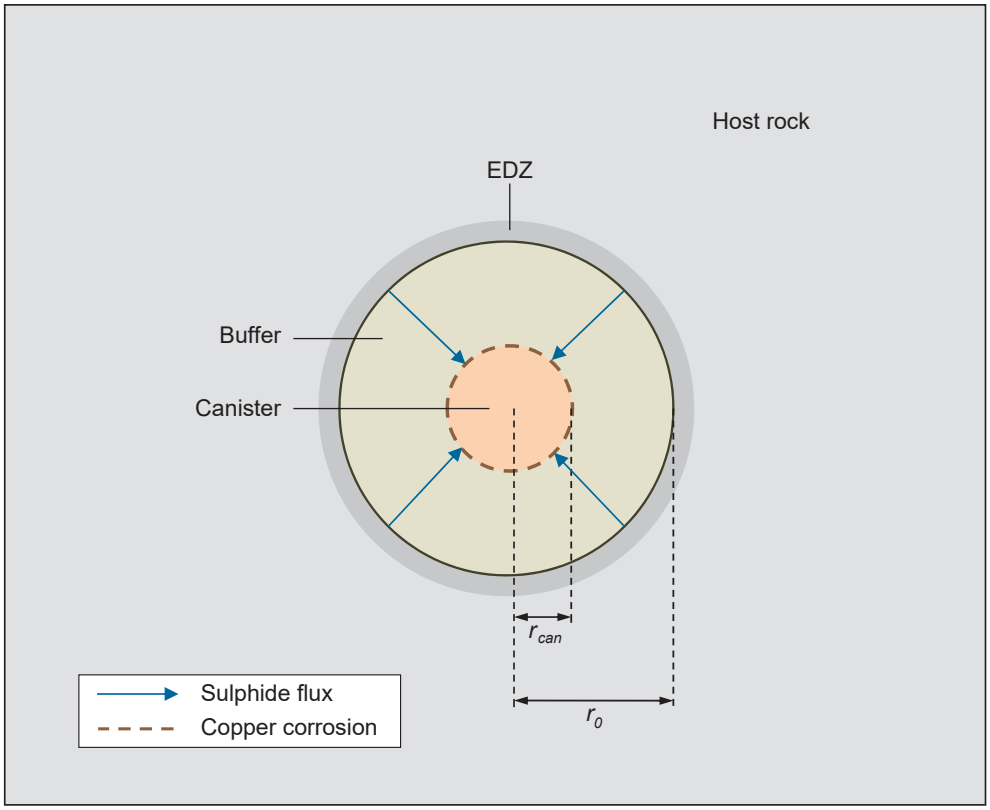

Fig. A-4: Model to determine the sulphide flux from the EDZ to the canister surface.

The sulphide flux to the canister surface is then:

$$F_s = \frac{2\pi r D_{e,sb} \frac{dC_{sb}}{dr} = 2\pi D_e C_z(t)}{ln\left(\frac{r_0}{r_{can}}\right)} \quad \text{(A-17)}$$

where $D_{e,sb}$ [m^2 a^{-1}] is the effective diffusion coefficient of sulphide in the buffer.

A.1.5 Diffusive sulphide flux from the EDZ to the rock

The diffusive sulphide flux from the EDZ back into the host rock, F_{rd}, is conceptualised as a 1-D process along a diffusive transport path that extends from the emplacement drift to the upper and lower boundaries of the host rock. The transport path is assigned a width equal to half the external surface area of the EDZ, to ensure that radionuclide transfer from the emplacement drifts to the rock by diffusion is represented by the proper contact area. The 1-D steady-state solution of the diffusion equation then gives a diffusive flux out of the EDZ of:

$$F_{rd} = 2\pi a \cdot D_{e,sr} \cdot \frac{C_z(t)}{L} \quad \text{(A-18)}$$

where $D_{e,sr}$ [m^2 a^{-1}] is the effective diffusion coefficient of sulphide in the rock, and L [m] is a diffusion distance, taken to be the distance from the centre of the tunnel to the upper or lower host-rock boundaries.

A.1.6 Advective sulphide flux from the EDZ to the rock

The expression for the advective sulphide flux from the EDZ back into the host rock, F_{ra}, is analogous to that for the advective sulphate flux from the host rock to the EDZ (Eq. A-15), i.e.:

$$F_{ra} = 4a \cdot K \cdot i \cdot C_z(t) \tag{A-19}$$

A.2 Scenario B and C: Sulphate-reducing bacteria active in the EDZ and buffer

As described in Section 4.2.3, three evolution phases can be distinguished:

- the dissolution front separating areas with precipitated sulphide minerals from areas depleted in these minerals resides within the buffer,
- the dissolution front separating areas with precipitated sulphide minerals from areas depleted in these minerals resides within the EDZ, and
- the dissolution front has reached the outer boundary of the EDZ, where sulphide originating from the host rock has been precipitated (precipitates assumed here to occupy a narrow ring).

The sulphide fluxes F_s to the canister surface in each of these three phases are described in the following sections.

A.2.1 Dissolution front resides within the buffer

The approach used to determine F_s, the diffusive sulphide flux to the canister, during the period that the dissolution front resides within the buffer is shown in Fig. A-5. It is assumed in this approach that the concentration $C_s(r,t)$ [mol m^{-3}] of sulphide in the buffer (as in the EDZ) is subject to a solubility limit S_s [mol m^{-3}]. This concentration is maintained outside the front, where sulphide minerals are present.

As previously, it is assumed that the time scale for diffusion across the depleted region is small compared with the rate of expansion of the depleted region, so, in calculating diffusion, a pseudo-steady state sulphate concentration distribution may be assumed. This distribution is the steady-state solution to the diffusion equation in cylindrical polar coordinates, with a zero concentration boundary condition at the inner boundary of the depleted region (the canister surface) due to consumption of sulphide by corrosion and a concentration S_s maintained at the outer boundary:

$$C_s(r,t) = S_s \cdot \begin{cases} \dfrac{\ln\left(\frac{r}{r_{can}}\right)}{\ln\left(\frac{r_f}{r_{can}}\right)} & r_{can} \le r < r_f \\ 1 & r_f \le r \le r_0 \end{cases} \tag{A-20}$$

where r_f [m] is radius of the depleted region.

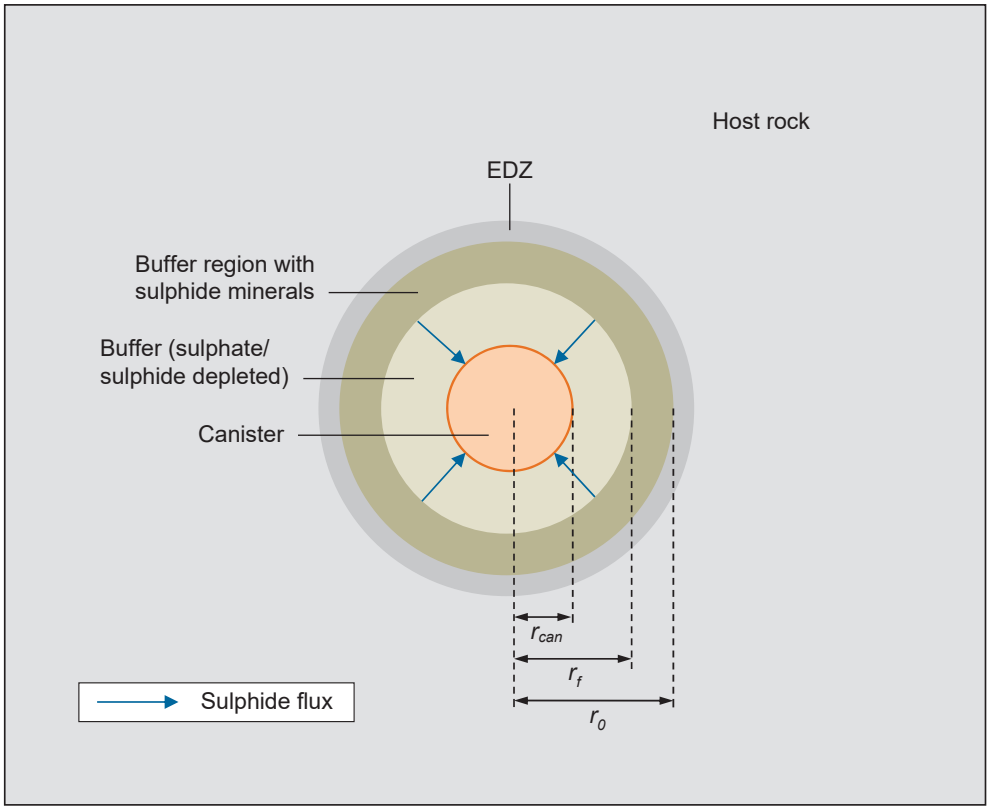

Fig. A-5: Model to determine the sulphide flux to the canister surface when the dissolution front resides within the buffer.

The (inwardly directed) sulphide flux across the depleted region, per unit tunnel length, is:

$$F_s = 2\pi \cdot S_s \cdot \frac{D_{e,sb}}{ln\left(\frac{r_f}{r_{can}}\right)} \tag{A-21}$$

where $\boldsymbol{D_{e,sb}}$ [m^2 a^{-1}] is the effective diffusion coefficient of sulphide in the buffer.

This sulphide flux can also be expressed in terms of the rate of change of the depleted region radius:

$$F_s = m_b \cdot 2\pi \cdot r_f \cdot \frac{dr_f}{dt} \tag{A-22}$$

where m_b [mol m^{-3}] is the mass of sulphide in the buffer per unit buffer volume at locations outside the front (where sulphide minerals are present), given by:

$$m_b = 10 \cdot n_b \cdot \frac{w_b}{f_b} \cdot \rho_b \tag{A-23}$$

Here, ρ_b [kg m^{-3}] is the dry density of the buffer (other symbols defined earlier).

From Eq. A-21 and Eq. A-22:

$$r_f \cdot \frac{dr_f}{dt} \cdot \ln\left(\frac{r_f}{r_{can}}\right) = D_{e,sb} \cdot \frac{S_s}{m_b} \tag{A-24}$$

The inner radius of the depleted region is obtained by integrating Eq. A-24:

$$\int_{r_{can}}^{r_f} r_f' \ln\left(\frac{r_f'}{r_c}\right) dr_f' = \frac{D_{e,sb} S_s t}{m_b} \tag{A-25}$$

$$r_{can}^2 \Big|_{r_f'=r_{can}}^{r_f} \left[\frac{1}{2}\left(\frac{r_f'}{r_{can}}\right)^2 \ln\left(\frac{r_f'}{r_{can}}\right) - \frac{1}{4}\left(\frac{r_f'}{r_{can}}\right)^2\right] = \frac{D_{e,sb} S_s t}{m_b} \tag{A-26}$$

$$\frac{r_f^2}{2}\left[\ln\left(\frac{r_f}{r_{can}}\right) - \frac{1}{2}\left(\frac{r_f^2 - r_{can}^2}{r_f^2}\right)\right] = \frac{D_{e,sb} S_s t}{m_b} \tag{A-27}$$

r_f is obtained by solving Eq. A-27 iteratively.

Having determined r_f, the sulphate flux F_s to the canister surface is obtained using Eq. A-21.

The time t_b[a] to deplete the entire buffer, is given by setting $r_f = r_0$:

$$t_b = \frac{r_0^2 m_b}{2 D_{e,sb} S_s}\left[\ln\left(\frac{r_0}{r_{can}}\right) - \frac{1}{2}\left(\frac{r_0^2 - r_{can}^2}{r_0^2}\right)\right] \tag{A-28}$$

This is the starting time for the next period, in which the dissolution front resides within the EDZ.

A.2.2 Dissolution front resides within the EDZ

The approach used to determine F_s, the diffusive sulphide flux to the canister period, during the period that the dissolution front resides within the EDZ, is essentially the same as when the front resides within the buffer. It is assumed that the concentration $C_s(r,t)$ [mol m^{-3}] of sulphide in the EDZ is subject to the same solubility limit S_s [mol m^{-3}] as in the buffer. This concentration is maintained outside the front, where sulphide minerals are present.

Once again, it is assumed that the time scale for diffusion across the depleted region is small compared with the rate of expansion of the depleted region, so, in calculating diffusion, a pseudo-steady state sulphate concentration distribution may be assumed. This distribution is the steady-state solution to the diffusion equation in cylindrical polar coordinates, this time for two concentric media (the buffer and the EDZ). A zero concentration boundary condition is imposed at the inner boundary of the depleted buffer region (the canister surface) due to consumption of sulphide by corrosion and a concentration S_s maintained at the outer boundary:

$$C_s(r,t) = S_s \cdot \begin{cases} \dfrac{\frac{D_{e,sz}}{D_{e,sb}}\ln\left(\frac{r}{r_{can}}\right)}{\frac{D_{e,sz}}{D_{e,sb}}\ln\left(\frac{r_0}{r_{can}}\right)+\ln\left(\frac{r_f}{r_0}\right)} & r_{can} \le r < r_0 \\ \dfrac{\frac{D_{e,sz}}{D_{e,sb}}\ln\left(\frac{r_0}{r_{can}}\right)+\ln\left(\frac{r}{r_0}\right)}{\frac{D_{e,sz}}{D_{e,sb}}\ln\left(\frac{r_0}{r_c}\right)+\ln\left(\frac{r_f}{r_0}\right)} & r_0 \le r < r_a \\ 1 & r_f \le r \le a \end{cases} \tag{A-29}$$

where $D_{e,sz}$ [m^2 a^{-1}] is the effective diffusion coefficient of sulphide in the EDZ.

The (inwardly directed) sulphide flux across the depleted region, per unit tunnel length, is:

$$F_s = 2\pi \cdot S_s \cdot \frac{D_{e,sz}}{\frac{D_{e,sz}}{D_{e,sb}}\ln\left(\frac{r_0}{r_c}\right)+\ln\left(\frac{r_f}{r_0}\right)} \tag{A-30}$$

This sulphide flux can also be expressed in terms of the rate of change of the depleted region radius:

$$F_s = m_z \cdot 2\pi \cdot r_f \cdot \frac{dr_f}{dt} \tag{A-31}$$

where m_z [mol m^{-3}] is the mass of sulphide in the buffer per unit buffer volume at locations outside the front (where sulphide minerals are present). Referring to Eq. 3-2, this mass is given by:

$$m_z = \frac{M_0}{2\pi(r_0\Delta - \Delta^2)}\,10 \cdot n_a \cdot \frac{w_a}{f_a} \cdot \rho_{EDZ} \tag{A-32}$$

From Eq. A-30 and Eq. A-31:

$$r_f \cdot \frac{dr_f}{dt} \cdot \left[\frac{D_{e,sz}}{D_{e,sb}}\ln\left(\frac{r_0}{r_{can}}\right)+\ln\left(\frac{r_f}{r_0}\right)\right] = D_{e,sz} \cdot \frac{S_s}{m_z} \tag{A-33}$$

The radius of the depleted region is obtained by integrating Eq. A-33:

$$\int_{r_0}^{r_f} r_f' \left[\frac{D_{e,sz}}{D_{e,sb}}\ln\left(\frac{r_0}{r_{can}}\right)+\ln\left(\frac{r_f'}{r_0}\right)\right] dr_f' = D_{e,sz} \cdot \frac{S_s}{m_z} \cdot (t - t_b) \tag{A-34}$$

$$\frac{1}{2}\Big|_{r_f'=r_0}^{r_f}\left[\frac{D_{e,sz}}{D_{e,sb}}(r_f^2 - r_0^2)\ln\left(\frac{r_0}{r_{can}}\right) + r_f'^2\ln\left(\frac{r_f'}{r_0}\right) - \frac{1}{2}r_f'^2\right] = D_{ez} \cdot \frac{S_s}{m_z} \cdot (t - t_b) \tag{A-35}$$

$$\frac{1}{2}\left\{\frac{D_{e,sz}}{D_{e,sb}}\left(r_f^2 - r_0^2\right)\ln\left(\frac{r_0}{r_{can}}\right) + r_f^2\left[\ln\left(\frac{r_f}{r_0}\right) - \frac{1}{2}\left(\frac{r_f^2 - r_0^2}{r_f^2}\right)\right]\right\} = D_{e,sz}\cdot\frac{S_s}{m_z}\cdot(t - t_b) \quad \text{(A-36)}$$

r_f is obtained by solving Eq. A-36 iteratively.

Having determined r_f, the sulphide flux F_s to the canister surface in this time interval is obtained using Eq. A-30.

The time t_z[a] to deplete the entire buffer, is given by setting $r_f = r_0$:

$$t_z = t_b + \frac{m_z}{2D_{e,sz}S_s}\left[\frac{D_{e,sz}}{D_{e,sb}}(a^2 - r_0^2)ln\left(\frac{r_0}{r_{can}}\right) + a^2\left[ln\left(\frac{a}{r_0}\right) - \frac{1}{2}\left(\frac{a^2 - r_0^2}{a^2}\right)\right]\right] \quad \text{(A-37)}$$

This is the starting time for the next period, in which the dissolution front resides at the outer boundary of the EDZ.

A.2.3 Dissolution front at the outer boundary of the EDZ

The (inwardly directed) sulphate mass transfer across from the intact rock to the EDZ is the same as calculate in Sections A.1.2 and A.1.3, i.e. $\boldsymbol{F_{czd} + F_{cza}}$.

In the present model, this sulphate flux is reduced to sulphide at the outer boundary of the EDZ, where it precipitates. Some then migrates back into the geosphere and the rest resides at the boundary until the dissolution front reaches that boundary at time t_z.

Summing and integrating the various fluxes, the mass of sulphide $M(t_z)$ [mol m^{-1}] in the EDZ at time t_z will be:

$$M(t_z) = \int_0^{t_z}(F_{czd} + F_{cza} - F_{rd} - F_{ra})\,dt \quad \text{(A-38)}$$

Thereafter, the mass is given by:

$$M(t) = M(t_z) + \int_{t_z}^{t}(F_{czd} + F_{cza} - F_s - F_{rd} - F_{ra})\,dt \quad \text{(A-39)}$$

Definitions and expressions to calculate the fluxes F_{czd}, F_{cza}, F_{rd} and F_{ra} are the same as for model scenario A and are given in Appendix A.1. The flux of sulphide F_s from the outer boundary of the bentonite to the canister surface is given by Eq. A-30, setting $r_f = a$:

$$F_s = 2\pi\cdot S_s\cdot\frac{D_{e,sz}}{\frac{D_{e,sz}}{D_{e,sb}}\ln\left(\frac{r_0}{r_c}\right) + \ln\left(\frac{a}{r_0}\right)} \quad \text{(A-40)}$$

This flux is maintained unless and until $M(t)$, as calculated using Eq. A-39, is zero. In practice, remains greater than zero for all calculation cases considered in the present study.

B The impact of a high pH concrete liner on canister corrosion

Shotcrete liners (ca. 30 cm thick) will be used to provide stable and safe conditions in the tunnels during the construction and operation of the facility. The liners have no long-term safety function, but at the same time they should not compromise any of the long-term safety functions of other repository components through interactions with them. The effect of increased pH was not included in the calculations presented in Chapters 5, 6 and 7, in order to keep the model setup lean. The effect of a shotcrete liner is evaluated in this appendix and it is shown that elevated pH would reduce sulphide solubility due to mackinawite equilibrium, resulting in reduced sulphide fluxes towards the canister and thus in lower corrosion depths.

B.1 Model description

The methodology employed in this calculation scenario comprises two main steps:

- First, a batch geochemical calculation (using as input the expected evolution of pH in the concrete liner) is performed to calculate a time series of sulphide solubility (concentration in porewater) in a portion of the EDZ in direct contact with the liner. Sulphide concentration is calculated assuming mackinawite equilibrium together with additional equilibrium constraints (described in more detail below).
- Then, the calculated sulphide concentration evolution in the EDZ in time is used as input for the simplified model (definition of sulphide source) to calculate sulphide fluxes towards the canister.

Batch geochemical model

Batch calculations were performed using the PHREEQC (Parkhurst & Appelo 2013) geochemical simulator and the Thermochimie v.9b thermodynamic database. The input chemical data for the Opalinus Clay is the same as that used for reactive transport calculations (Section 5.2.2.) The assumption is made that low-pH shotcrete will be used as a liner. The evolution of pH in the concrete liner is approximated for a period of 1'000'000 years based on previous modelling results reported by Bradbury et al. (2014) for the initial 56'200 years, and expert judgment for later times. Six pH evolution phases are defined (see Fig. B-1):

- The initial 126 years, where pH drops from the starting value of 11.1 to 10.6
- From 126 to 1'000 years, where pH decreases from 10.6 to 10.4
- From 1'000 to 10'000 years, where pH decreases from 10.4 to 10.1
- From 10'000 to 56'200 years, where pH decreases from 10.1 to 9.6
- From 56'200 to 100'000 years, where pH decreases from 9.6 to 8.0
- The remaining time up to 1'000'000 years, where pH remains constant at 8.0

pH evolution up to 56'200 years was modelled by Bradbury and collaborators, and the pH values they reported for specific times (126, 1'000, 10'000 and 56'200 years) are used with linear interpolation in-between them. Beyond the 56'200 years of the modelled evolution, an assumption is made that pH would linearly decrease towards 8 and remain constant thereafter (in agreement with estimations made by the authors for the long time pH evolution).

The batch geochemical equilibrium calculation was performed with the following constraints:

- pH is imposed (fixed to the desired value)
- S(-II) is controlled by mackinawite equilibrium
- Fe is controlled by siderite equilibrium
- C(IV) is controlled by calcite equilibrium
- Ca is controlled by equilibrium with clay exchanger (along with Na, Mg and K).

This calculation aims to simplistically represent the composition of the EDZ porewater under the impact of elevated pH due to cement dissolution. The expected pH evolution of the shotcrete liner and the calculated concentration of total dissolved sulphide are presented in Fig. B-1. The figure highlights the importance of pH for sulphide solubility under mackinawite equilibrium: a pH decrease by three units translates into an approximate three orders of magnitude increase in sulphide concentration. Therefore elevated pH conditions are expected to decrease sulphide concentrations in the EDZ, and (in direct proportion) reduce sulphide fluxes towards the canister. For comparison, at pH 7.3 (initial pH value in undisturbed Opalinus Clay) the sulphide concentration is evaluated at 2.6×10^{-6} mol/L, while at pH 6.6 (the minimum value calculated in RT simulation for scenario A) at 2.3×10^{-5} mol/L.

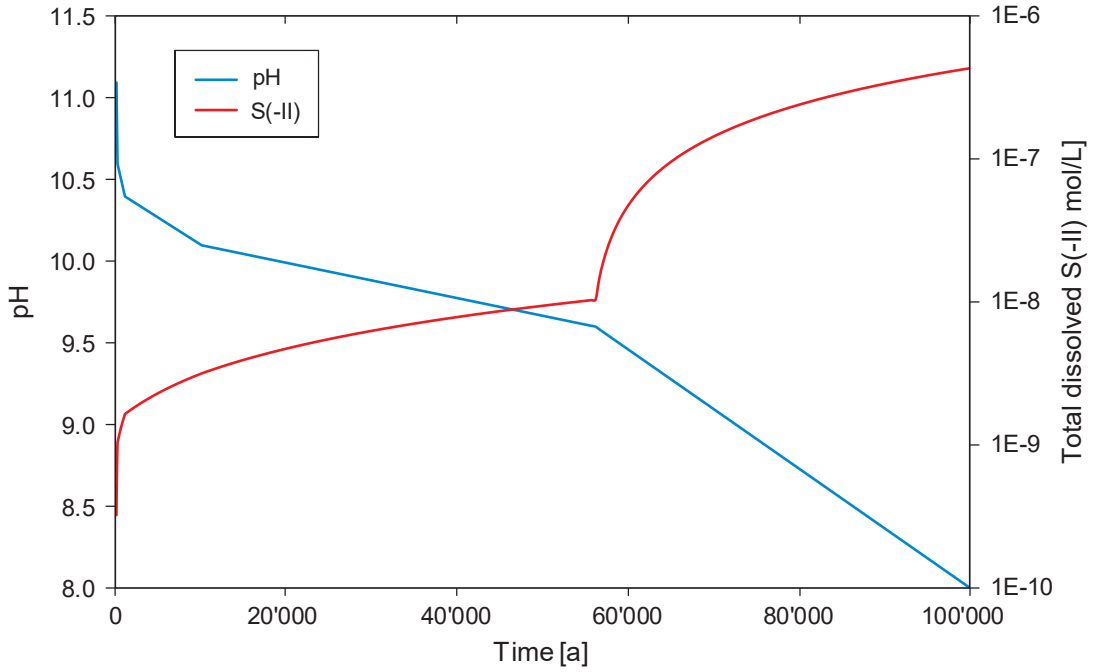

Fig. B-1: The estimated pH evolution of the low-pH concrete liner and the corresponding sulphide solubility due to mackinawite equilibrium.

Only the initial 100'000 years are shown, after that pH and sulphide concentration values remain constant.

B.2 Model results

The impact of the high pH liner on the sulphide solubility was illustrated in the previous section. It can thus be expected that in the presence of a shotcrete liner, the sulphide flux towards the canister and hence the corrosion depth will be further decreased. This effect is most pronounced at times t < 60'000 years. After 60'000 years, the pH decreases and sulphide concentrations continue to increase. To restrict computational complexity and because this effect would add to the lower boundary of corrosion depth, it was decided to assess the impact of this pH-dependent using the simplified model (see Section 4.2.2).

Fig. B-2 shows the corrosion calculated by taking into account the high pH conditions set by the shotcrete liner and compared with cases where different sulphide solubilities where assumed. In the initial period upto 60'000 years the corrosion depths calculated for the case with a shotcrete liner are insignificant. After 60'000 years, a time coinciding with a significant drop of the pH of the liner, the corrosion depth increases but is still significantly lower than the depths calculated by the different cases in Scenario A. These results indicate that the pH has a significant influence on corrosion and the presence of the shotcrete liner will lead to corrosion depths lower than those calculated in Chapters 5, 6 and 7. Leaving out the shotcrete liner from the model setup leads to an overestimation of the calculated corrosion depth.

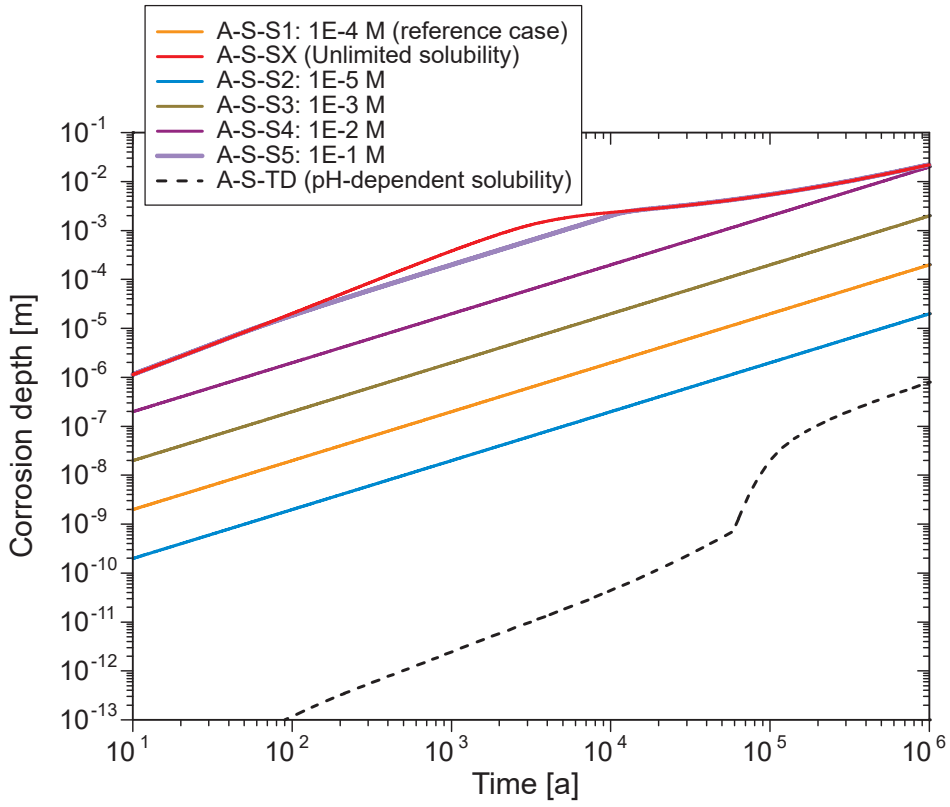

Fig. B-2: Corrosion depths calculated by the simplified model, illustrating the impact of a pH-dependent solubility (A-S-TD), compared with the calculation cases without any solubility limit (A-S-SX) and calculation cases with a fixed solubility limit (A-S-S1 to A-S-S5).

C The impact of hydrogen generated by anaerobic steel corrosion on canister corrosion

The current disposal concept considers that structural steel elements (e.g. reinforcing steel meshes, rock bolts and ancors) used for tunnel construction and operation of the repository may be left in place after closure of the facility. Once anaerobic conditions have developed, corrosion of steel will produce hydrogen. The effect of hydrogen as a second electron donor to SRB was not included in the calculations presented in sections 5, 6 and 7. The objective of this appendix is to quantify this effect and compare the results with the calculations for scenario A as described in Chapter 5.

C.1 Model description

The model (geometry, dimensions, geochemical composition of materials) is based on that defined for Scenario A (A-RT-RC) and described in Section 5.2. The main differences are the following:

- A steel compartment is defined between the buffer and EDZ. The thickness of this compartment is assumed to be 5 cm.
- The physical properties (porosity and effective diffusion coefficient) of the steel compartment are the same as those of the EDZ.
- SRB are present within both the steel and EDZ compartments, and utilise hydrogen generated by anaerobic corrosion of steel as an electron donor for sulphate reduction.
- The evolved hydrogen is decoupled from the redox system and is assumed not to form a separate gas phase.
- The rates of microbial consumption of hydrogen are assumed to be sufficiently fast so as to consume all generated hydrogen (a limiting assumption testing the maximum rates of sulphide generation due to hydrogen).
- The role of organic matter as electron donor is disregarded.

Corrosion of reinforcing steel mesh and the steel anchors is considered. The following corrosion reaction is assumed:

$$Fe(s) + 2H^+(aq) \Rightarrow Fe^{2+}(aq) + H_2(aq) \quad \text{(C-1)}$$

The rates of steel corrosion reported by NTB 16-01 (volume of hydrogen gas at standard temperature and pressure conditions per unit length of the tunnel) are used in the model. The reported hydrogen gas volumes are converted into hydrogen moles per unit volume of the steel compartment. A linear approximation of the hydrogen generation (constant rate) is implemented in the RT model (Fig. C-1), corresponding to ca. 7 moles of hydrogen generated per litre bulk of the steel compartment in 100'000 years (or ca. 50 moles of hydrogen per 1 litre porewater, assuming porosity of 0.14). The hydrogen associated with steel corrosion is assumed to be decoupled from the redox system. SRB activity utilising hydrogen as an electron donor is assumed to follow according to the reaction:

$$4H_2(aq) + SO_4^{2-}(aq) + H^+(aq) \Rightarrow HS^-(aq) + 4H_2O \quad \text{(C-2)}$$

Iron released by steel corrosion can precipitate as magnetite following:

$$2Fe^{3+}(aq) + Fe^{2+}(aq) + 4H_2O \Leftrightarrow Fe_3O_4(s) + 8H^+(aq) \quad \text{(C-3)}$$

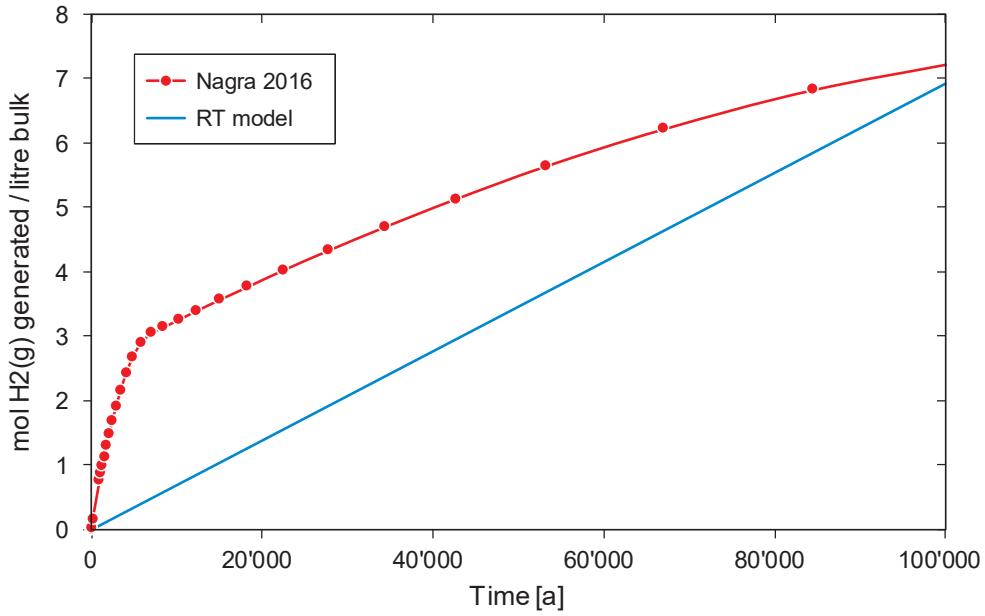

Fig. C-1: Hydrogen gas generation per litre bulk of the steel compartment (recalculated from data of hydrogen volume at standard temperature and pressure, assuming the corrosion of reinforcing steel mesh and steel anchors; Nagra 2016) and its linear approximation implemented in the RT model.

C.2 Model results

Anaerobic steel corrosion has a relevant impact on the predicted evolution of pH (Fig. C-2), which tends to increase to a level controlled by magnetite solubility. The increased pH values decrease sulphide solubility due to mackinawite equilibrium in the EDZ, where sulphide is generated (Fig. C-3). Fig. C-4 shows that the decreased sulphide concentrations correlate directly with a lower calculated corrosion depth compared to the reference case of scenario A (A-RT-RC). It is noted that due to the fast microbial activity rates allowed, all hydrogen generated is completely consumed by bacteria.

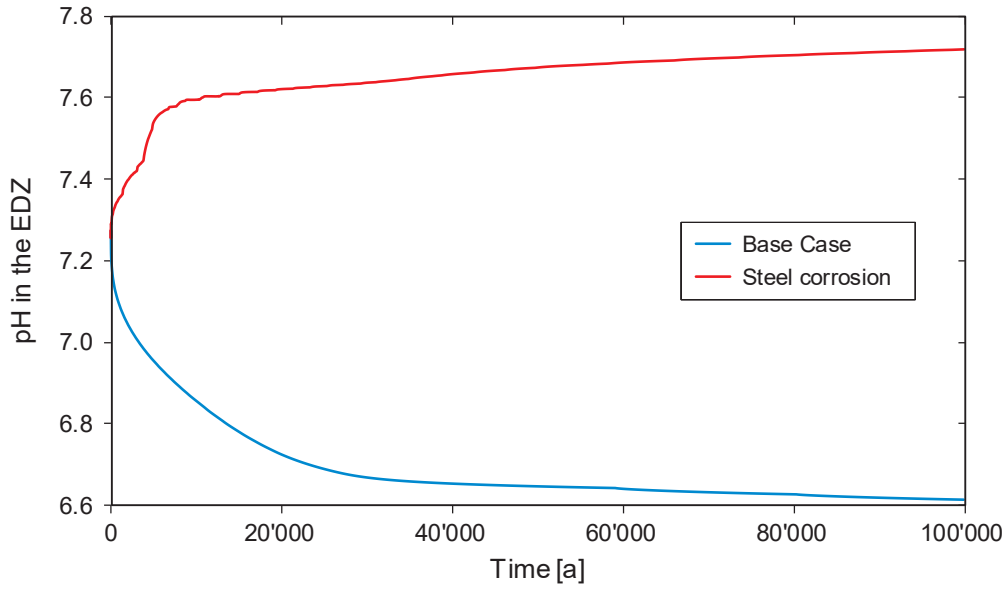

Fig. C-2: Comparison of evolution of pH in the middle of the EDZ in the Base Case calculation (A-RT-RC) and in the calculation considering steel corrosion and hydrogen generation (red line).

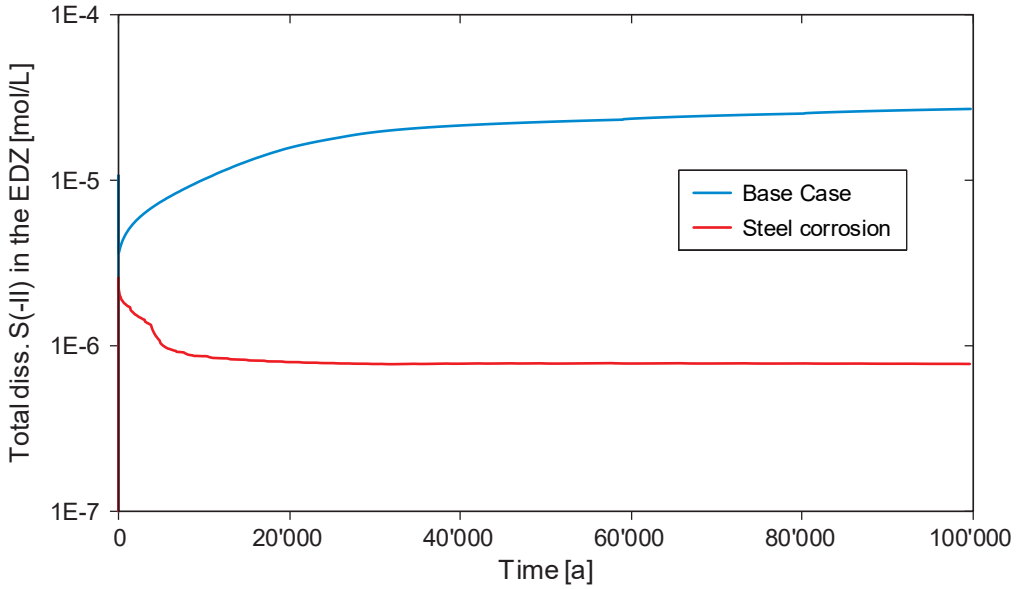

Fig. C-3: Comparison of evolution of total dissolved sulphide concentrations in the middle of the EDZ in the Base Case calculation (A-RT-RC) and in the calculation considering steel corrosion and hydrogen generation (red line).

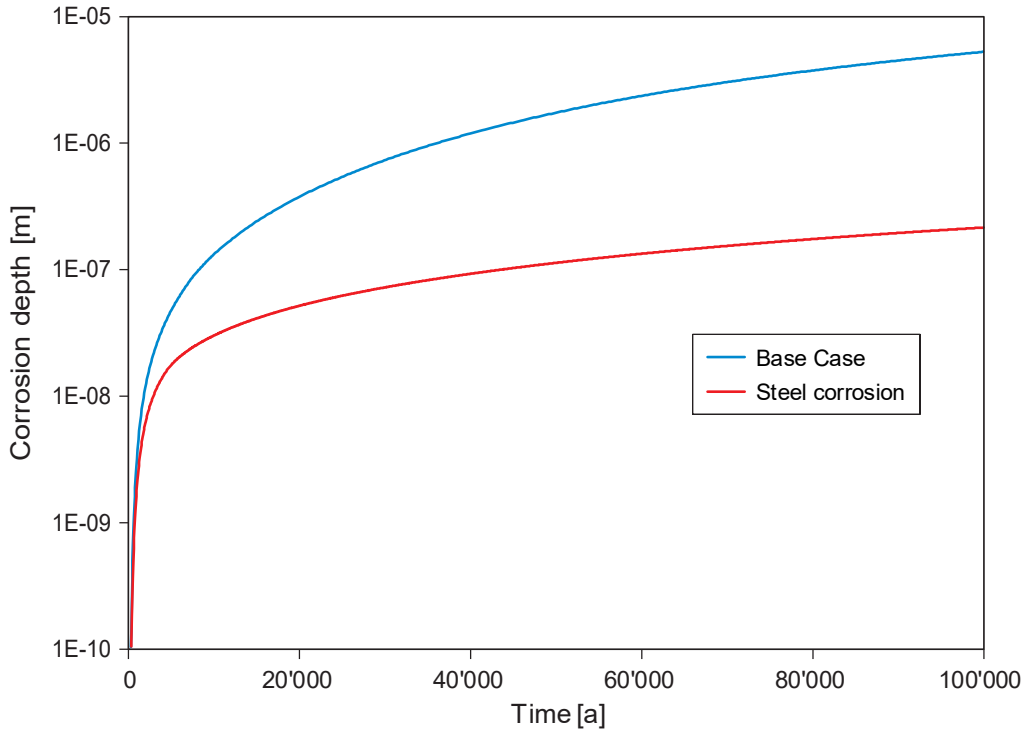

Fig. C-4: Comparison of canister corrosion depths calculated in the Base Case (A-RT-RC, blue line) and in the calculation considering steel corrosion and hydrogen generation (red line).

D Impact of a reduced pH on sulphide solubility in the EDZ

Because of the important impact that pH has on sulphide solubility we consider the impact of a lower pH (more acidic regime) in more detail below. As mentioned in Section 5.2.3, the model considers that (under a given pH) the concentration of dissolved sulphide in the EDZ is controlled by the simultaneous equilibrium of mackinawite and siderite. Because microbial activity in the EDZ releases H^+ and drives the precipitation of calcite and mackinawite adding to acidification, it cannot be excluded that the pH is slightly reduced. On the other hand the pH is also buffered by the dissolution of siderite which consumes H^+ and releases Fe for mackinawite precipitation. There also exists some uncertainty on the extent to which pH could decrease due to microbial activity, which is related to the overall uncertainty on the rate of microbial activity and the efficiency of pH buffering in Opalinus Clay.

Fig. D-1 presents a comparison between the evolution of total dissolved sulphide in the EDZ porewater as a function of pH calculated using the RT model over a period of 100'000 years and sulphide concentrations calculated in a batch mode. Batch calculations were performed using the PHREEQC (Parkhurst & Appelo 2013) geochemical simulator and the Thermochimie v.9b thermodynamic database. The input chemical data for the Opalinus Clay is the same as that used for reactive transport calculations (Section 5.2.2.) The batch calculation is based on the following assumptions:

- The pH is fixed to the desired value,
- Dissolved sulphide is controlled by mackinawite equilibrium,
- Dissolved iron is controlled by siderite equilibrium,
- Dissolved carbonate is controlled by calcite equilibrium, and
- Dissolved calcium is controlled by equilibrium with exchanger (along with Na, Mg and K).

The figure shows that the sulphide concentrations calculated by the two models agree closely. This verifies the assumption regarding solubility control on dissolved iron and sulphide during the RT calculation. Based on these results, the batch equilibrium model can be used to make predictions about the potential effect of pH on sulphide concentrations in the EDZ and to quantify the uncertainty regarding pH impact.

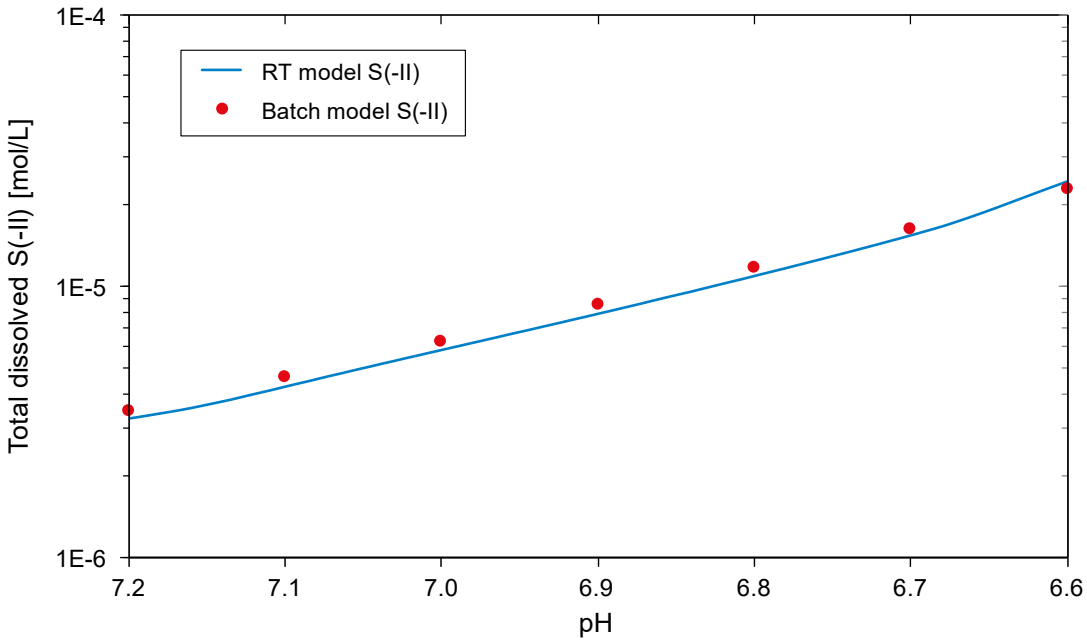

Fig. D-1: Comparison of total dissolved sulphide concentration in the EDZ as a function of pH, calculated by the reactive transport model or the batch model.

There exists little experimental information regarding the minimum pH values that could be generated by SRB activity under repository conditions. Wersin et al. (2011) report the "in situ" values of pH continuously measured during the Porewater (PC) experiment in Opalinus Clay at the Mont Terri Underground Research Laboratory (Fig. D-2). The lowest value of pH measured was 6.8 (with 0.2 pH unit uncertainty). Considering the analytical uncertainty, this is roughly within the minimum pH range predicted by the RT model.

In the following, we consider a pessimistic (theoretical) scenario, whereby due to very fast microbial activity and limited buffering capacity, the pH in the EDZ decreases to a value of 6, and use the batch model to calculate the corresponding concentration of dissolved sulphide (Fig. D-3).

Fig. D-3 shows that for a pH between 6.2 and 6.0 the model predicts that the total dissolved sulphide in the EDZ would be limited to values around $1 - 2 \times 10^{-4}$ mol/L. The impact of an increased sulphide solubility value on canister corrosion has been explored by the simplified model applied to the three scenarios, as presented in Sections 5, 6 and 7. The general effect is that the total corrosion depth scales in direct proportion with the sulphide solubility in the EDZ.

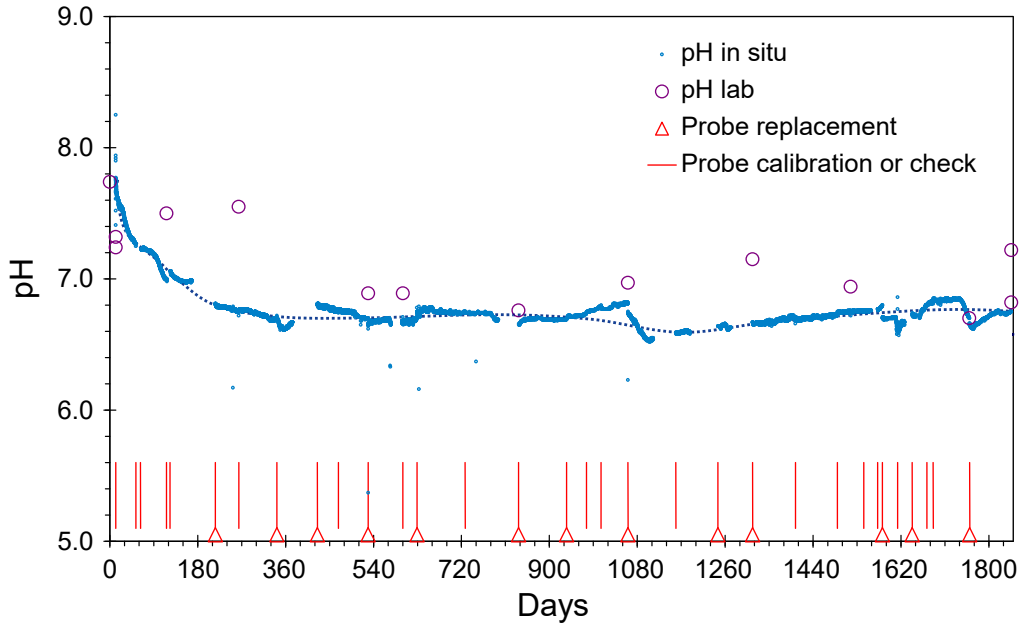

Fig. D-2: Measured pH versus time continuously measured "in situ" values and laboratory values measured on the sampled water during the Porewater (PC) experiment in Opalinus Clay at the Mont Terri Underground Research Laboratory (Wersin et al. 2011).

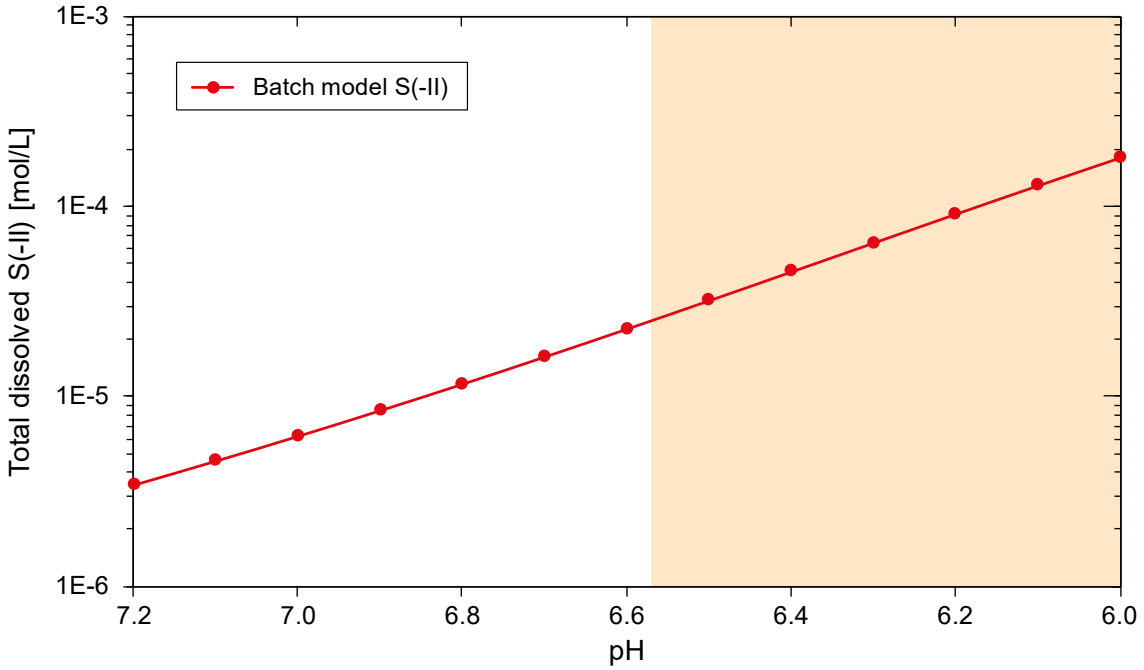

Fig. D-3: The concentration of total dissolved sulphide calculated using the batch model for a pH range between 7.2 and 6.0.

In light orange is indicated the pH range below that predicted by the RT model.